2004-12

Development of a Control Moment Gyroscope controlled, three axis satellite simulator, with active balancing for the bifocal relay mirror initiative

Kulick, Wayne J.

Monterey, California. Naval Postgraduate School

NAVAL POSTGRADUATE SCHOOL

MONTEREY, CALIFORNIA

THESIS

DEVELOPMENT OF A CONTROL MOMENT GYROSCOPE CONTROLLED, THREE AXIS SATELLITE SIMULATOR, WITH ACTIVE BALANCING FOR THE BIFOCAL RELAY MIRROR INITIATIVE

by

Wayne J. Kulick

December 2004

Thesis Advisor:	Brij N. Agrawal
Second Reader:	Jong-Woo Kim

Approved for public release; distribution is unlimited

THIS PAGE INTENTIONALLY LEFT BLANK

REPORT DOCUMENTATION PAGE			Form Approved OMB No. 0704-0188

1. AGENCY USE ONLY *(Leave blank)*	2. REPORT DATE	3. REPORT TYPE AND DATES COVERED
	December 2004	Master's Thesis

4. TITLE AND SUBTITLE: Development Of A Control Moment Gyroscope Controlled, Three Axis Satellite Simulator, With Active Balancing For The Bifocal Relay Mirror Initiative	5. FUNDING NUMBERS
6. AUTHOR(S) Wayne Joseph Kulick	
7. PERFORMING ORGANIZATION NAME(S) AND ADDRESS(ES) Naval Postgraduate School Monterey, CA 93943-5000	8. PERFORMING ORGANIZATION REPORT NUMBER
9. SPONSORING /MONITORING AGENCY NAME(S) AND ADDRESS(ES) N/A	10. SPONSORING/MONITORING AGENCY REPORT NUMBER

11. SUPPLEMENTARY NOTES The views expressed in this thesis are those of the author and do not reflect the official policy or position of the Department of Defense or the U.S. Government.

12a. DISTRIBUTION / AVAILABILITY STATEMENT	12b. DISTRIBUTION CODE
Approved for public release; distribution is unlimited	

13. ABSTRACT (maximum 200 words)

This thesis develops and implements a Control Moment Gyroscope (CMG) steering law, controller and active balancing system for a three-axis satellite simulator (TASS). The CMGs are configured in a typical pyramid configuration (the fourth CMG position being null). The development was done primarily with simulation and experiments utilizing Real Time Workshop and XPC Target of MATLAB and SIMULINK. The TASS is a double circular platform mounted on a spherical air bearing with the center of rotation (CR) about the approximate physical geometric center of the simulator. The TASS utilizes three moveable masses in the three body axes for balancing which actively eliminate any center of gravity (CG) offset and return the CG to the CR. The TASS supports an optics payload designed to acquire, track and point a received laser beam onto an off-satellite target. The target may be stationary or moving. Actively balancing the TASS reduces the torque output requirement for the CMGs while maintaining either a stabilized level platform or a particular commanded attitude. Reduction or elimination of torque output from the CMGs results in a more stabilized platform, less structural induced vibration, less jitter in payload optics and less power required in spacecraft applications.

14. SUBJECT TERMS Satellite Simulator, Active Balancing, Auto Balancing, Control Moment Gyroscope, CMG, Air Bearing,	15. NUMBER OF PAGES 125
	16. PRICE CODE

17. SECURITY	18. SECURITY	19. SECURITY	20. LIMITATION OF ABSTRACT
Unclassified	Unclassified	Unclassified	UL

NSN 7540-01-280-5500 Standard Form 298 (Rev. 2-89)
Prescribed by ANSI Std. 239-18

THIS PAGE INTENTIONALLY LEFT BLANK

Approved for public release; distribution is unlimited

DEVELOPMENT OF A CONTROL MOMENT GYROSCOPE CONTROLLED, THREE AXIS SATELLITE SIMULATOR, WITH ACTIVE BALANCING FOR THE BIFOCAL RELAY MIRROR INITIATIVE

Wayne J. Kulick
Lieutenant Commander, United States Navy
B.S., University of North Florida, 1995

Submitted in partial fulfillment of the
requirements for the degree of

MASTER OF SCIENCE IN ASTRONAUTICAL ENGINEERING

from the

NAVAL POSTGRADUATE SCHOOL
December 2004

Author: Wayne J. Kulick

Approved by: Dr. Brij N. Agrawal
Thesis Advisor

Dr. Jong-Woo Kim
Thesis Co-Advisor

Anthony J. Healey
Chairman, Department of Mechanical and Astronautical Engineering

THIS PAGE INTENTIONALLY LEFT BLANK

ABSTRACT

This thesis develops and implements a Control Moment Gyroscope (CMG) steering law, controller and active balancing system for a three-axis satellite simulator (TASS). The CMGs are configured in a typical pyramid configuration (the fourth CMG position being null). The development was done primarily with simulation and experiments utilizing Real Time Workshop and XPC Target of MATLAB and SIMULINK. The TASS is a double circular platform mounted on a spherical air bearing with the center of rotation (CR) about the approximate physical geometric center of the simulator. The TASS utilizes three moveable masses in the three body axes for balancing which actively eliminate any center of gravity (CG) offset and return the CG to the CR. The TASS supports an optics payload designed to acquire, track and point a received laser beam onto an off-satellite target. The target may be stationary or moving. Actively balancing the TASS reduces the torque output requirement for the CMGs while maintaining either a stabilized level platform or a particular commanded attitude. Reduction or elimination of torque output from the CMGs results in a more stabilized platform, less structural induced vibration, less jitter in payload optics and less power required in spacecraft applications.

THIS PAGE INTENTIONALLY LEFT BLANK

TABLE OF CONTENTS

LIST OF FIGURES

LIST OF TABLES

THIS PAGE INTENTIONALLY LEFT BLANK

LIST OF SYMBOLS, ACRONYMS AND ABBREVIATIONS

δ_i	Individual CMG gimbal angle (rad)
$\dot{\delta}_i$	Individual CMG gimbal rate (rad/sec)
d_i	Δ position from $r_{i,0}$ to current m_i position
h_B	Momentum of rigid body
h_{CMG}	Momentum of CMGs
h_i	Momentum of single CMG
H_S	Total system momentum
I_B	Inertia of rigid body (Kg-m^2)
I_{CMG}	CMG rotor inertia (Kg-m^2)
m_i	Mass of an individual balance mass
m_j	CMG_j mass
M	Mass of the TASS minus sum of balance masses
r_{CG}	Position vector of the CG offset from the CR
r_j	CG position of CMG_j
$r_{i,0}$	CR to initial m_i position
$\boldsymbol{s}_i$	Unit vector along m_i axis
h_{CMG}	CMG angular momentum (N-m-s)
τ_{CMG}	Torque output of one CMG (N-m)
τ_{EXT}	Total torque acting on system (N-m)
$\boldsymbol{u}$	Control torque
ω_n	Natural frequency
ω_r	CMG rotor angular speed (rad/sec)

ACEI	Automated Controlled Environments Inc.
AFRL	Air Force Research Lab
BFRM	Bifocal Relay Mirror
CG	Center of Gravity
CMG	Control Moment Gyroscope
CR	Center of Rotation
DOF	Degrees of Freedom
FSM	Fast Steering Module
GDC	Guidance Dynamics Corporation
IEC	Industrial Embedded Computer
IMU	Inertial Measurement Unit
MOI	Moment of Inertia
NPS	Naval Postgraduate School
NRO	National Reconnaissance Office
PSD	Position Sensing Device
PSM	Position Sensing Module
SGVSCMG	Single Gimbal variable Speed CMG

TASS	Three axis satellite simulator
TASS1	1st generation TASS
TASS2	2nd generation TASS

LIST OF EQUATIONS

THIS PAGE INTENTIONALLY LEFT BLANK

ACKNOWLEDGMENTS

The author would like to thank several people whom had a direct influence on the outcome of this thesis:

Distinguished Professor Brij Agrawal. Dr. Agrawal knows how to make research a truly enjoyable learning experience. His guidance kept my research focused and on track.

Dr. Jong-Woo Kim. Dr. Kim was always there to answer questions and work shoulder to shoulder on the simulator. He either had ready answers to difficult questions or knew where to find them. His patience is outstanding and he has a great ability to make the difficult concepts easily understood.

Professor Mason Peck of Cornell University. I had the unique pleasure of working with Dr. Peck when he was with Honeywell in Glendale, AZ. His work in this area is unparalleled. He was always available to answer my incessant questions and make his concepts easily understood. Not only a great academic, but a great engineer as well. Cornell is lucky to have him.

Last, but most important, my wonderful wife Melissa. Her patience through this research was incredible. She kept me on track during the times it was most difficult and reminded me of the goal when I needed it most. She is truly the answer to my prayers.

THIS PAGE INTENTIONALLY LEFT BLANK

I. INTRODUCTION

A. BACKGROUND

1. Bifocal Relay Mirror (BFRM)

This thesis builds upon the previous work of Vincent S. Chernesky [Ref. 4] and his work with the initial three axis satellite simulator (TASS1). This second and improved capability three axis satellite simulator (TASS2, also referred to as TASS within this document) continues the work on the first with an upgraded structure, control system and BFRM payload. The history of the BFRM project will be briefly summarized here. A more detailed history for the interested can be found in Chernesky's thesis on the TASS1.

In 2000, a preliminary satellite design for scissors-like BFRM was completed by Naval Postgraduate School (NPS) masters degree students' senior design project to validate a concept study performed by the Air Force Research Laboratory (AFRL) in Albuquerque, NM. The design consisted of two optical telescopes in a scissors-like configuration (Figure 1)where a laser beam was received from the earth by one of the orbiting optical telescopes, passed to the second optical telescope on the satellite where it was then relayed back to earth to either a cooperative or uncooperative target. The optical path between the telescopes includes adaptive optics for wave front aberration correction, jitter correction and beam steering.

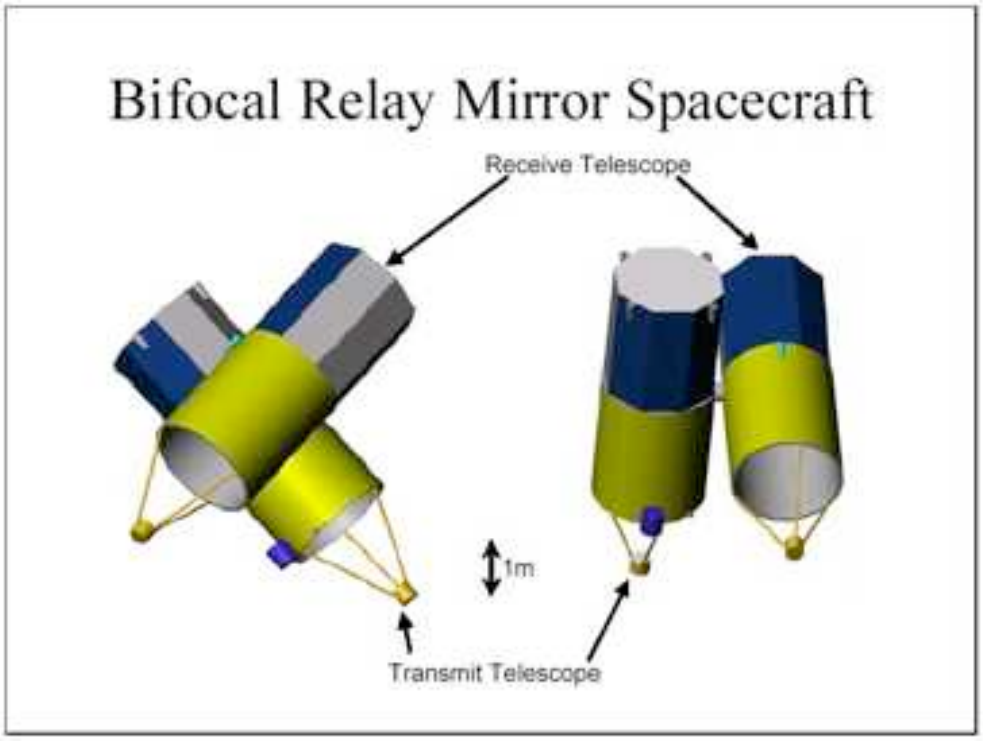

Figure 1. BFRM [Ref. 4]

In January 2001, a joint contract was awarded by the National Reconnaissance Office (NRO) to both NPS and AFRL as a joint project to develop the concept in more detail. Work was divided up between AFRL and NPS such that AFRL would develop the optical payload while NPS developed the controls for acquisition, tracking and pointing.

2. Spacecraft Research and Design Center (SRDC)

The SRDC at NPS consists of a satellite servicing lab, Fleet Satcom lab, flexible dynamics lab, attitude control and dynamics lab and a satellite design center. The satellite attitude control and dynamics lab is host to both TASS1 and TASS2 with each simulator occupying opposite sides of the lab. This arrangement allows for development of each simulator and future enhancements such as cooperative experiments between the two.

II. HARDWARE DEVELOPMENT

The TASS2 is comprised of several subsystems integrated to form a notional satellite with subsystems for power, attitude determination and control, command and data handling and an optical payload: the bifocal relay mirror. This section outlines the physical description, development and integration of the various subsystems onboard the TASS. Also covered are difficulties encountered during development, remaining work to be pursued and discrepancies between simulation and experimentation.

TASS2 is to support the acquisition, tracking and pointing requirements for the BFRM project. The ultimate goal of the project is to deliver pointing accuracy, for the spacecraft bus, in the milliradian region. The optical payload goal is to support nanoradian pointing accuracy. This is not possible with the current lab equipment, but will allow "proof of concept." Accuracy to that degree will require highly sophisticated sensors and equipment.

What the TASS2 will do is prove the concept of such pointing accuracy within the limits of the accuracy on the onboard equipment.

A. OVERVIEW

The TASS (shown in Figure 2) was constructed by Guidance Dynamics Corporation (GDC) with electronics and controllers designed and integrated by Automated Controlled Environments Inc., (ACEI). The main structure is built upon 2 circular steel decks 1.25cm thick, 1.83m in diameter and the two decks separated into upper and lower decks by 15, 0.5m long, circular standoffs with rubber vibration

isolation on the lower deck end. The center of rotation (CR) is located 21.3cm below the upper deck and is comprised of a spherical bearing ~30cm in diameter. The spherical bearing rests in a spherical cup supplied with 80 psi air for floated operations. During floated operations, air supplying the pedestal base raises the TASS ~1cm for near frictionless floated motion. During floated operations, the table is restricted to 3 degrees of freedom (DOF) about the CR.

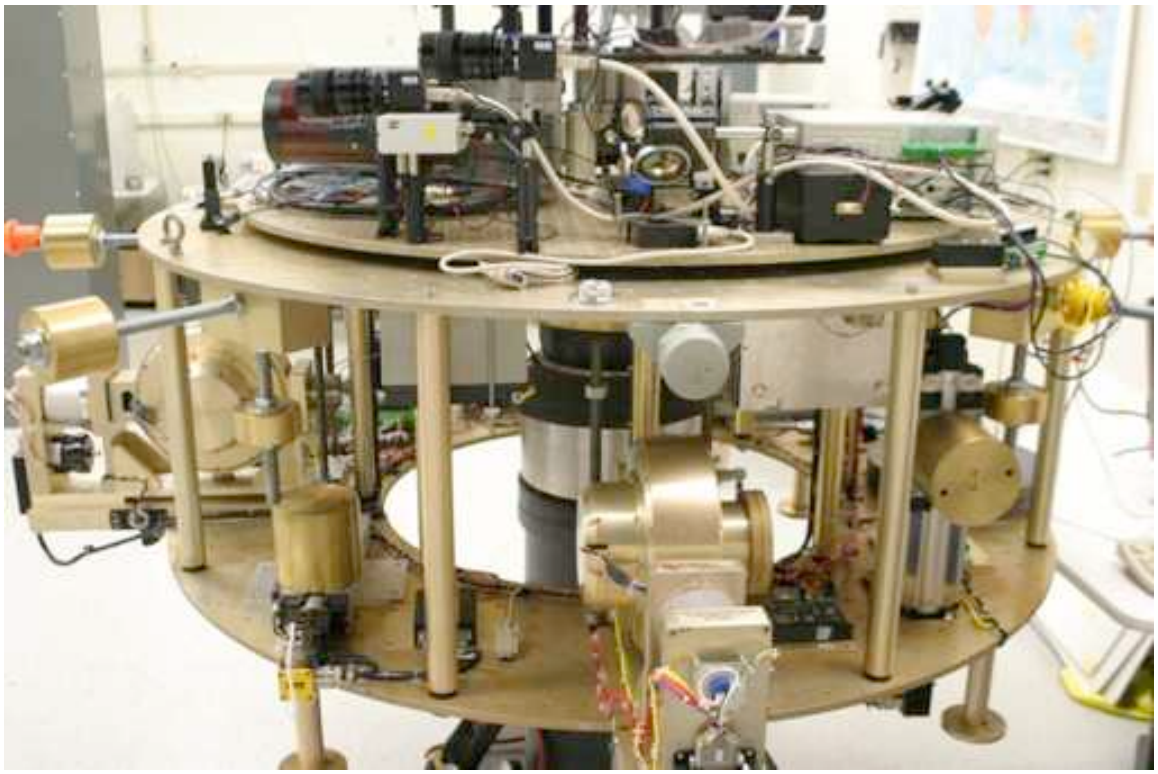

Figure 2. TASS2 Overview

Attached to the upper deck is a main optical deck slightly smaller in diameter than the upper deck. On this deck is attached the targeting optics which consist of a 102mm diameter Orion Maksutov-Cassegrain telescope with a 1300mm focal length, fast steering mirror (FSM) for beam

positioning, optics train components for beam steering, three computers for optical payload control, position sensing devices (PSDs) for fine pointing control of the simulator structure, moveable masses for balance and various power distribution and switching components. Attached to the center of the TASS and raised above the main optical is the upper optical deck. This deck is motorized and has one degree of freedom with respect to and parallel to the main optical deck for tracking of a source beam. This deck contains the source beam receive optics consisting of an Orion telescope identical to the targeting Orion telescope, FSM and PSD for jitter control, controllers for the FSM and PSD and optics for routing the received beam to the main optical deck through the hollow center section of the TASS.

Balance of the TASS is accomplished in part by manual and automatic adjustable masses. Manual, radially adjustable masses, are located and attached slightly below the upper deck at six locations. The masses are essentially located every 45° with exception of the positive and negative X axis. If a mass adjustment is required along this axis, the adjustment can be made by moving the two masses offset 45° from the axis. Four vertically adjustable masses are located on the periphery and are used for adjusting the center of gravity (CG) along the Y axis. Three linear adjustable masses are located along the three principal axes and attached to a Daedal linear actuator operated by a Compumotor rotary brushless DC motor.

Attitude control is maintained by three single gimbal GDC Control Moment Gyroscopes (CMGs) configured in a modified pyramid configuration (Figure 3) with the

traditional fourth position empty and filled by ballast mass to maintain simulator balance. The CMGs are attached to a hinged frame and canted to a beta angle (β) of −35.25° relative to the lower deck. The β, or skew angle, is measured with the vertex of the skew angle at the center of mass of the CMG, one side of the angle parallel to the lower deck of the TASS facing inward and the other side passing through, and parallel to, the plane of the CMG rotor such that the angle less than 90° is measured. This is not a "traditional" pyramid arrangement of CMGs. In the traditional configuration, the gimbal axis vectors are aligned such that they are perpendicular to the face of the tetrahedron, resulting in a skew angle of 54.75°.

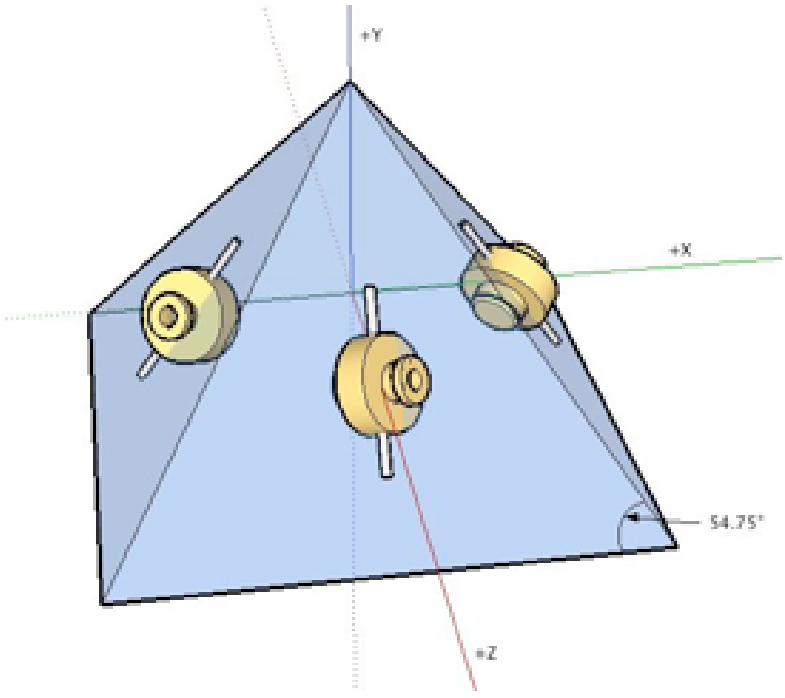

Figure 3. CMG pyramid configuration

Attitude determination is made with a combination of sensors including a Northrup Grumman (formerly Litton) LN-200 IMU (Figure 21) mounted to the underside of the upper deck, a three axis magnetometer mounted to the upper deck and a three axis inclinometer mounted to the underside of the upper deck.

A VersaLogic industrial embedded PC (Figure 24) houses a Diamond MM32-AT PC104 for program control, execution and C&DH functions. Communication between the embedded PC and off-simulator computer (desktop PC running Matlab/Simulink) is performed via a wireless Dlink router (Figure 4) using 802.11G wireless technology and Ethernet cable from the router to the embedded PC. Major equipment locations are shown in Figure 5.

Figure 4. DLink wireless 802.11g router

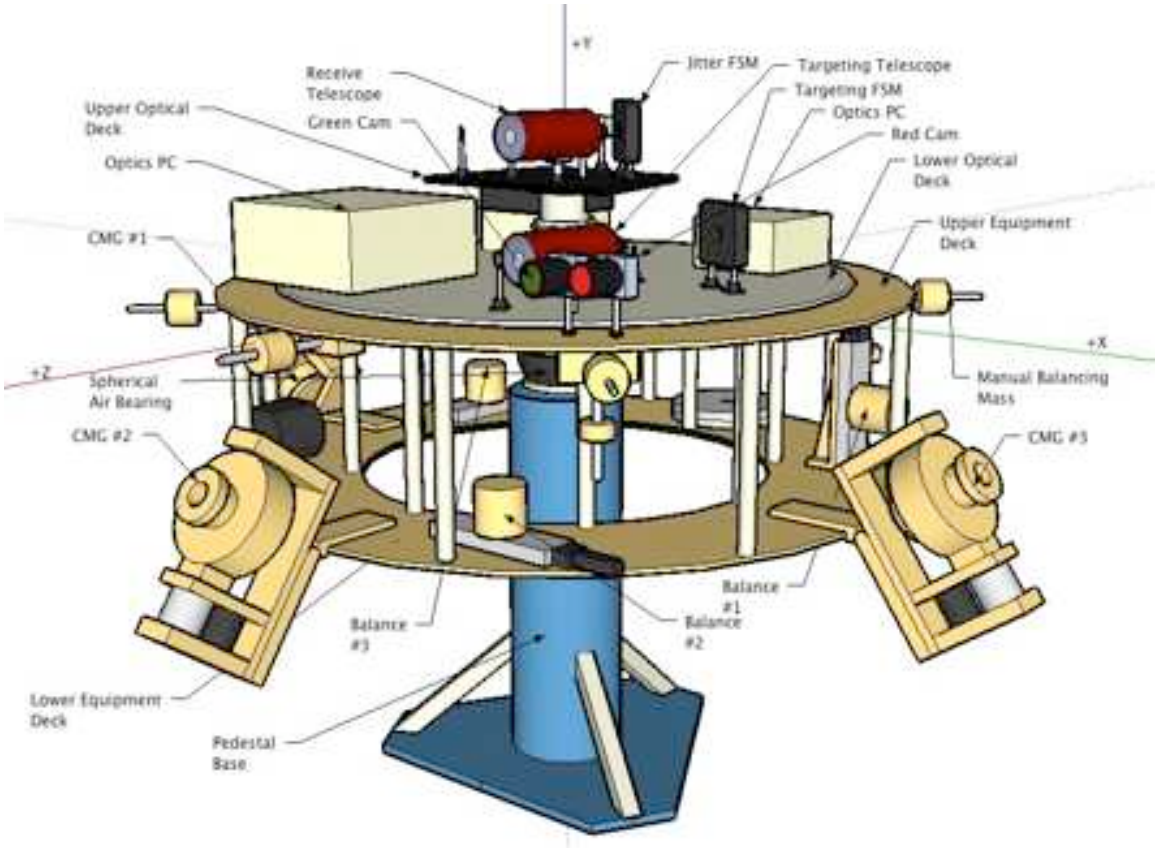

Figure 5. TASS2 equipment locations

B. REFERENCE FRAMES AND AXES

1. GDC Axes

The TASS was delivered with an assumed reference frame during construction and documented in the mass properties spreadsheet. The assumed reference frame was a left handed (LH) coordinate system of roll, pitch and yaw with yaw being from the CR downwards, towards the earth, as positive. Roll and pitch axes then formed the horizontal plane parallel to the upper and lower decks in a LH fashion. The positive X axis was from the CR through the center of CMG#1 ballasting weights. The positive Z axis was from the CR and passing through the ballasting weights added in the position of the absent CMG#4 completing the LH

body frame. The demonstration program supplied with the TASS was also based in this reference frame.

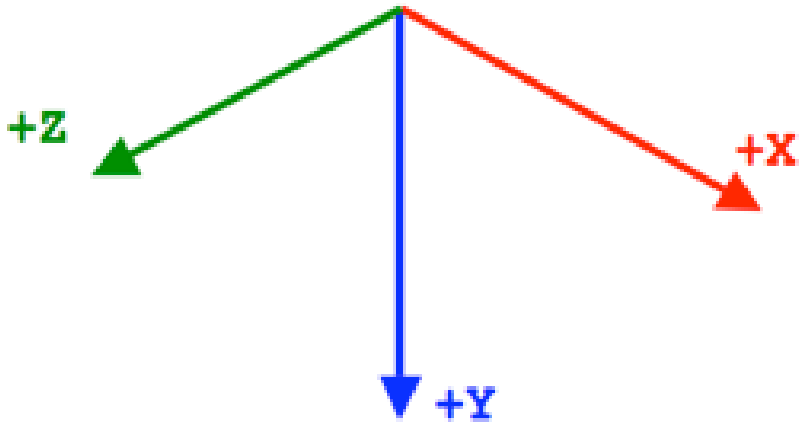

Figure 6. Left handed coordinate system

2. Inertial Axes

Inertial axes will be denoted by the subscript "N". For operation and simulation of a satellite in orbit, it was necessary to redefine the axes as defined by GDC to correspond to industry and educational standards.

Though the intuitive yaw axis (Z) would appear to be the vertical axis passing through the CR and air bearing pedestal base, this would not agree with our payload pointing and where the laser source and targets were located. In our case, the TASS is assumed to be "flying" such that the far wall of the lab is earth and the flight path is parallel with the floor. Since in traditional satellite control the +Z axes points towards the earth, that determined our $+Z_N$ axis.

The desired flight path for simulations is parallel to the lab floor and in order to align the Y_N axis upwards (for

convenience), produced a direction of flight to the right as one faces the TASS ($-Z_N$ direction). The resulting RH coordinate system located the pitch axis (Y_N) upwards, the roll axis (X_N) parallel to the floor and to the right and the yaw axis (Z_N) down the length of the lab.

3. Body Axes

Body axes will be denoted with the subscript "B". The body axes are identical to the control axes used. The $+Y_B$ axis was set originating from the CR vertically through the TASS. The $-Y_B$ correspondingly passes downward through the air bearing pedestal base. The $+X_B$ axis was set passing through CMG#3 and the $+Z_B$ passing through CMG#2. In a stationary situation, this aligned the body axes with the inertial axes. The body axes can be seen in Figure 5 in relation to the equipment and in Figure 7 for graphical representation.

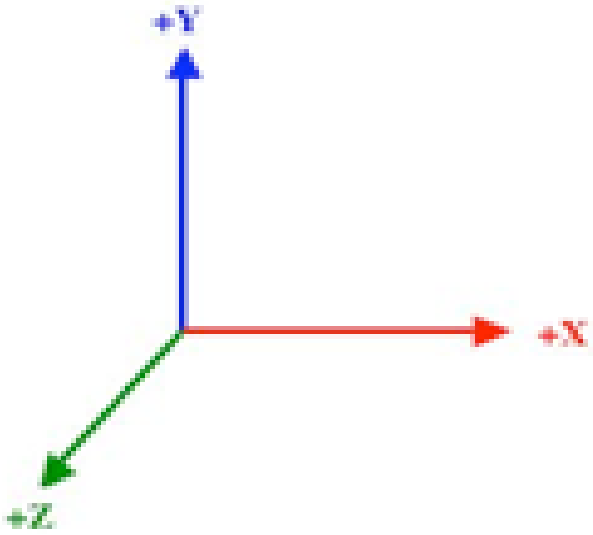

Figure 7. Right handed coordinate system

3. Principal Axes

Principal axes were assumed to coincide with the body axes for simulation purposes. The moment of inertia matrix as calculated in the mass properties spreadsheet (Appendix B) shows close symmetry between the X_B and Z_B axes. Since equipment on the TASS is changing often, calculation of the exact principal axes is left for a later date. It is anticipated there should be little control influence in early experiments with a slight difference between the body axes and principal axes.

4. Orbit Axes

The body axes origin is centered at the CR. Since the TASS is fixed relative to the inertial reference frame, no orbit reference frame is required. All coordinate transformations can be accomplished from body to inertial, or reverse, directly.

5. Mass Properties Axes

The mass properties spreadsheet [Ref. 9](Appendix A) was delivered by GDC based on their LH coordinate systems explained previously. It was necessary to convert equipment positions based in the GDC body reference frame to a right handed reference frame standard to the SRDC, academia and commercial institutions.

C. CONTROL MOMENT GYROSCOPES

1. Description

The CMGs (Figure 8)were built by GDC and are 24.4 N-m-s (based on a max rotor speed of 2800 rpm), single gimbal, variable speed CMGs (SGVSCMG). The controller hardware was built, supplied and integrated by ACEI. The controllers include rotor speed controllers (Figure 9) and gimbal controllers (Figure 10). The CMGs can be operated in either single gimbal CMG mode, maintaining a constant rotor speed

and gimbaling the axis, or in reaction wheel mode by fixing the gimbal axis and operating the CMG in variable speed mode to control attitude. The CMGs provide gimbal angle feedback by rotary encoders monted on the gimbal shaft (Figure 11)

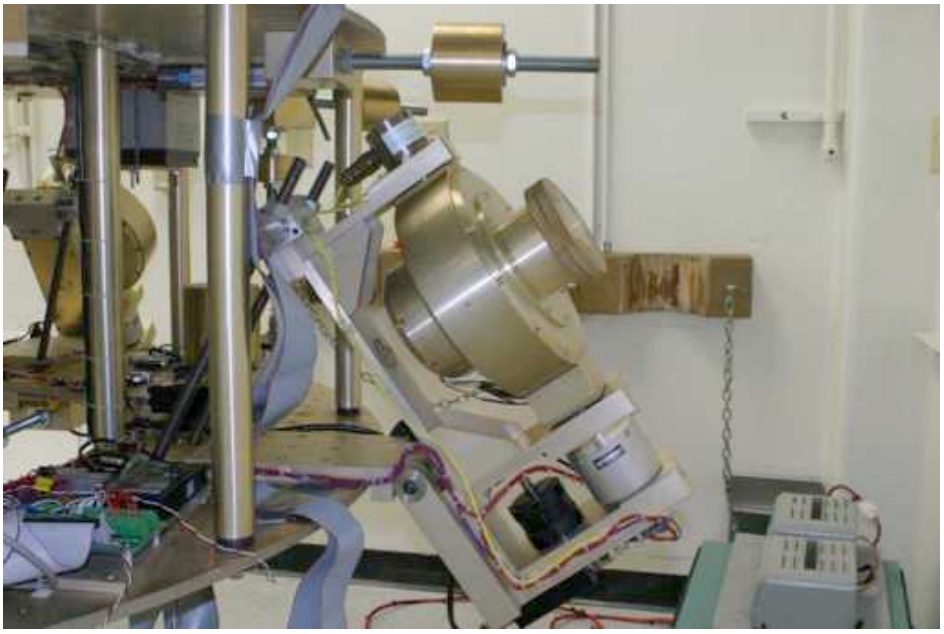

Figure 8. GDC SGVSCMG

Figure 9. CMG Rotor speed controller

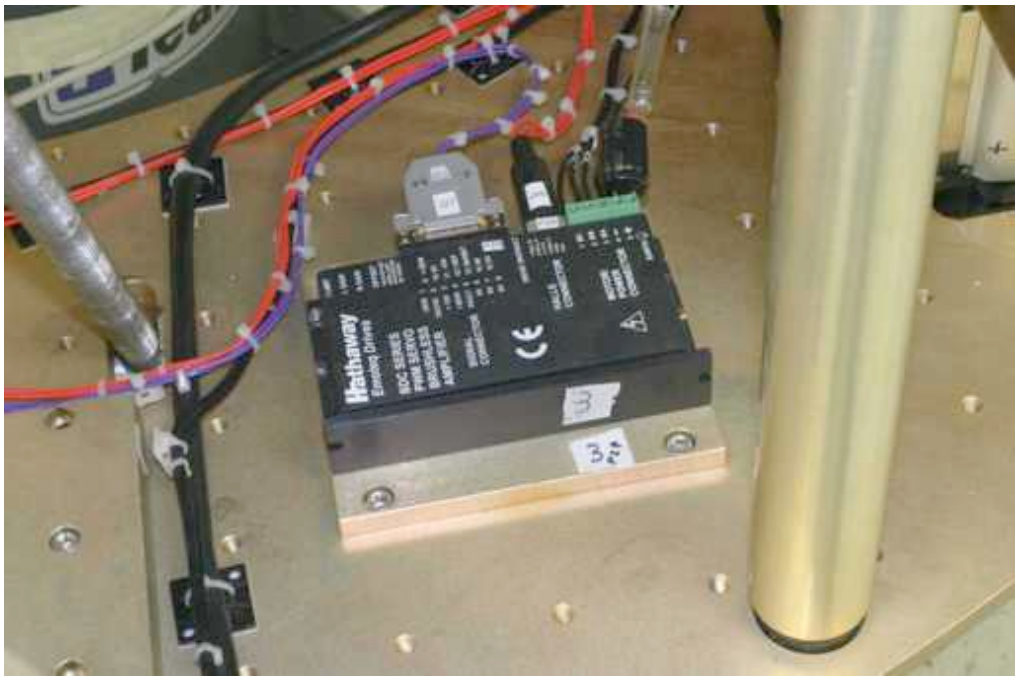

Figure 10. CMG gimbal controller

Figure 11. CMG gimbal position encoder

2. Failures and Troubleshooting

During simulation, it was noted that control movements were non-smooth at times. For the CMGs, being commanded via a PD controller, gains were initially suspect. Gains were

tuned using the Nichols-Ziegler method. Slight variations in gains did not alter the sporadic, seemingly uncommanded movements of the CMGs. Next, hardware was investigated. Investigation revealed a 10°-20° play in the gear system connecting the DC motor to the gimbal. The gimbal position feedback was not seen as changing for 10°-20° of commanded gimbal angle. This resulted in an almost bang-bang control system. Disassembling the gear system revealed loose set screws securing the gears to their respective shafts.

CMG #1 was discovered to have an oscillatory noise on it's gimbal position feedback signal. Figure 12 shows commanded position in blue and feedback position in green. Periodic spikes up to 1.4° in magnitude can be seen. CMG#2 is depicted in Figure 13 and is also representative of CMG#3. Feedback position is identical to commanded position as would be expected. It is unknown as to the cause of the ~10Hz oscillatory noise, but the controller electronics is suspect. The CMG and controller has been returned to the manufacturer for modification the controller electronics.

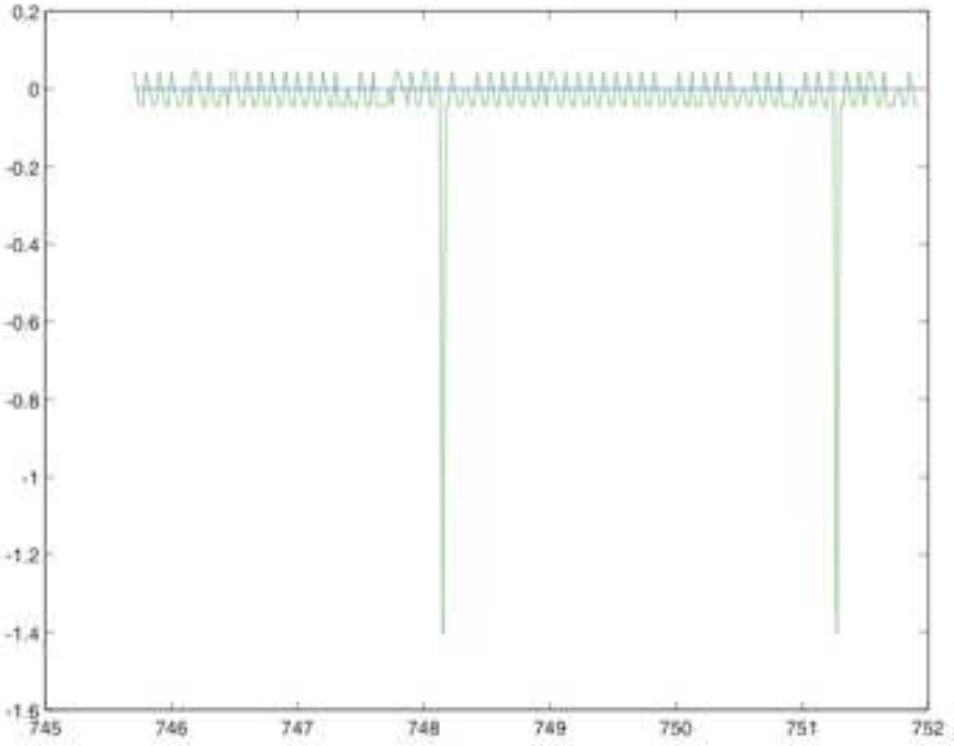

Figure 12. CMG#1 Commanded vs. Feedback Position

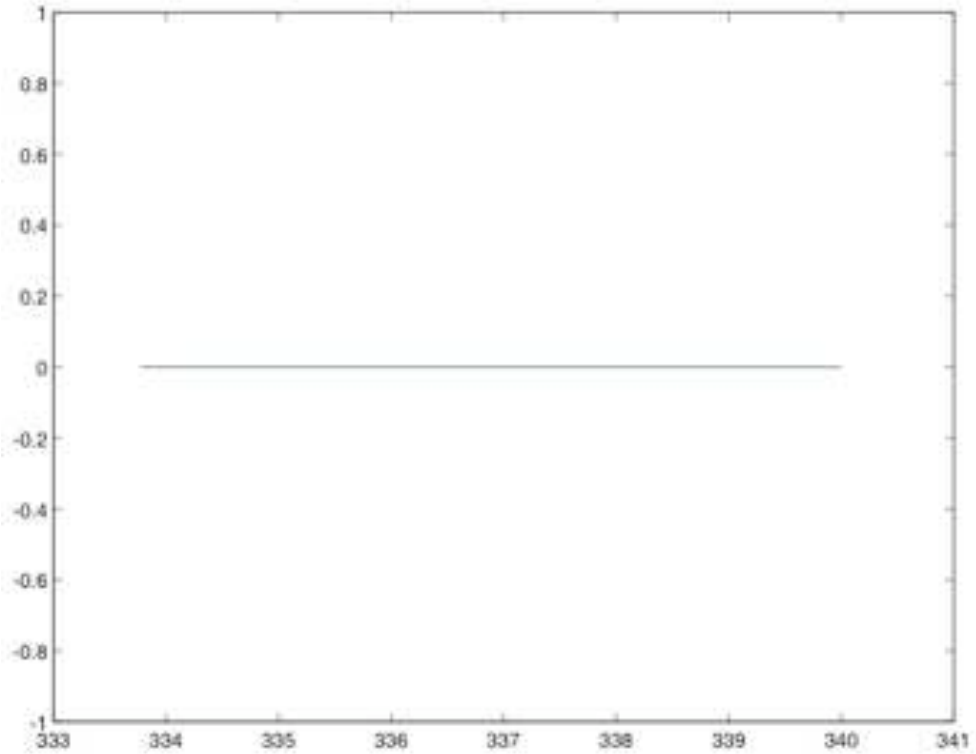

Figure 13. CMG#2 Commanded vs. Feedback Position

D. POWER SWITCHING AND DISTRIBUTION SYSTEM

The power subsystem is a 24.8 Vdc (nominal) bus rated at 100A and is composed of the power switch box, power switching electronics assembly, batteries, external power and external battery charger. At a zero-torque, CMG rotors not rotating condition, current draw is no more than ~4A. Operation in this configuration can continue for up to 6 hours. CMG operation will reduce this time. Under actual conditions with CMGs operating and applying a torque to the TASS, a maximum of two hours continuous operation was observed.

The power system allows for flexibility in operation of the TASS. For example, the batteries may be charged while operating the TASS from external power, CMG rotors can also be powered via battery while operating the TASS on external power. As a safety measure, CMG rotors may only be operated from battery power to prevent over current conditions on external power. CMG gimbals, however, may be operated on external power.

1. Power Switch Box

The switch box (Figure 14) is the main user interface for powering TASS2 components. The front panel contains individual power switches for the CMGs, Balance Controllers, IMU, Top Deck Controller and Payload Electronics. The switchbox provides overcurrent protection for components by automatically switching off power if bus voltage drops below 18.5V.

Figure 14. Power switch box

2. Power Switching Electronics (PSE)

The PSE provides an interface for the Industrial Embedded Computer (IEC) to communicate with all the digitally controlled devices on the TASS via a single RS-232 interface. The PSE also contains analog conditioning electronics for the sun sensor.

3. Batteries

For floated, internal power operation, two Yuasa 12V-24Ah sealed gel-cell batteries (Figure 15) are connected in series providing a nominal 24.8 Vdc bus.

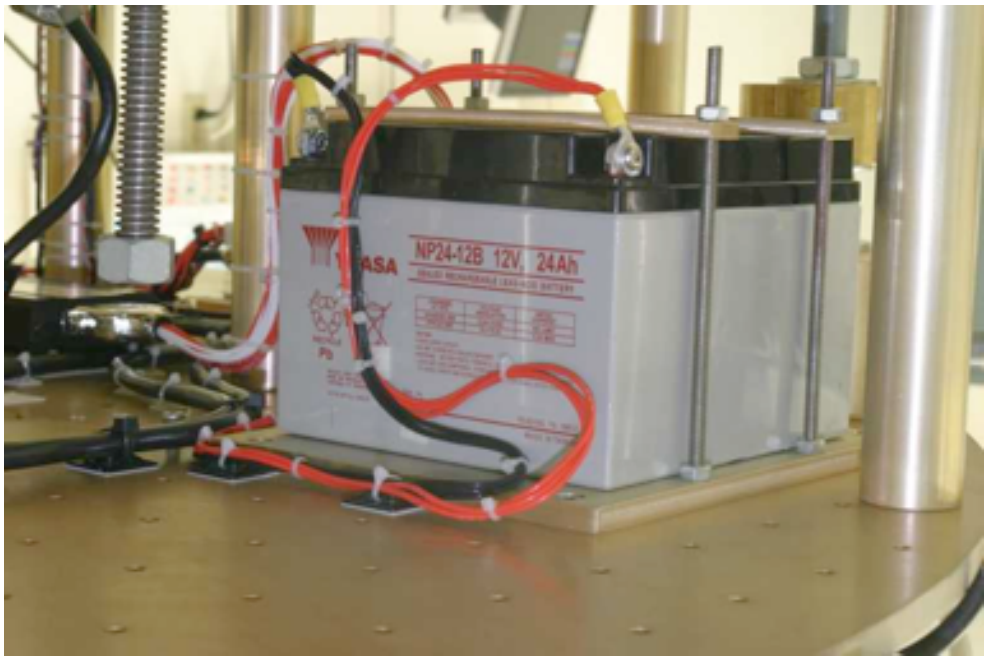

Figure 15. Gel cell battery

4. External Power

External power is provided via an umbilical from an external 24 Vdc source to the power switch box receptacle. The red switch controls the source of power. Out selects internal power while "IN" selects external power.

5. Battery Charger

The battery charger is external to the TASS and connects to the TASS via the same umbilical used for external power (Figure 16). Two chargers (one for each battery) connect to a quick disconnect in the umbilical which then plugs into the power switch box receptacle.

Figure 16. Battery chargers

E. SUN SENSOR

The sun sensor (Figure 17) utilizes a four-sensor array that determines the average location of the maximum point of light along a vertical and horizontal axis in its field of view (±10°). Average location is output in the form of an error signal with an analog value of 1.5 to 3.5 Vdc in each axis. An "on center" condition is indicated by a 2.5 Vdc output in each axis. The corresponding average scale factor is 44mV/deg.

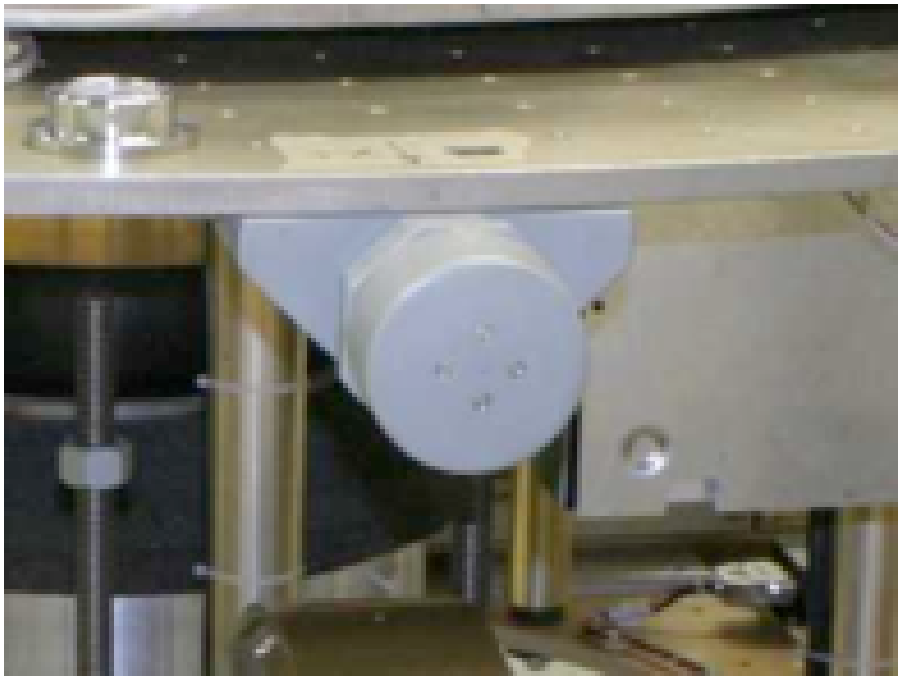

Figure 17. Sun sensor (IR)

F. STAR SENSORS

A "pseudo" star sensor (Figure 18) was implemented in a previous thesis [Ref. 12] by using an attitude sensor based on a laser (Figure 19) and position sensing device (PSD) capable of an accuracy down to 10 μrad. The PSD chosen was a position sensing module (PSM) by ON-TRAK Photonics, Inc. A 20mm sensor, the PSM is capable of discriminating 4.883×10^{-6} meters.

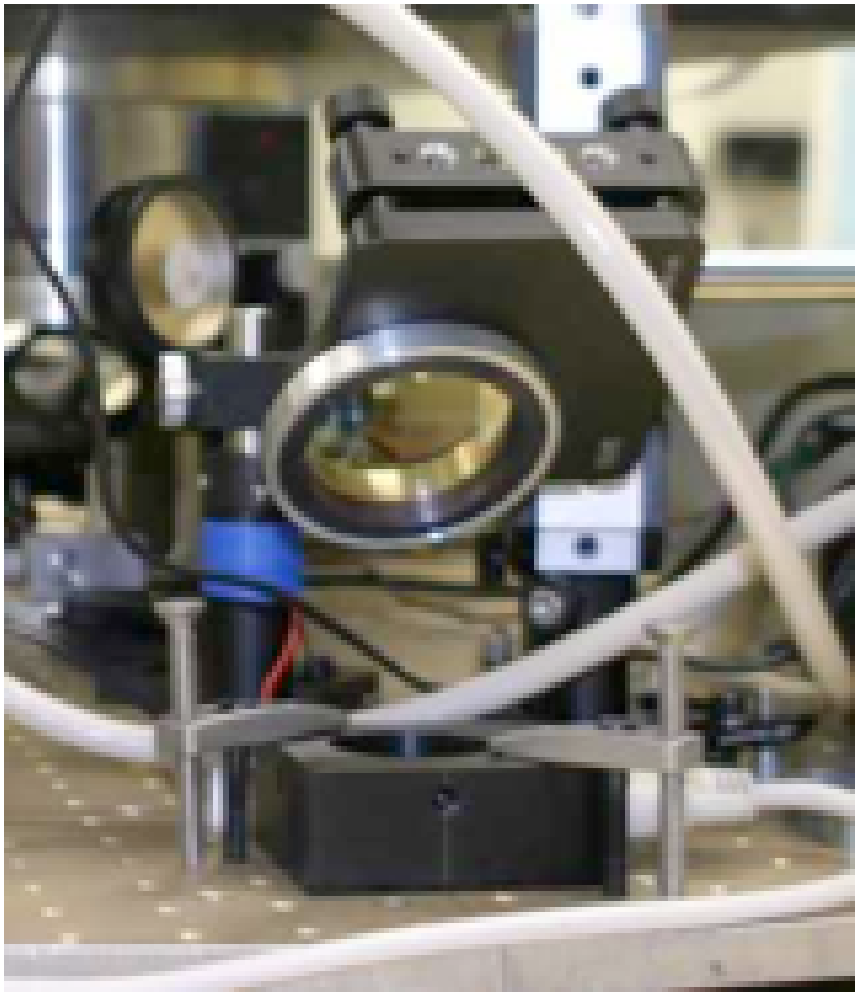

Figure 18. Fine position (Star) sensor

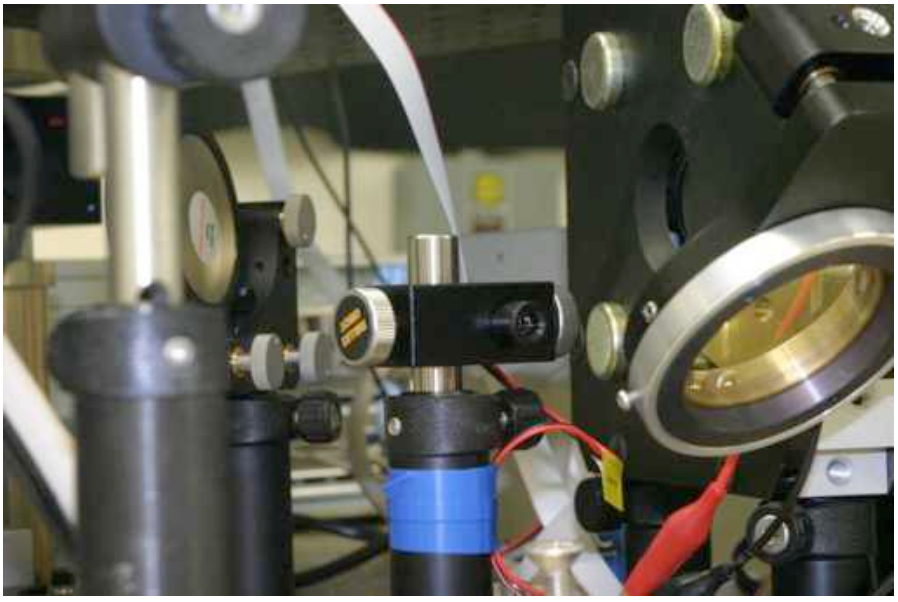

Figure 19. Star sensor laser

The star sensor uses a laser mounted on the TASS, transmitted through the star sensor beam splitter to a mirror (Figure 20) mounted on the lab wall (one for the +X axis and one for the –Z axis). The beam is reflected back to the star sensor beam splitter where is then directed downward to the PSM. Any deviation in the TASS attitude will appear as a corresponding deviation of the laser beam on the PSM.

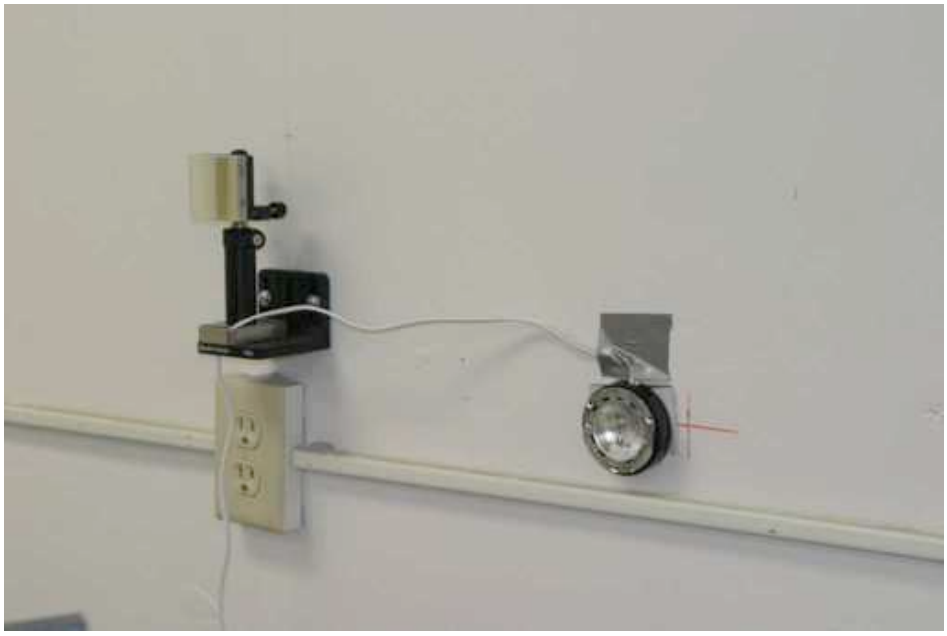

Figure 20. Star sensor inertial mirror

G. INERTIAL MEASUREMENT UNIT (IMU)

The IMU (Figure 21) is a Northrop Grumman (formerly Litton) LN-200 fiber optic gyro (FOG) with silicon accelerometers. Spin-up time is a minimum of 0.8 sec with maximum accuracy being achieved after 5 sec. Bias variation is a maximum of 0.35 deg/hr with repeatability of 1 deg/hr to 10 deg/hr (1 sigma).

Figure 21. IMU

H. MAGNETOMETER

A Billingsley Magnetics TFM100-G2 three axis magnetometer (Figure 22) is used on the TASS. While the outputs can be noisy, operating it in a differential mode with an additional magnetometer could prove to provide a very accurate "north" for the pitch (Y) axis.

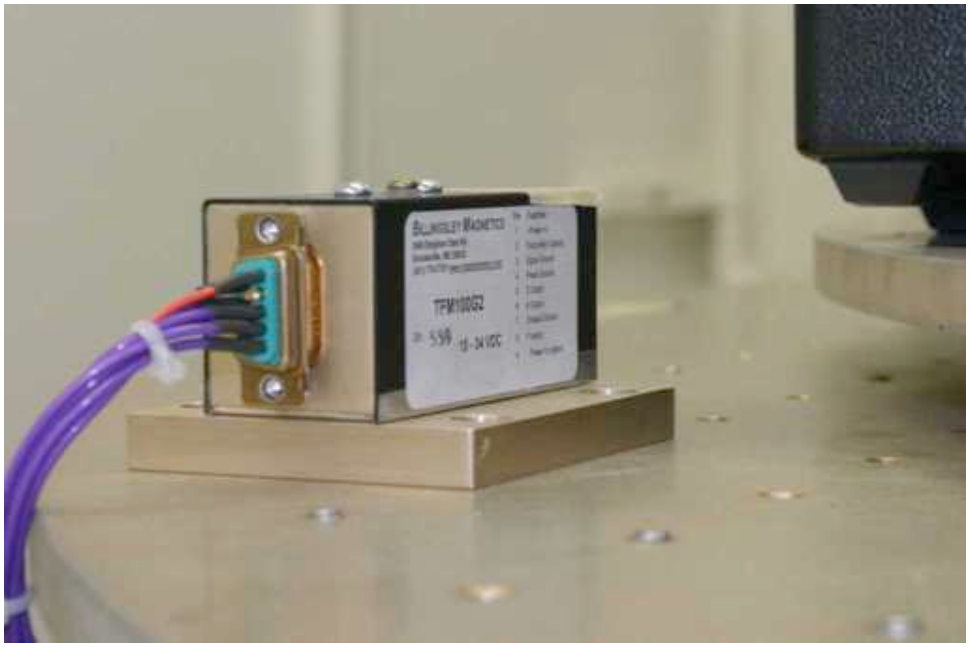

Figure 22. Magnetometer

Added difficulty in incorporating the Magnetometer arises in calibration. Completely removing surrounding ferrous material is impossible. The lab structure (walls, ceiling), TASS hardware (equipment, wiring) and other stray magnetic fields will make calibration difficult.

I. INCLINOMETERS

Angles measured to the horizontal inertial axes are done with two Rieker N3 inclinometers. Full measuring range of ±30°, they have a resolution of <.005°. The stated maximum non-linearity is <0.2% of the measured value implying a max non-linearity of <0.06°. Response time is stated to be <.3 sec which might have an influence on controllability.

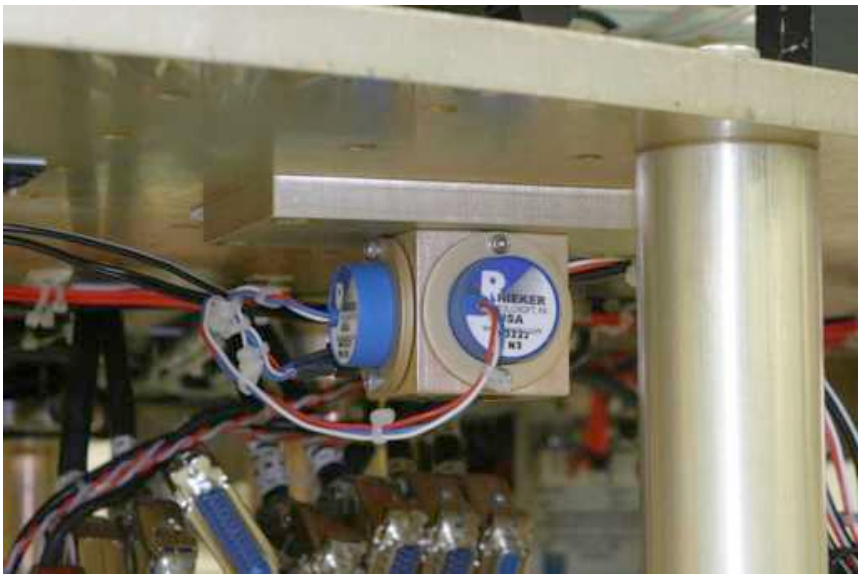

Figure 23. Inclinometer

Early on in development while measuring inclinometer signals in the X axis, a noted non-linearity was observed as can be seen in Table 1. Though not exhaustive data, it appears a non-linearity greater than the manufacturer's stated 0.2%. AECI plans on upgrading controller electronics to remove circuitry that was added to increase the sensor's

signal to noise (SNR) ratio. When in operation, the circuitry was noted to produce unwanted distortions in the sensor signal.

Actual Angle	Recorded Angle	Bias	%
0°	0.86°	+0.86°	--
-3.48°	-3.08°	+0.40°	11%
-7.18°	-6.63°	+0.55°	7.7%
-12.38°	-11.76°	0.62°	5%

Table 1. Inclinometer non-linearity

J. INDUSTRIAL EMBEDDED COMPUTER

The IEC is a PC-104 format computer based on the Intel Pentium III running at 750Mhz and running Matlab xPC onboard. The IEC utilizes two cards, a Diamond MM32-AT and Diamond Ruby MM8 for monitoring analog sensor inputs and communicating with the PSE assembly via a RS-232 interface.

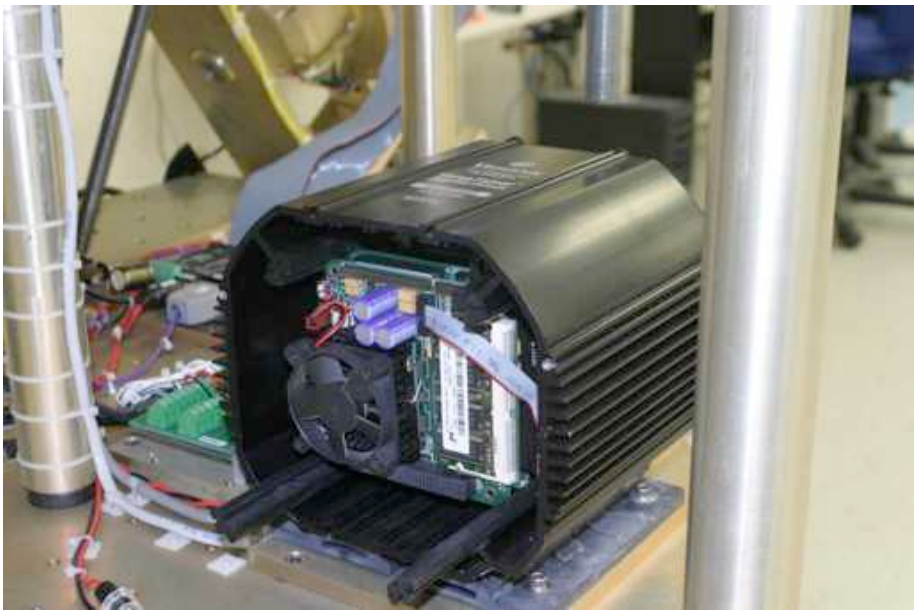

Figure 24. Industrial Embedded Computer (IEC)

K. MASS BALANCING SYSTEM

The mass balancing subsystem (Figure 25) is composed of three proof masses (cylindrical 10.89 Kg masses), three linear actuators with linear position encoders and leveling mass interfaces. All linear actuators are identical except the vertical axis which is equipped with an actuator brake to prevent mass movement in the vertical direction due to gravity.

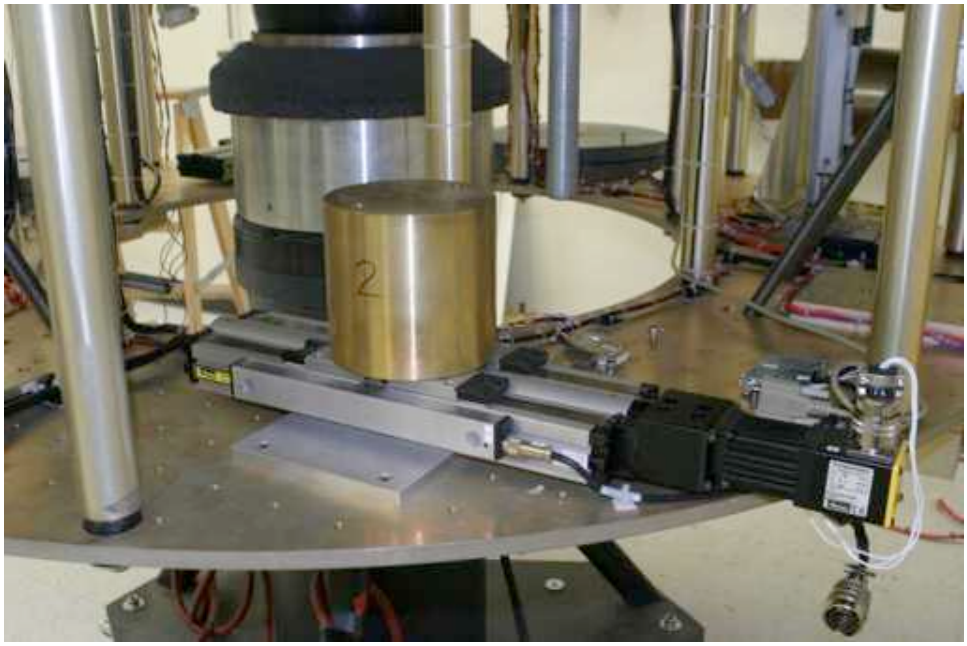

Figure 25. Mass balancer

1. Linear Actuators

The linear actuators are 404XR Series standard precision Parker-Hannifin Daedal leadscrew tables capable of 150mm of travel with an accuracy of 18µm and bidirectional repeatability of ±5µm. Maximum acceleration is rated at 20m/sec^2.

2. Linear Encoder

The linear encoder converts linear position into a digital output. The encoder has a positional accuracy of ±3 microns and a resolution that is dependent on selected speed of the actuator as shown in Table 2.

Actuator Speed	Encoder Resolution
3.0 m/sec	1.0 micron
1.5 m/sec	0.5 micron
0.3 m/sec	0.1 micron

Table 2. Linear Encoder Resolution

Home repeatability is based on encoder resolution with repeatability ±2 counts times the encoder resolution with best case being 1 micron. Home repeatability is shown in Table 3.

Encoder Resolution	Home Repeatability
1.0 micron	±2 microns
0.5 micron	±1 micron
0.1 micron	± micron

Table 3. Home Repeatbility Accuracy

3. Leveling Mass Interface (LMI)

The interface (Figure 26) converts serial inputs into commands to control the linear actuator it is attached to. The interface can save the last “home” position to non-volatile memory (NVRAM) so, when powered up, the controller can seek the last saved position. A command is provided to automatically center the actuator and set it as “home”.

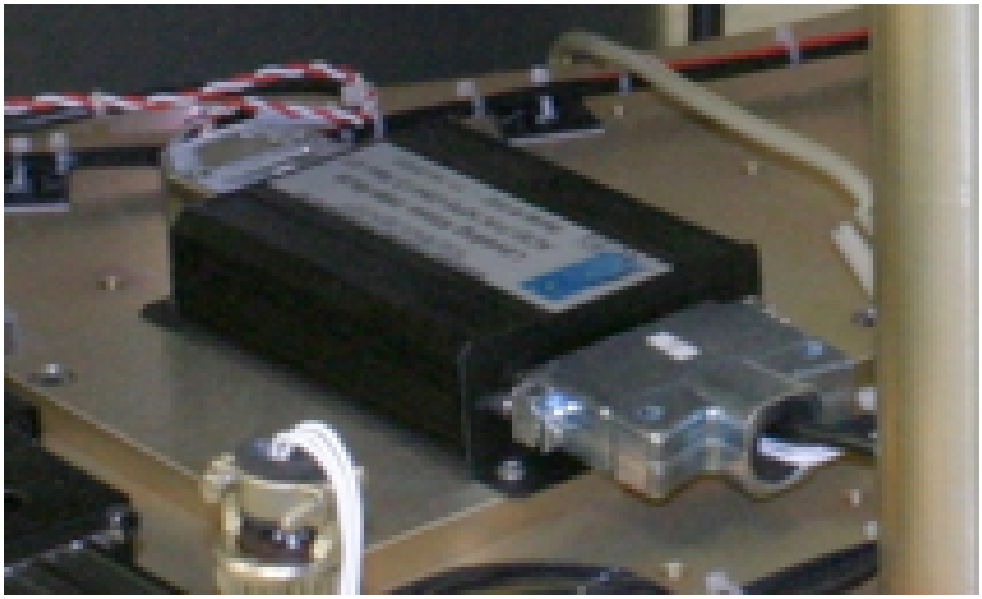

Figure 26. Leveling mass interface (LMI)

The LMI accepts bitwise commands as an unsigned 8 bit integer with bits performing commands in Table 4.

Bit	Mode CMD	Description
0	Enable	1-motor on; 0-motor off
1	Save	0 to 1 transition sets new home position
2	Brake	1-brake on; 0-brake off (normally not used)
3	Center	Seeks center of travel and sets home 1-active; 0-inactive
4	Home	Seeks saved home pos: 1-active; 0-inactive
5	NULL	
6	NULL	
7	NULL	

Table 4. Balance LMI commands

Actual position commands are issued as a signed 16 bit integer. The command is converted into a delta position

(+/-) from the saved home position. The decimal value of 32768 indicates a delta of zero while decimal zero is a maximum negative delta position and decimal 65536 is a maximum positive delta position. The scale factor is 1916.3 counts/cm. The balancer table has a maximum travel of 15cm, so the maximum position command in counts that can be issues is 61512 for a maximum positive delta and 4023 for a maximum negative delta position.

4. Failures/Troubleshooting

During initial operations, it was noted that on TASS powerup, #2 mass balancer would move and position the balance mass to an off-center position. Two reasons this was abnormal: the power switch on the switchbox for the mass balancers was off and previous simulations had set the NVRAM home position at the center. The mass was not only moving with the power switch off, but moving to a non-stored position. The balance controllers are currently back with the manufacturer undergoing modifications.

L. VIDEO SYSTEM

The video system is composed of two Dalsa cameras for differentiating targeting and tracking laser beams. Identical camera, one is affixed with a red filter, the other with a green filter as shown in Figure 27. One of the other two camera used for field of view determination can be seen as well.

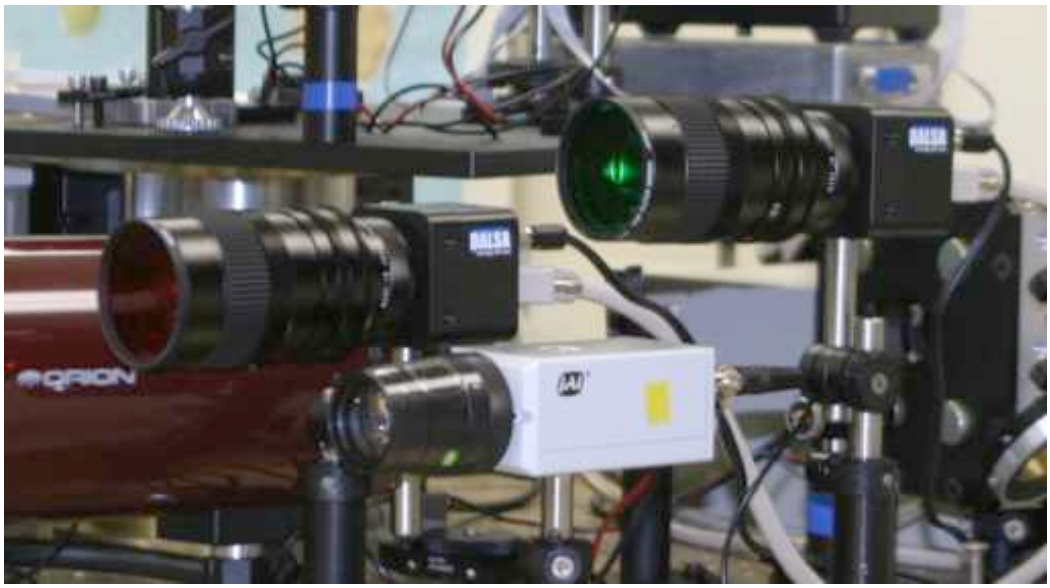

Figure 27. Video camera

M. OPTICS

The optics payload was supplied by AFRL. The optics consist of two 102mm diameter Orion Maksutov-Cassegrain telescopes with a 1300mm focal length, two Baker Adaptive Optics fast steering mirrors (FSM) (Figure 28) for jitter control and beam positioning and various optics train components for beam routing and alignment. The payload can be seen in Figure 29.

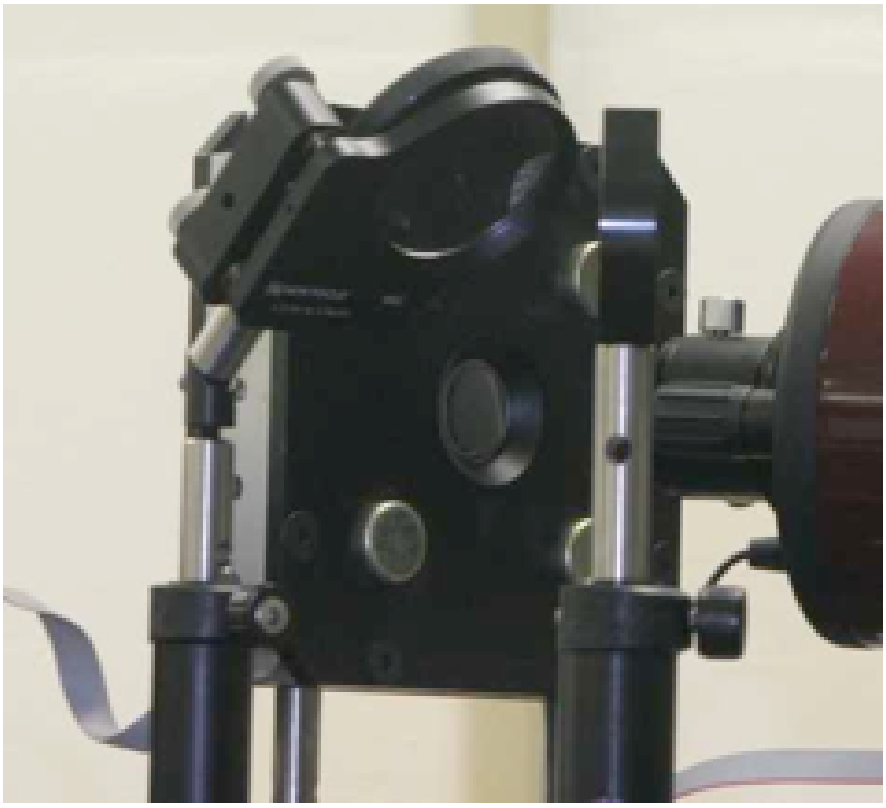

Figure 28. Fast Steering Mirror (FSM)

Figure 29. BFRM payload

N. OPTICS CONTROL

The payload optics program and control is provided by two personal computers (PCs) seen in Figure 29. Provided by AFRL, these computers run the software for calibration, testing and operational tracking. FSM and Jitter PSD controllers are shown in Figure 30.

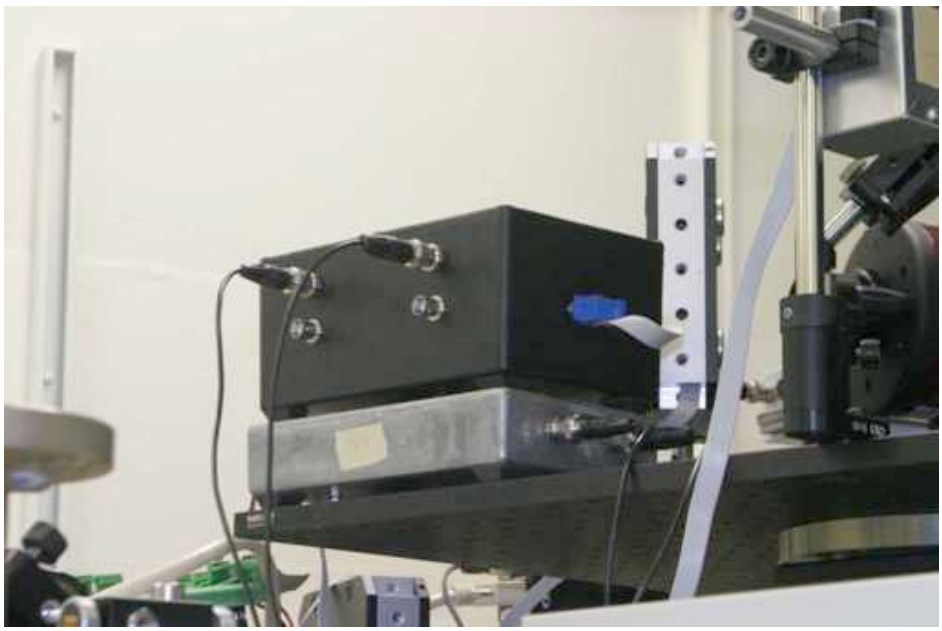

Figure 30. FSM Controller (top), PSD Controller (bot)

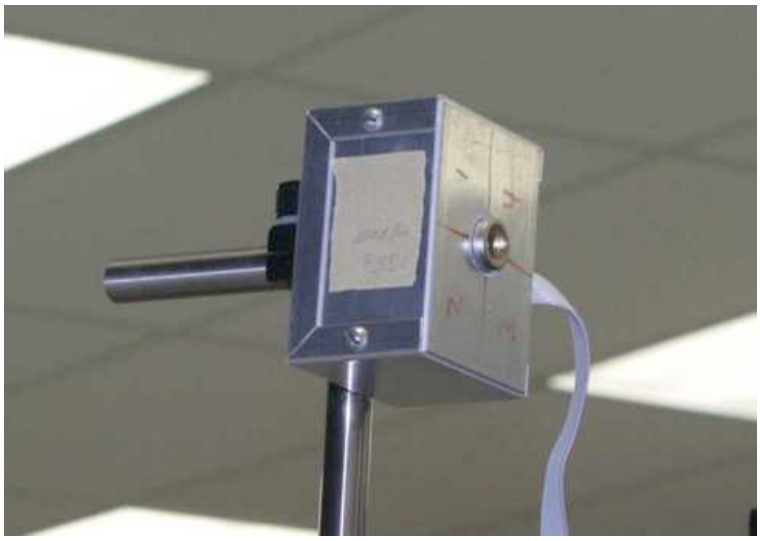

Figure 31. Jitter PSD

The upper optics deck that supports the receive telescope, jitter elimination equipment and controllers is motorized with one DOF with respect to the vertical body axis. it is controlled via a table drive motor shown in Figure 32.

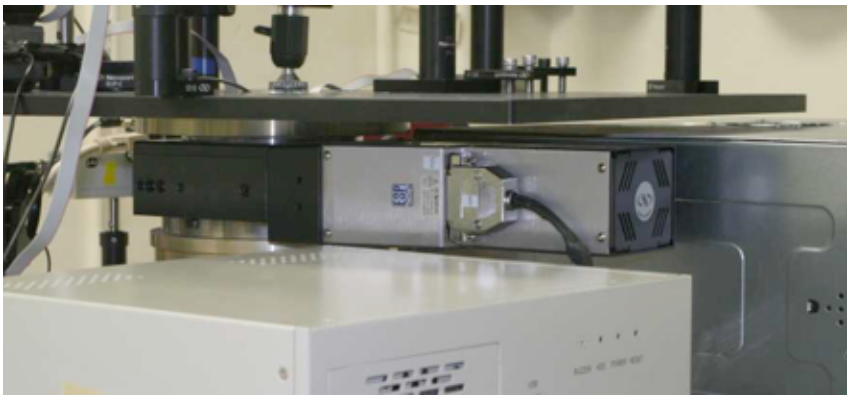

Figure 32. Optical deck motorized drive

O. MASS PROPERTIES

1. Background

The initial mass properties, as delivered by GDC, were specified and provided in the form of a Microsoft Excel spreadsheet. The initial mass properties were specified using the GDC assumed coordinate system and had to be transformed to the body coordinate system in use. As development progressed and new equipment was added to the simulator, it was necessary to update the spreadsheet with the new equipment data. Where practicable, equipment was weighed. If not, geometry, density and material were used for equipment mass property.

2. Moments of Inertia and Principal Axes

The principal axes coincide with the body axes for purposes of my simulations. The total inertia dyadic of the platform is the sum of the inertia for the rigid body platform plus the parallel axis inertia contribution from

each of the CMGs since the moment of inertia (MOI) for each CMG is not constant with respect to time in the body reference frame. This inertia dyadic can be shown by Equation 1:

$$\vec{I} = \vec{I}_B + \sum_{j=1}^{3} m_j \left(\left[r_j\right]^T \left[r_j\right]\left[1\right] - \left[r_j\right]\left[r_j\right]^T \right)$$

Equation 1. Inertia dyadic

Where $\left[1\right]$ is a 3x3 identity matrix, $\left[r_j\right]$ is the mass center position of the j^{th} CMG and m_j is the mass of the individual CMG.

The inertia of the body was calculated based on scaling the original MOI from GDC for the mass changes made to the platform. There is ongoing effort in progress to develop an accurate MOI for the platform from detailed mass and measurements of the equipment changes. MOI can also be compared from inertial parameter measurements during operation to validate the spreadsheet calculation of the platform MOI.

The spreadsheet as updated for equipment currently installed shows a total TASS2 mass of 652.8 Kg. This differs from the weighed (using a strain meter) mass of 624 Kg. An estimated mass can be calculated once fully operational using attitude measurements.

The MOI matrix calculated by the spreadsheet shows a MOI of:

$$I_S = M \begin{bmatrix} 262.1 & -56.5 & 4.09 \\ -56.5 & 373.7 & 52.4 \\ 4.09 & 52.4 & 270.3 \end{bmatrix} \times 10^{-3}$$

Equation 2. TASS2 inertia matrix

I_{XX} and I_{ZZ} are very close to the same value which shows near symmetry about both the X and Z axes. The actual principal axes can be found based on spreadsheet values or more accurately by experimental determination.

THIS PAGE INTENTIONALLY LEFT BLANK

III. SOFTWARE DEVELOPMENT

Software development was carried out primarily within Mathworks Matlab and Simulink programs. Simulation was performed first when practicable followed by experimentation to validate simulation results.

A. REAL-TIME WORKSHOP AND XPC TARGET INTEGRATION

Real-Time Workshop and xPc Target modules in Matlab and Simulink were used to interface the simulink control program with the onboard IEC. Real-Time Workshop generates the stand alone C code to run on the IEC. XPc Target allows a real-time connection to the IEC for control and provides IEC specific blocks for control and signal processing.

Development was done primarily in Simulink with some Matlab M files written for initialization code. Following modifications to the Simulink program, the program was then compiled under Real-Time Workshop and uploaded to the IEC. Once uploaded to the onboard IEC, the program was executed. With xPc Target, the capability exists to connect to the running program on the target (IEC) from the host (desktop PC where development is done) and dynamically update parameters, observe signals and interact real-time with the executing program.

THIS PAGE INTENTIONALLY LEFT BLANK

IV. CMG CONTROL ANALYSIS

A. BACKGROUND

CMGs are momentum devices. Angular momentum of the CMG is aligned with the spinning rotor axis. Equation 3 defines angular momentum for the CMG.

$$h_{CMG} = I_{CMG}\omega_r$$

Equation 3. General CMG angular momentum

In a single gimbal configuration, a rate of change in the gimbal angle, δ produces torque according to the relationship in Equation 4 and shown graphically in Figure 33.

$$\tau_{CMG} = h_{CMG} \times \dot{\delta}$$

Equation 4. CMG torque

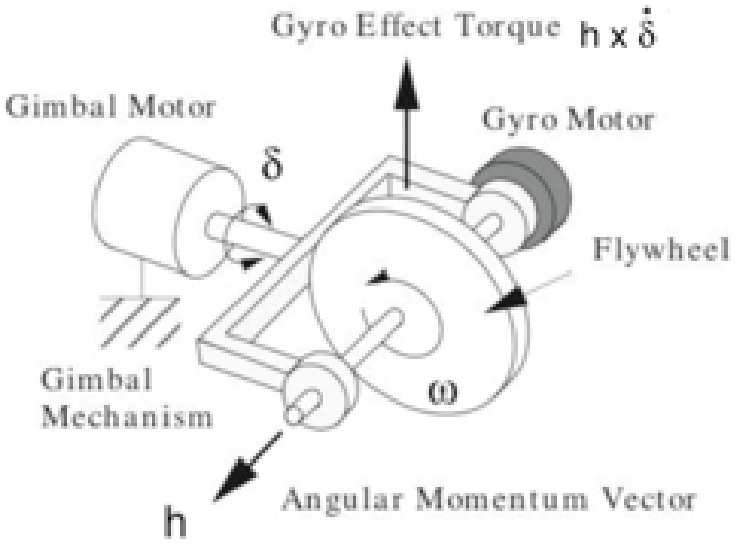

Figure 33. CMG torque

The above equations help determine the sizing of the CMGs as well. For our TASS, we used the max rotor speed and thus the max angular momentum. The maximum torque is then limited by the maximum gimbal rate. The CMG steering law block (written by MAJ Timothy Sands, USAF) has a saturation limit of $\pi \frac{rad}{s}$ imposed on $\dot{\delta}$. This limits the maximum torque from any single CMG to:

$$\tau_{CMG} = h_{CMG} \times \dot{\delta} = 24.4\ Nms \cdot \pi \frac{rad}{s} = 76.7\ Nm$$

Equation 5. CMG torque output

The maximum torque of the three CMG arrangement is therefore $3 \times 76.7\ Nm = 230.1\ Nm$.

The total angular momentum of the TASS, represented by H_s is the sum of the angular momentum of the rigid body h_B and the CMGs, $h_{CMG} \Rightarrow$

$$H_S = h_B + h_{CMG}$$

Equation 6. System angular momentum

Since $h_B = I_B \omega_B$:

$$H_S = I_B \omega_B + h_{CMG}$$

Equation 7. System H, function of *I*, ω

The rotational equation of motion (EOM) is given by:

$$\dot{H}_S + \omega_B \times H_S = \tau_{EXT}$$

Equation 8. Rotational EOM

Substituting,

$$\left(I_B\dot{\omega}_B + \dot{h}_{CMG}\right) + \omega_B \times \left(I_B\omega_B + h_{CMG}\right) = \tau_{EXT}$$

Equation 9. Expanded rotational EOM

Similarly, CMG torque can be defined as:

$$\dot{h}_{CMG} + \omega_B \times h_{CMG} = \tau_{CMG}$$

Equation 10. CMG torque

Since τ_{CMG} is the control torque, we can represent it as $-\boldsymbol{u}$ (I use negative to simplify math and keep the convention used in Wie) and adding it to both sides result in:

$$I_B\dot{\omega}_B + \omega_B \times I_B\omega_B = \tau_{EXT} + \boldsymbol{u}$$

and

$$\dot{h}_{CMG} = -\boldsymbol{u} - \omega_{CMG} \times h_{CMG}$$

This is the form of control torque used as the input to the steering logic block in the simulation.

B. CMG STEERING LAW

The CMGs are configured in a modified pyramid configuration. The traditional pyramid configuration and would be Figure 34 including the null fourth CMG.

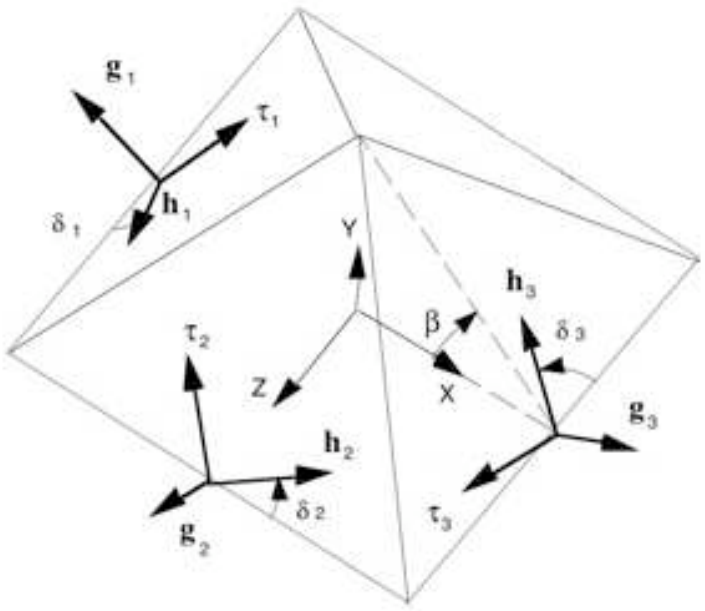

Figure 34. Pyramid CMG configuration [Ref. 5]

The exception with the TASS is the gimbal axes are not perpendicular to the pyramid faces as in Figure 34 but lie parallel an in the face. The operation is similar since the gimbal axis **g**, angular momentum axis **h** and torque axis τ are orthogonal. This results in a skew angle, β, of –35.25°.

Though not developed by the author, the CMG steering law follows the relationship where the CMG angular momentum, ***h*** and torque τ vectors lie in the plane of their respective CMG rotor and perpendicular to the side of the tetrahedron they occupy. The maximum range determined by a circle based on the maximum angular momentum and maximum torque developed by each CMG. This relationship can be seen in Figure 35 rotated 90° to coincide with our configuration. Future configurations of the CMGs might likely be a box configuration (with gimbal axes parallel to the lower equipment ring) allowing a simple setting of β = -

90° allowing simpler calculations, or an inverted pyramid configuration (top of pyramid aligned along the –Y axis) and a β = 35.25°.

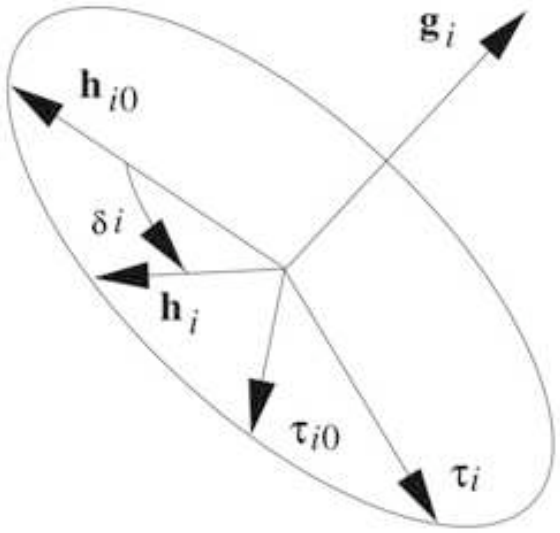

Figure 35. CMG angular momentum, torque plane [Ref. 5]

The steering law follows the relationship in Bong Wie [Ref. 7], where $\boldsymbol{h}_{\text{CMG}}$ is a function of the gimbal angle $\Rightarrow h_{CMG} = h(\delta)$. To find gimbal angle trajectories to generate the commanded $\boldsymbol{h}$ trajectory, we have to find a matrix $[A(\delta)]$ that is a function of the gimbal angle, δ, such that:

$$\dot{h}_{CMG} = [A(\delta)]\dot{\delta}$$

$[A]$ is a 3x3 Jacobian matrix that maps the gimbal rates to torque such that $\dot{h}_{CMG} = [A]\dot{\delta}$

$$\Rightarrow \begin{bmatrix} a_1 & a_2 & a_3 \end{bmatrix} \begin{bmatrix} \dot{\delta}_1 \\ \dot{\delta}_2 \\ \dot{\delta}_3 \end{bmatrix} = \sum_{i=1}^{3} a_i \dot{\delta}_i$$

The required gimbal rates are then solved for by solving $\dot{h}_{CMG} = [A]\dot{\delta}$ for $\dot{\delta}$:

$$[A]^{+}\dot{h}_{CMG} = \dot{\delta}$$

Equation 11. Steering law gimbal rates

Since $[A]$ is singular, a direct inverse cannot be taken. We use Matlab's Pinv() command to take the Moore-Penrose pseudo-inverse in the steering block.

Bong Wie outlines the steering logic for a four CMG pyramid configuration as [Ref. 7]:

$$h_{CMG} = \sum_{i=1}^{4} h_i(\delta_i)$$

$$= \begin{bmatrix} -c\beta \sin\delta_1 \\ \cos\delta_1 \\ s\beta \sin\delta_1 \end{bmatrix} + \begin{bmatrix} -\cos\delta_2 \\ c\beta \sin\delta_2 \\ s\beta \sin\delta_2 \end{bmatrix} + \begin{bmatrix} c\beta \sin\delta_3 \\ -\cos\delta_3 \\ s\beta \sin\delta_3 \end{bmatrix} + \begin{bmatrix} \cos\delta_4 \\ c\beta \sin\delta_4 \\ s\beta \sin\delta_4 \end{bmatrix}$$

For the TASS configuration, there is no CMG#4, so this term is left off. Add to that, our $\beta = 54.75° - 90° = -35.25°$, then the TASS equation is:

$$h_{CMG} = \sum_{i=1}^{3} h_i(\delta_i)$$

$$= \begin{bmatrix} -.817 \sin\delta_1 \\ \cos\delta_1 \\ .577 \sin\delta_1 \end{bmatrix} + \begin{bmatrix} -\cos\delta_2 \\ .817 \sin\delta_2 \\ .577 \sin\delta_2 \end{bmatrix} + \begin{bmatrix} .817 \sin\delta_3 \\ -\cos\delta_3 \\ .577 \sin\delta_3 \end{bmatrix}$$

Equation 12. Individual CMG angular momentum

$$[\mathrm{A}] = \begin{bmatrix} -.817\sin\delta_1 \\ \cos\delta_1 \\ .577\sin\delta_1 \end{bmatrix} + \begin{bmatrix} -\cos\delta_2 \\ .817\sin\delta_2 \\ .577\sin\delta_2 \end{bmatrix} + \begin{bmatrix} .817\sin\delta_3 \\ -\cos\delta_3 \\ .577\sin\delta_3 \end{bmatrix}$$

Equation 13. [A] matrix

Where $\dot{\delta}$ represents the gimbal angle rate and $C^T\left(CC^T\right)^{-1}$ the pseudo-inverse of *C*. Thus Equation 11 can be reduced to Equation 14 where ***k*** represents an arbitrary vector of n elements.

$$\dot{\delta} = \begin{bmatrix} -.817\sin\delta_1 & -\cos\delta_2 & .817\sin\delta_3 \\ \cos\delta_1 & .817\sin\delta_2 & -\cos\delta_3 \\ .577\sin\delta_1 & .577\sin\delta_2 & .577\sin\delta_3 \end{bmatrix}^{+} \dot{h}_{CMG}$$

Equation 14. TASS2 CMG steering law

The pseudo-inverse is commonly represented by the notation $[A]^{+} = [A]^{T}\left([A][A]^{T}\right)^{-1}$ [Ref. 7]. The CMG steering law implemented in Simulink can be seen in Figure 59.

C. CMG CONTROLLER

The CMG controller was simulated using two control methods. First a PID controller was implemented based on Euler angle errors. Difficulty was encountered in getting the simulation stable and adjusting the gains so a different feedback method was attempted. The second method was based on quaternion error feedback control. There were a few advantages to pursuing this method.

TASS1, a reaction wheel (RW) based simulator was controlling using quaternion error feedback, Dr. Kim (thesis co-advisor/second reader) had already developed a

controller and the Extended Kalman Filter (EKF) for TASS1 and quaternion feedback was free of singularities. Not that our testbed would pass through any region of singularity, but quaternion feedback allowed us the freedom to ignore singularities.

The quaternion controller can be seen in Figure 65. Since quaternion attitude control was already being performed, it was a trivial task to extract the current attitude quaternion q_a and calculate the target or desired quaternion q_t. Unlike error determination in a typical controller, subtraction of the actual attitude from the desired attitude can not be done with quaternions. Quaternion error is calculated by multiplication, such that the quaternion error is calculated by [Ref. 7,11]:

$$q_e = q_a \cdot q_t$$

Equation 15. Quaternion error

The output of the quaternion feedback controller was commanded torque. This was sent to the CMG steering block for CMG gimbal angle commands.

D. SINGULARITY AVOIDANCE

In any CMG steering law, singularities can be expected. Each CMG geometrical configuration has its advantages, but inevitably must plan to avoid singular regions. Singularity avoidance schemes were not implemented in this thesis.

E. CMG SIMULATION ANALYSIS

The controller was implemented in Simulink with some initialization done in Matlab 'M' files. The block diagrams can be seen in Appendix B. For simplification in running

multiple simulations and varying parameters, a graphical interface was created as shown in Figure 36.

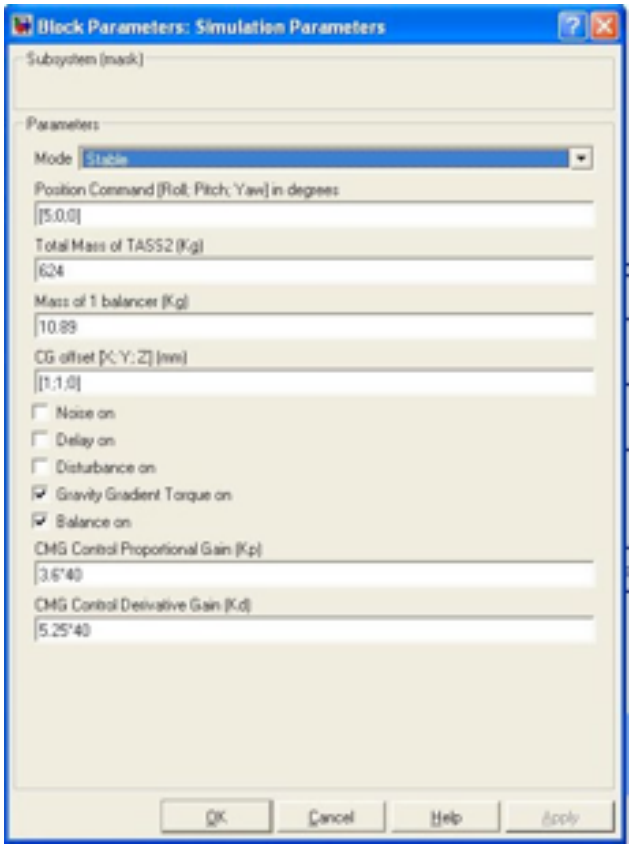

Figure 36. Simulation graphical interface

From this interface it was possible to specify parameters such as CG offset, CMG controller gains, TASS and balancer masses, commanded position for slew maneuvers and mode of operation: stability or position command. Check boxes were also available for selecting noise, delay, disturbance, gravity torque or whether to compensate with the mass balancers.

The noise parameter was based on observed noise from the sensors and added to simulated sensor outputs for CMG gimbal position and measured TASS angular velocity. The

noise was a Gaussian distribution with a variance of 2×10^{-4} rad (.01°) and frequency of 100 hz as shown in Figure 37.

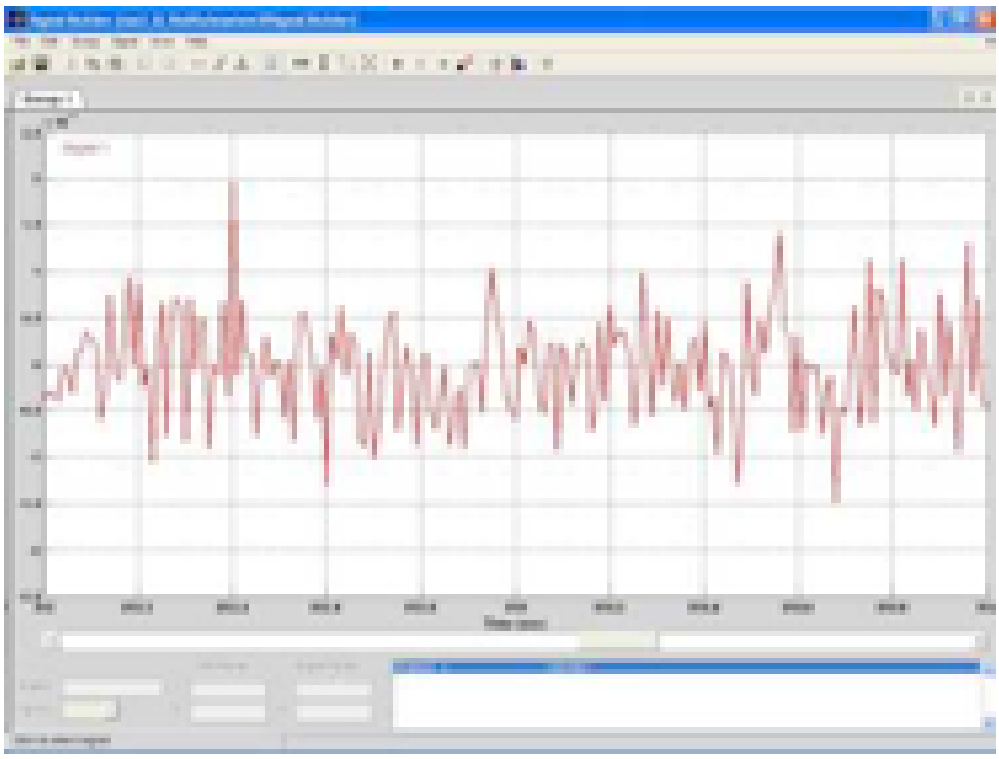

Figure 37. Gaussian noise

Delays used were varied depending on the signal line being delayed. Any delay used was an integer multiple of the sample time. The largest delay used anywhere in the simulation was four times the sample time. Though no actual times were measured from the TASS, due to the wireless connection, delays can be higher than a direct connected control system. Sample time was set at .025 to correspond to a worst case hardware sample frequency of 40 Hz.

The first simulation is an ideal run for comparisons. No noise, delays, disturbances or gravity torque were

introduced. The first was a commanded position slew +5° about the X axis as seen in Figure 38.

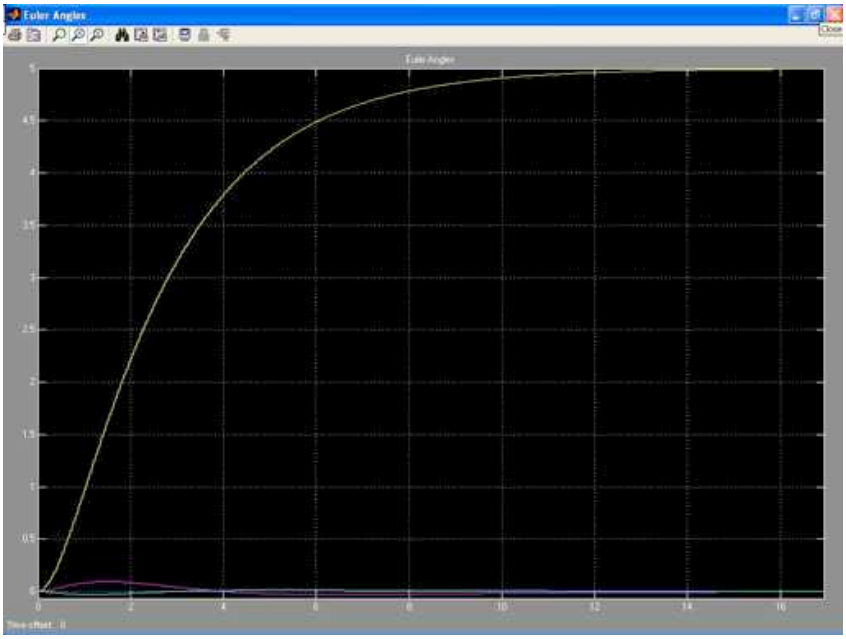

Figure 38. Euler angles, 5 degree slew about +X, ideal

Critically damped, rise time (T_r) can be seen to be 5.25 sec, settling time T_s = 10 sec.

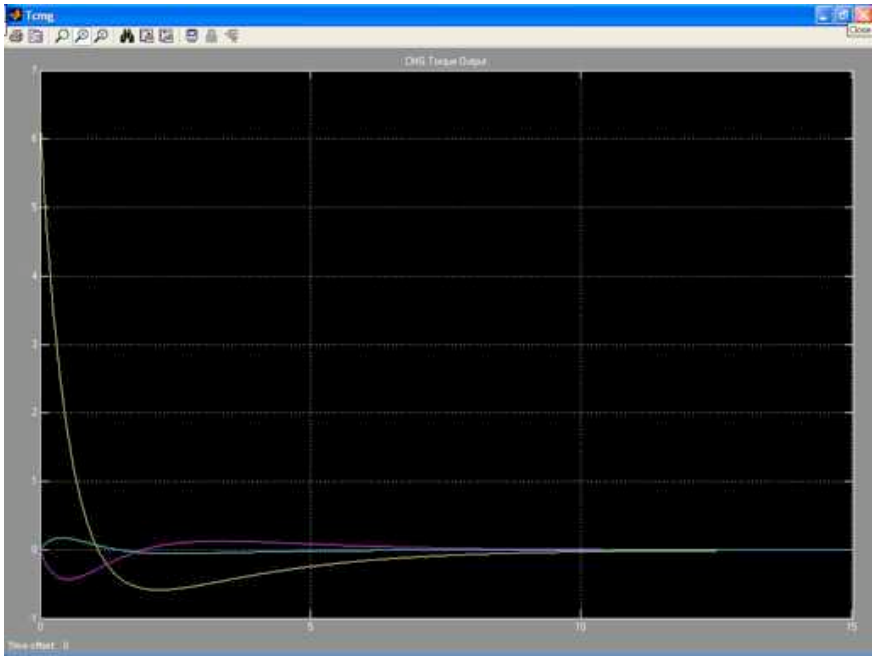

Figure 39. CMG torque, 5° slew in +X, ideal

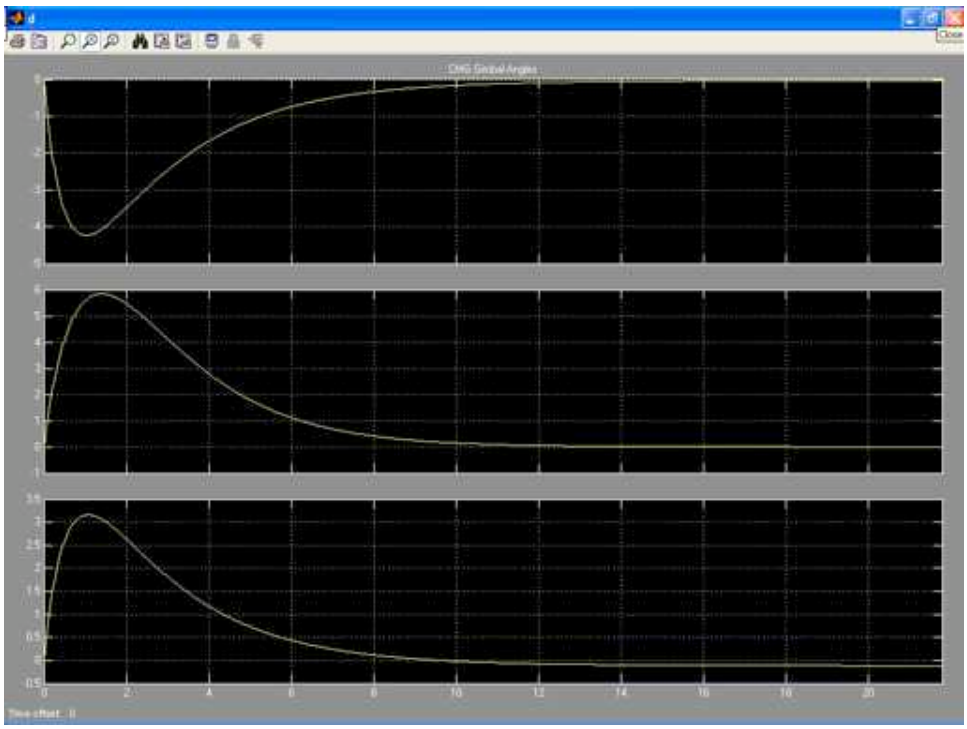

Figure 40. CMG gimbal angles, 5° slew in +X, ideal

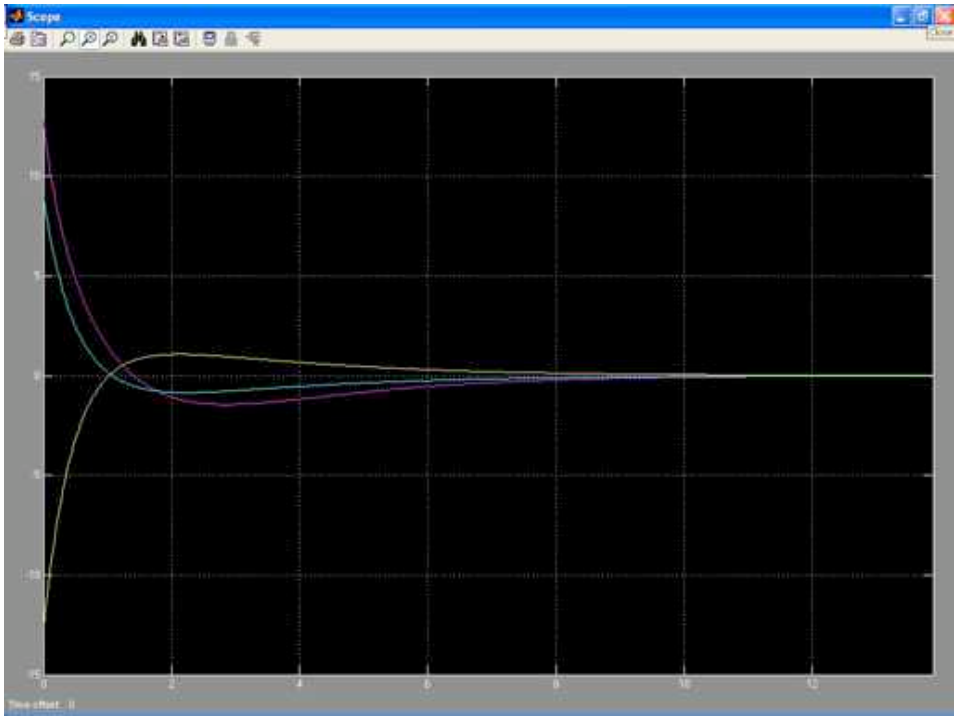

Figure 41. CMG gimbal rates, 5° slew in +X, ideal

Gimbal angles, rates and torque can all be seen to settle by about 14 seconds. To be noted is the fact they do settle to zero. Under ideal conditions with no CG offset, the simulator remains balanced throughout the maneuver eliminating the necessity for the CMGs to produce torque. In an unbalanced condition, not corrected for, the CMGs would have a positive δ as long as the unbalanced situation remained. Eventually, the CMGs would saturate and the simulator would no longer be controllable. Saturation results can be seen in Figure 42, Figure 43, Figure 44 and Figure 45. The 180°/sec limit imposed on gimbal rates can be clearly seen at saturation in Figure 45.

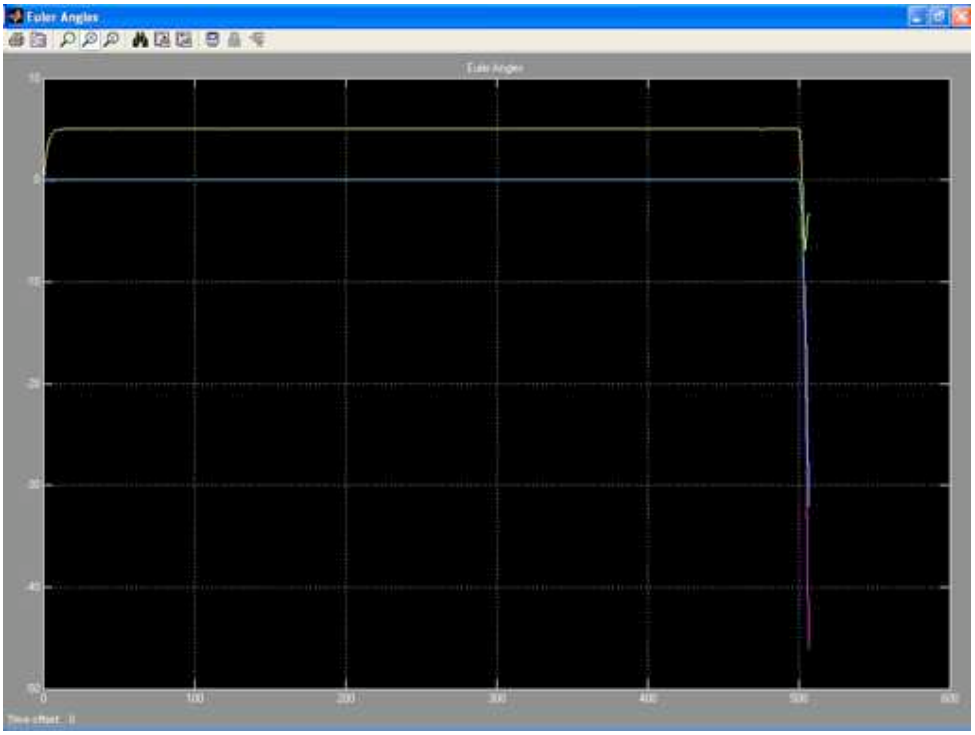

Figure 42. Euler angles, 5° slew, saturated

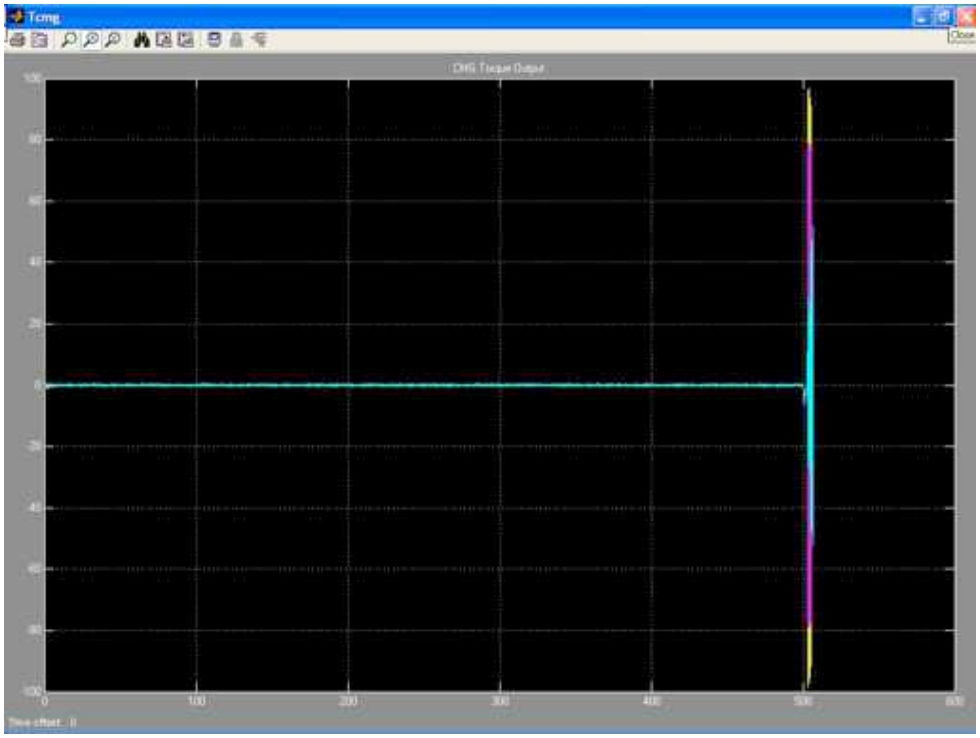

Figure 43. CMG torque, 5° slew, saturated

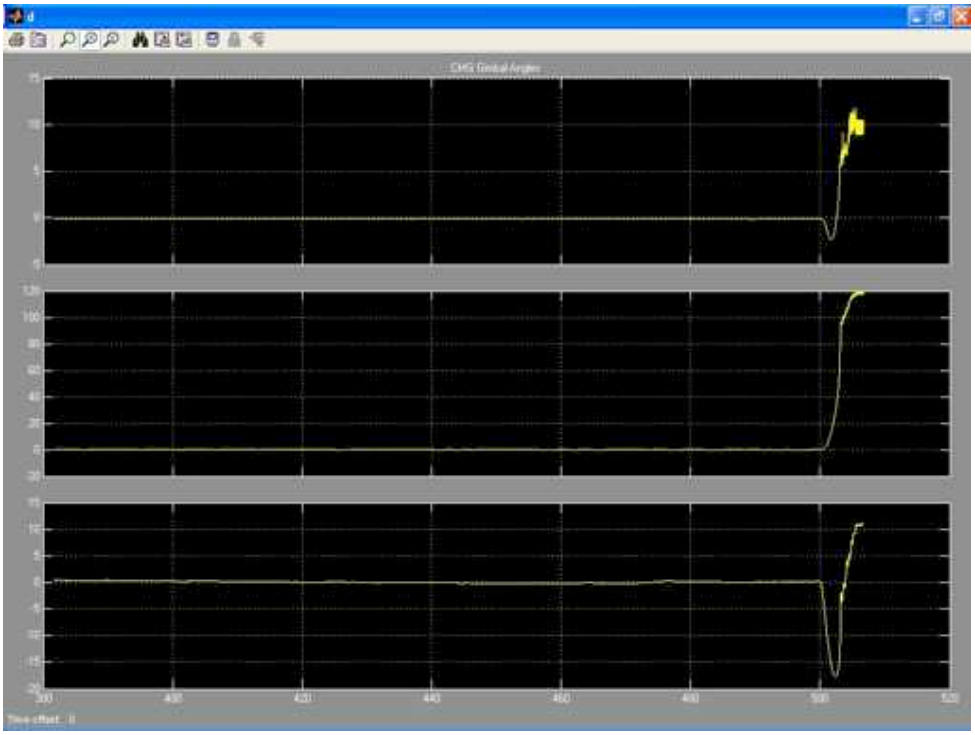

Figure 44. CMG gimbal angle, 5° slew, saturated

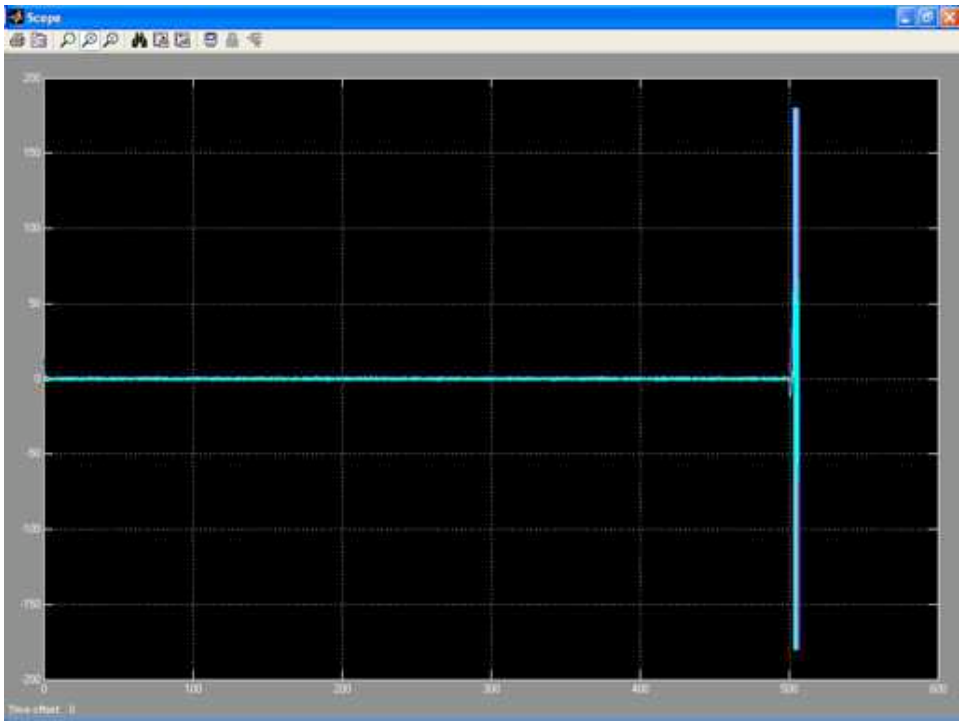

Figure 45. CMG gimbal rates, 5° slew, saturated

THIS PAGE INTENTIONALLY LEFT BLANK

V. MASS BALANCING AND ANALYSIS

A. BACKGROUND

The TASS is required to support the BFRM in such a way as to allow milliradian pointing accuracy. In order to accomplish this, eliminating not only disturbances in the laser beam, but disturbances in the bus. One of the major external disturbances affecting the platform is due to the gravity torque (τ_g) present with any offset in the CG perpendicular to gravity.

With an offset in the CG, the CMGs will be commanded in such a way as to counter this τ_g and maintain the commanded attitude. CMG gimbal position will be commanded to produce the required torque. Any motion of the CMGs will introduce vibration and unwanted disturbances into the bus that would need to be eliminated at some point in the optical path.

By actuating the three masses on the platform in such a way so as to return the CG back to the CR (or a vertical line passing through this point) would eliminate any torque requirement from the CMGs to maintain a desired attitude. A reduction in torque output would have a corresponding reduction in disturbances and an increase in pointing accuracy.

B. DERIVATION OF EQUATIONS

For reference during derivation, Figure 46 shows graphically the entities involved and their relative positions.

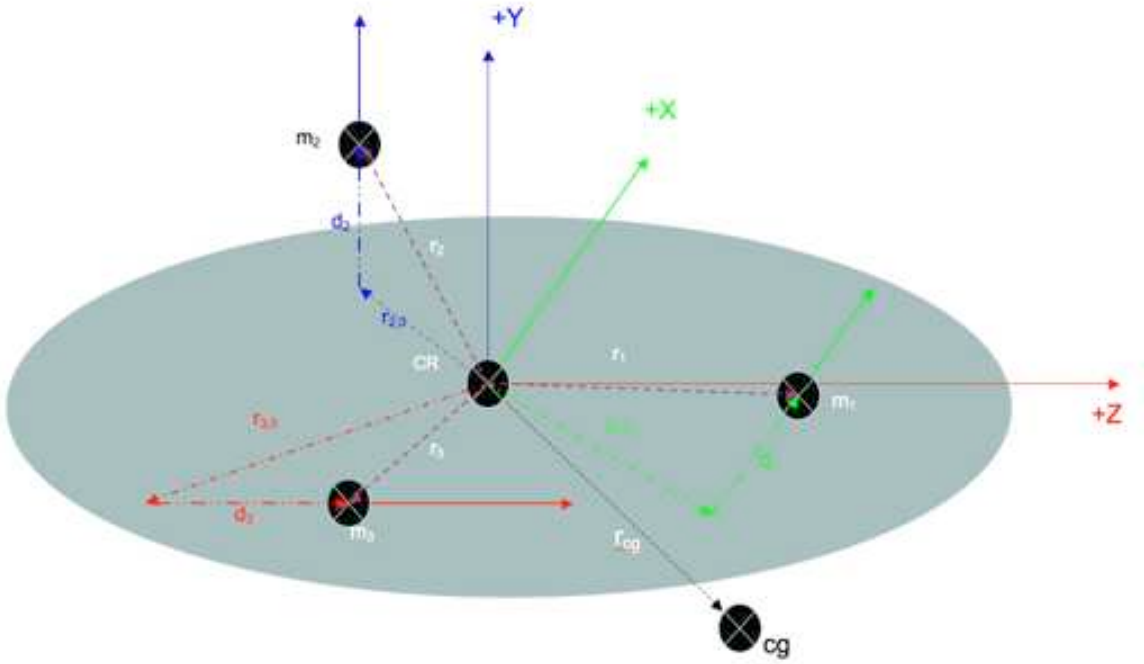

Figure 46. Mass Coordinate System

r_i represents the position of any of the balance masses m_i. $r_{i,0}$ is the starting position of mass m_i. r_{CG} is the position vector for the center of gravity offset. s_i is a representative unit vector along the path of the balance mass. d_i is the distance traveled for any mass m_i.

The torque, τ, on the center of gravity, due to gravity is designated by τ_{cg}. τ_{cg} follows the relationship shown in Equation 16, where $\vec{F} = M\vec{g}$ and M is the mass of the platform minus the balance masses [Ref. 1,2].

$$\vec{\tau}_{cg} = \vec{r}_{CG} \times \vec{F}$$

Equation 16. General torque

$$\vec{\tau}_{cg} = \vec{r}_{CG} \times M\vec{g}$$

Equation 17. Torque as a function of gravity

Accounting for the gravity torque contribution due to the balance masses is done in the same manner with each of the masses and its associated position vector shown in Equation 18.

$$\vec{\tau}_b = \vec{r}_i \times m_i\vec{g}$$

Equation 18. Single balance mass torque

Equation 18 represents the contribution on one balance mass. The contribution of all three balance masses is simply the summation of the three individual mass components as in

$$\vec{\tau}_b = \sum_{i=1}^{3} \vec{r}_i \times m_i\vec{g}$$

Equation 19. Total balance mass torque

The total gravity torque, $\vec{\tau}_g$, is the sum of the two torques:

$$\vec{\tau}_g = \vec{\tau}_{cg} + \vec{\tau}_b \Rightarrow \vec{\tau}_{gg} = \vec{r}_{CG} \times M\vec{g} + \sum_{i=1}^{3} \vec{r}_i \times m_i\vec{g}$$

Equation 20. Gravity torque

As can be seen in Figure 46, r_i is the sum of the components $\vec{r}_{i,0}$ and $\vec{d}_i$:

$$\vec{r}_i = \vec{r}_{i,0} + \vec{d}_i$$

Equation 21. Mass position vector

Since position commands for the balance mass controllers will be issued in terms of body coordinates, it will be advantageous to represent the above equations in terms of the body reference frame. All terms in the above equations are already specified in terms of the body

reference frame with the exception of gravity $\vec{g}$ which is expressed in the inertial reference frame as ${}^{N}\vec{g}$. To convert ${}^{N}\vec{g}$ to the body reference frame, a coordinate transformation with an appropriate rotation matrix ${}^{B}R^{N}$:

$$ {}^{B}\vec{g} = {}^{B}R^{N}\,{}^{N}\vec{g} $$

Equation 22. Gravity transformation

$$ \Rightarrow \vec{\tau}_{g} = \vec{r}_{CG} \times M\,{}^{B}R^{N}\,{}^{N}\vec{g} + \sum_{i=1}^{3} \vec{r}_{i} \times m_{i}\,{}^{B}R^{N}\,{}^{N}\vec{g} $$

In a balanced condition, $\vec{\tau}_{g} = 0 = \vec{\tau}_{cg} + \vec{\tau}_{b}$ and

$$ 0 = \vec{r}_{CG} \times M\,{}^{B}R^{N}\,{}^{N}\vec{g} + \sum_{i=1}^{3} \vec{r}_{i} \times m_{i}\,{}^{B}R^{N}\,{}^{N}\vec{g} \;\Rightarrow $$

$$ 0 = \vec{r}_{CG} \times M\,{}^{B}\vec{g} + \sum_{i=1}^{3} \vec{r}_{i} \times m_{i}\,{}^{B}\vec{g} $$

Equation 23. Balanced torque condition

If there is not an unbalanced situation, there is no CG offset and by definition, the balance masses must be in their home, balanced position.

If the TASS CG deviates from its position while in a balanced condition, it is necessary for the balance masses to move in such a manner so as to return the TASS CG to a position along the vertical axis passing through the CR. To find the required balance mass positions to return to a balanced condition, one need only solve Equation 23 for each of the three $\vec{d}_{i}$ vectors. It is instructive to note each balance mass is constrained to move along one primary axis and thus $\vec{d}_{i}$ is measured along one unit vector for its respective axis:

$$\vec{d}_1 = d_1 \begin{bmatrix} 1 \\ 0 \\ 0 \end{bmatrix}, \vec{d}_2 = d_2 \begin{bmatrix} 0 \\ 1 \\ 0 \end{bmatrix}, \vec{d}_3 = d_3 \begin{bmatrix} 0 \\ 0 \\ 1 \end{bmatrix}$$

$$\Rightarrow \vec{d}_1 = \begin{bmatrix} d_1 \\ 0 \\ 0 \end{bmatrix}, \vec{d}_2 = \begin{bmatrix} 0 \\ d_2 \\ 0 \end{bmatrix}, \vec{d}_3 = \begin{bmatrix} 0 \\ 0 \\ d_3 \end{bmatrix} \text{ and } \vec{d} = \begin{bmatrix} d_1 \\ d_2 \\ d_3 \end{bmatrix}$$

Converting to matrix notation allows easier manipulation of the equations. The skew symmetric notation to convert ${}^{B}\vec{g}$ to a 3x3 matrix where:

$${}^{B}\vec{g}^{\times} = \begin{bmatrix} 0 & -g_3 & g_2 \\ g_3 & 0 & -g_1 \\ -g_1 & g_1 & 0 \end{bmatrix}$$

Equation 24. Skew symmetric notation of gravity

Reversing the cross product operations gives:

$$0 = -M\,{}^{B}\vec{g} \times \vec{r}_{CG} + \sum_{i=1}^{3} -m_i\,{}^{B}\vec{g} \times \vec{r}_i$$

$$0 = -M\left[{}^{B}g^{\times}\right]\left[r_{CG}\right] - \sum_{i=1}^{3} m_i\left[{}^{B}g^{\times}\right]\left[r_i\right]$$

since m_i and $\left[{}^{B}g^{\times}\right]$ are constant and identical for all three masses and position vectors, they can be brought outside the summation:

$$0 = -M\left[{}^{B}g^{\times}\right]\left[r_{CG}\right] - m_i\left[{}^{B}g^{\times}\right]\sum_{i=1}^{3}\left[r_i\right]$$

From Equation 21:

$$0 = -M\left[{}^{B}g^{\times}\right]\left[r_{CG}\right] - m_i\left[{}^{B}g^{\times}\right]\sum_{i=1}^{3}\left[r_{i,0}\right] + \left[d_i\right]$$

Since $\left[r_i\right] = \left[r_{i,0}\right] + \left[d_i\right]$:

$$\left[r_1\right] = \begin{bmatrix} r_{1x,0} \\ r_{1y,0} \\ r_{1z,0} \end{bmatrix} + \begin{bmatrix} d_1 \\ 0 \\ 0 \end{bmatrix}, \left[r_2\right] = \begin{bmatrix} r_{2x,0} \\ r_{2y,0} \\ r_{2z,0} \end{bmatrix} + \begin{bmatrix} 0 \\ d_2 \\ 0 \end{bmatrix}, \left[r_3\right] = \begin{bmatrix} r_{3x,0} \\ r_{3y,0} \\ r_{3z,0} \end{bmatrix} + \begin{bmatrix} 0 \\ 0 \\ d_3 \end{bmatrix}$$

$$\Rightarrow \sum_{i=1}^{3}\left[r_{i,0}\right] + \left[d_i\right] = \begin{bmatrix} r_{1x,0} \\ r_{1y,0} \\ r_{1z,0} \end{bmatrix} + \begin{bmatrix} d_1 \\ 0 \\ 0 \end{bmatrix} + \begin{bmatrix} r_{2x,0} \\ r_{2y,0} \\ r_{2z,0} \end{bmatrix} + \begin{bmatrix} 0 \\ d_2 \\ 0 \end{bmatrix} + \begin{bmatrix} r_{3x,0} \\ r_{3y,0} \\ r_{3z,0} \end{bmatrix} + \begin{bmatrix} 0 \\ 0 \\ d_3 \end{bmatrix}$$

$$= \begin{bmatrix} r_{1x,0} \\ r_{1y,0} \\ r_{1z,0} \end{bmatrix} + \begin{bmatrix} r_{2x,0} \\ r_{2y,0} \\ r_{2z,0} \end{bmatrix} + \begin{bmatrix} r_{3x,0} \\ r_{3y,0} \\ r_{3z,0} \end{bmatrix} + \begin{bmatrix} d_1 \\ 0 \\ 0 \end{bmatrix} + \begin{bmatrix} 0 \\ d_2 \\ 0 \end{bmatrix} + \begin{bmatrix} 0 \\ 0 \\ d_3 \end{bmatrix}$$

$$= \begin{bmatrix} r_{1x,0} + r_{2x,0} + r_{3x,0} \\ r_{1y,0} + r_{2y,0} + r_{3y,0} \\ r_{1z,0} + r_{2z,0} + r_{3z,0} \end{bmatrix} + \begin{bmatrix} d_1 \\ d_2 \\ d_3 \end{bmatrix} \quad \text{or} \quad \left[r_0\right] + \left[d\right]$$

where: $\left[r_0\right] = \begin{bmatrix} r_{1x,0} + r_{2x,0} + r_{3x,0} \\ r_{1y,0} + r_{2y,0} + r_{3y,0} \\ r_{1z,0} + r_{2z,0} + r_{3z,0} \end{bmatrix}$ and $\left[d\right] = \begin{bmatrix} d_1 \\ d_2 \\ d_3 \end{bmatrix}$

Continuing to solve and eliminating the summation we have:

$$0 = -M\left[{}^{B}g^{\times}\right]\left[r_{CG}\right] - m_i\left[{}^{B}g^{\times}\right]\left(\left[r_0\right] + \left[d\right]\right)$$

$$M\left[{}^{B}g^{\times}\right]\left[r_{CG}\right] = -m_i\left[{}^{B}g^{\times}\right]\left(\left[r_0\right] + \left[d\right]\right)$$

$$\frac{-M}{m}\left[{}^{B}g^{\times}\right]\left[{}^{B}g^{\times}\right]^{+}\left[r_{CG}\right] - \left[r_0\right] = \left[d\right]$$

Equation 25. Balance mass positions

where $\left[\ \right]^{+}$ represents the pseudoinverse.

C. DETERMINATION OF CG OFFSET

The controller developed for mass balancing assumes the CG offset is known. This was done in order to simulate and collect data while developing an initial software control program. This will often not be the case in actual TASS operation.

The CG vector r_{CG} has components both perpendicular to gravity and parallel and only the perpendicular component can be measured directly [Ref. 1,2,8].

$$r_{CG} = r_{CG\perp} + r_{CG||}$$

Equation 26. CG components

The perpendicular component can be measured by measuring the individual d_i positions when a balanced condition is achieved and solving Equation 25 for r_{CG}. This also assumes $\boldsymbol{g}$ is known in testbed coordinates.

The TASS is then maneuvered to a new attitude and a new set of measurements are taken. Since the change in attitude should be readily measured from onboard sensors, a rotation matrix from attitude **a** to attitude **b** can be

determined: ${}^{b}[R]^{a}$. ***g*** from measurement **a** can be transformed to measurement **b** by: ${}^{b}g = {}^{b}[R]^{a}\,{}^{a}[g]$. Since $r_{CG} = r_{CG\perp} + r_{CG||}$,

$$[r_{CG}] = {}^{a}[r_{a\perp}] + {}^{a}[r_{a||}]\,{}^{a}[g]$$

and

$$[r_{CG}] = {}^{b}[r_{b\perp}] + {}^{b}[r_{b||}]\,{}^{b}[R]^{a}\,{}^{a}[g]$$

Setting the two measurements equal:

$${}^{a}[r_{a\perp}] + {}^{a}[r_{a||}]\,{}^{a}[g] = {}^{b}[r_{b\perp}] + {}^{b}[r_{b||}]\,{}^{b}[R]^{a}\,{}^{a}[g]$$

Solving for $r_{CG||}$:

$${}^{a}[r_{a\perp}] - {}^{b}[r_{b\perp}] = {}^{b}[r_{b||}]\,{}^{b}[R]^{a}\,{}^{a}[g] - {}^{a}[r_{a||}]\,{}^{a}[g]$$

$${}^{a}[r_{a\perp}] - {}^{b}[r_{b\perp}] = \begin{bmatrix} {}^{a}[r_{a||}] \\ {}^{b}[r_{b||}] \end{bmatrix} \begin{bmatrix} {}^{a}[g] & {}^{b}[R]^{a}\,{}^{a}[g] \end{bmatrix}$$

$${}^{a}[r_{a\perp}] - {}^{b}[r_{b\perp}] \begin{bmatrix} {}^{a}[g] & {}^{b}[R]^{a}\,{}^{a}[g] \end{bmatrix}^{+} = \begin{bmatrix} {}^{a}[r_{a||}] \\ {}^{b}[r_{b||}] \end{bmatrix}$$

Equation 27. Parallel components of CG

D. MASS BALANCE SIMULATION

The next phase of the development modified the CMG quaternion controller with a mass balance controller. All files and models can be found in Appendix B. Once the balance mass positions were solved for in Equation 25, a controller and steering logic were designed.

Essentially, the objective was to eliminate the effect of τ_g. A PD controller was initially designed for simplicity

and evaluation of the control algorithm. Some unwanted effects such as the desired error not reaching zero completely (a characteristic of PD control), unwanted perturbations and difficulty in selecting gains were observed with this method. An integral gain was added to complete a PID controller which removed unwanted behavior and was more stable.

Choosing τ_g as our error to minimize allowed a compact calculation for $[d]$. Equation 20 showed that $\vec{\tau}_g = \vec{\tau}_{cg} + \vec{\tau}_b \Rightarrow \vec{\tau}_{gg} = \vec{r}_{CG} \times M\vec{g} + \sum_{i=1}^{3} \vec{r}_i \times m_i\vec{g}$. Solving for $[d]$ can be implemented as [Ref. 1,2]:

$$\vec{\tau}_g - \vec{\tau}_{cg} = \vec{\tau}_b = \sum_{i=1}^{3} \vec{r}_i \times m_i\vec{g}$$

$$= -m_i \left[{}^B g^{\times}\right] \sum_{i=1}^{3} [r_i]$$

Based on the relationship for $\vec{r}_i$ in Equation 21,

$$[r_i] = [r_{i,0}] + [d_i]$$

and

$$[\tau_g] - [\tau_{cg}] = -m_i \left[{}^B g^{\times}\right] \sum_{i=1}^{3} [r_i]$$

$$\Rightarrow [\tau_g] - [\tau_{cg}] = -m_i \left[{}^B g^{\times}\right] \sum_{i=1}^{3} \left([r_{i,0}] + [d_i]\right)$$

and solving for $[d]$ in similar fashion as in Equation 25:

$$[\tau_g] - [\tau_{cg}] = -m_i [{}^B g^{\times}]([r_0] + [d])$$

$$\frac{-1}{m_i}[[\tau_g] - [\tau_g]][{}^B g^{\times}]^{+} - [r_0] = [d]$$

Equation 28. Calculation of [d] in terms of torque.

E. MASS BALANCE ANALYSIS

The next simulations introduced noise, sinusoidal disturbance, delays and gravity torque one at a time noting the results at each point. Only the ideal case presented earlier and the case with all anomalies will be shown for brevity. If the simulation works with worst case anomalies, it should work for those cases in between worst case and ideal.

Conditions for the following results are shown in Figure 47.

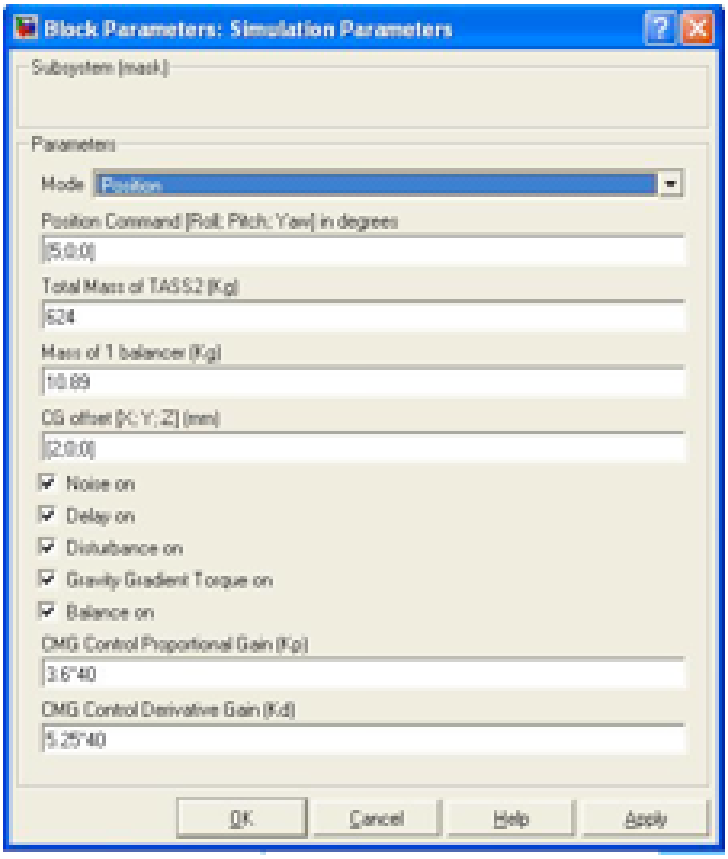

Figure 47. Simulation parameters, 2mm CG, worst case

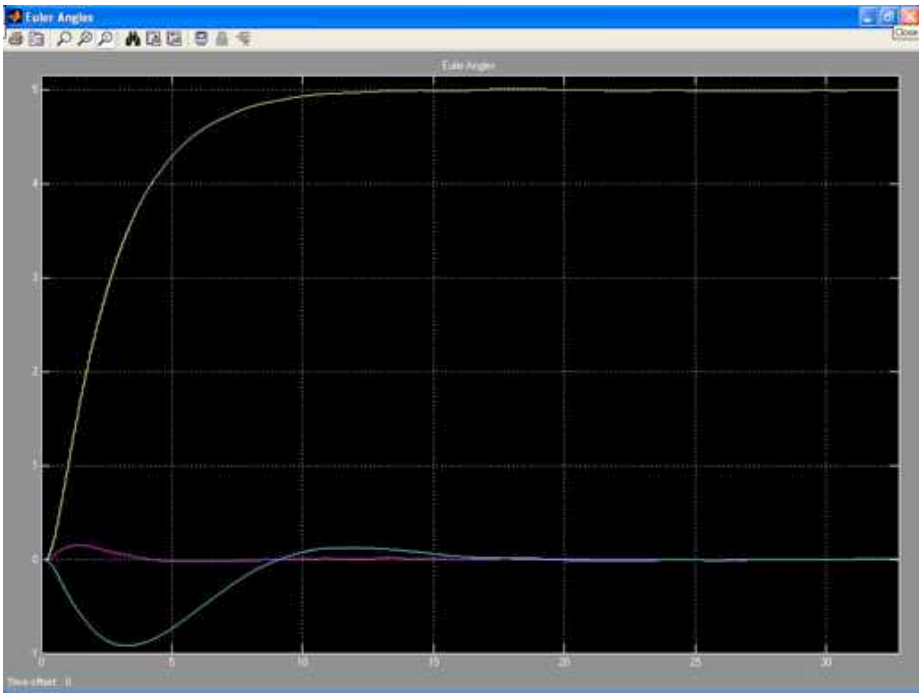

Figure 48. Euler angles, 2mm CG offset, worst case

The X axis, shown in yellow, took about the same time to settle to the commanded 5° position and only slightly greater rise time (by .25 seconds). The more notable difference occurred on the Y and Z axes. Where the ideal situation had disturbances in these axes settled, in about 16 seconds, here it took almost twice as long to fully settle to the commanded position.

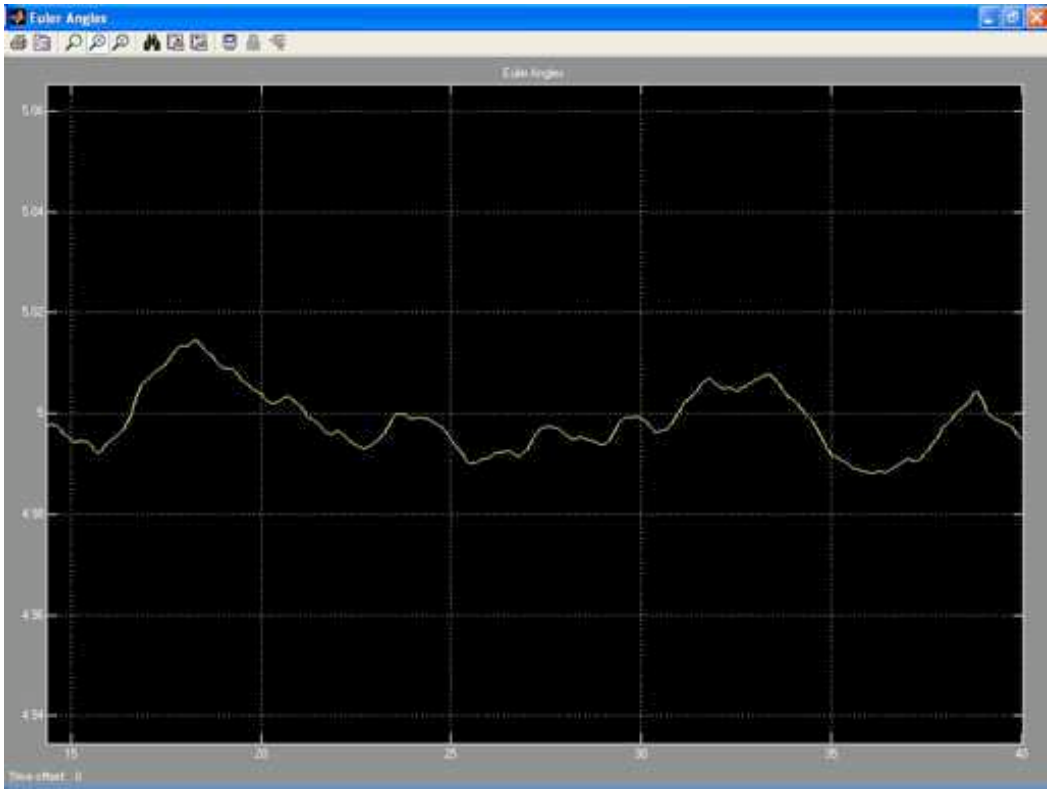

Figure 49. Euler X axis, 2mm CG offset, zoomed

Upon closer inspection of the commanded angle of 5°, a fluctuation (due to the inserted sensor noise shown in Figure 37) of ±0.02° can be observed.

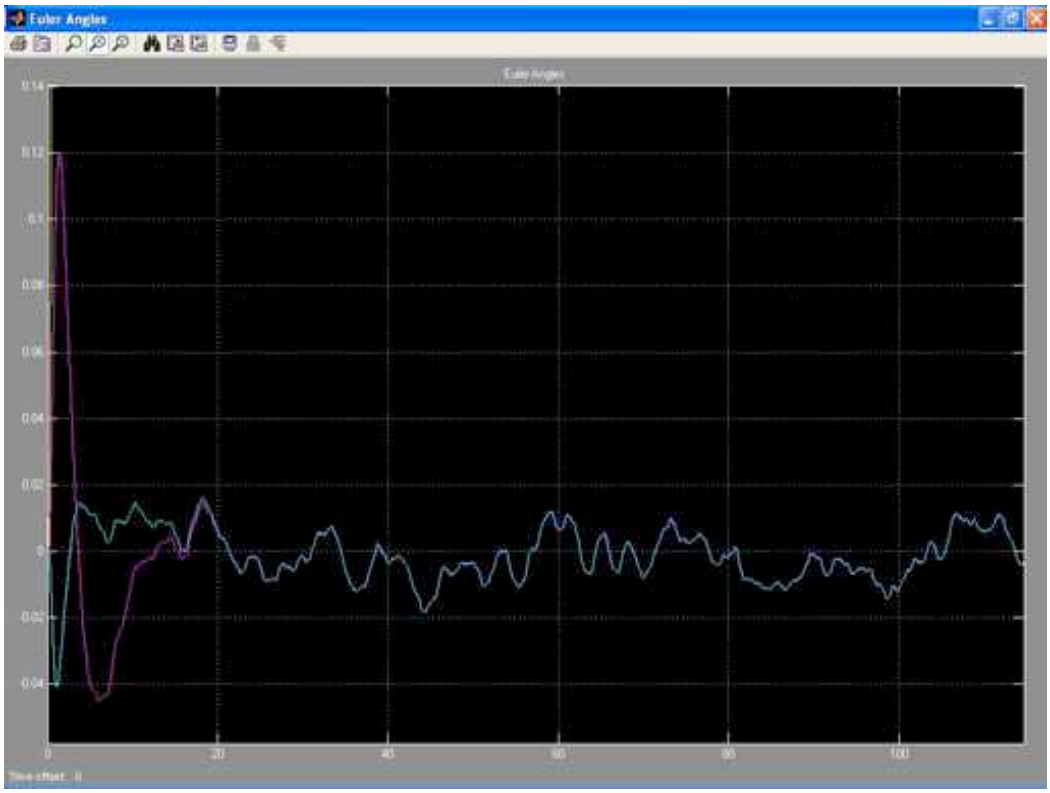

Figure 50. Euler Y, Z axes, 2mm CG offset, zoomed

Figure 50 shows a fluctuation (due to the inserted sensor noise) of ±0.02° can be observed in the Y and Z axes as well.

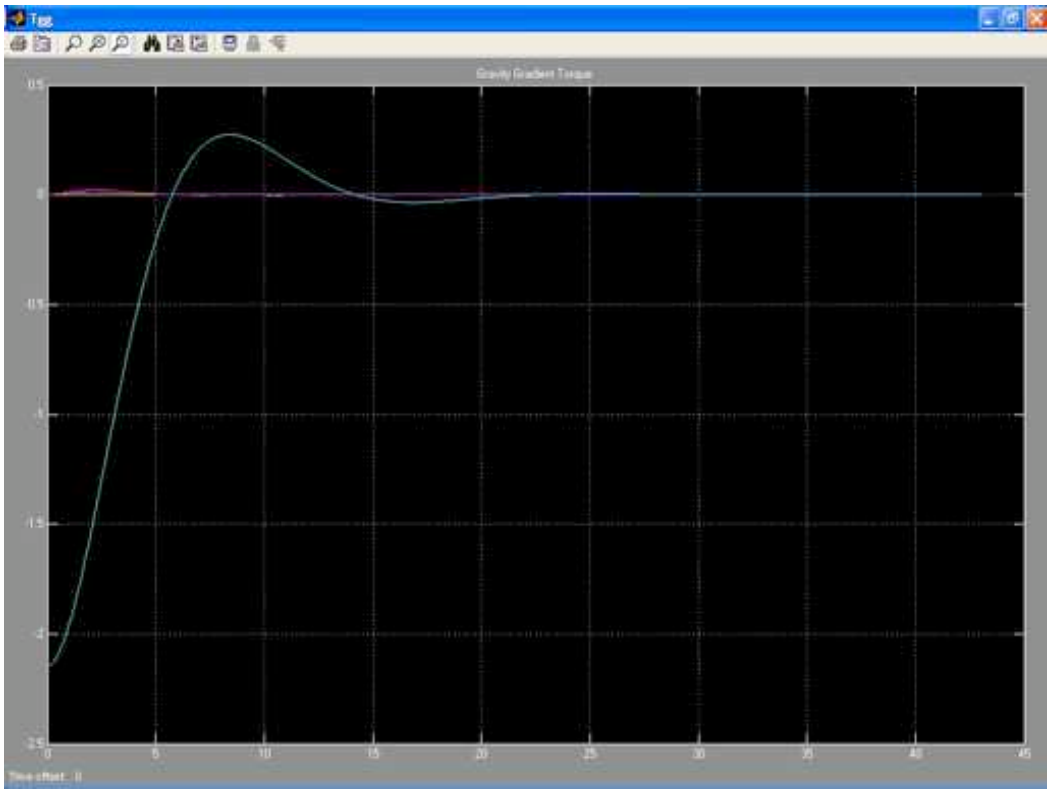

Figure 51. Gravity torque, 2mm CG offset, worst case

Figure 51 shows the gravity torque response for the 2mm CG offset during a commanded 5° slew. Without balance mass movement, this would be constant throughout the maneuver. Coupling in the axes can be seen by the slight perturbation in gravity torque for one of the other axes.

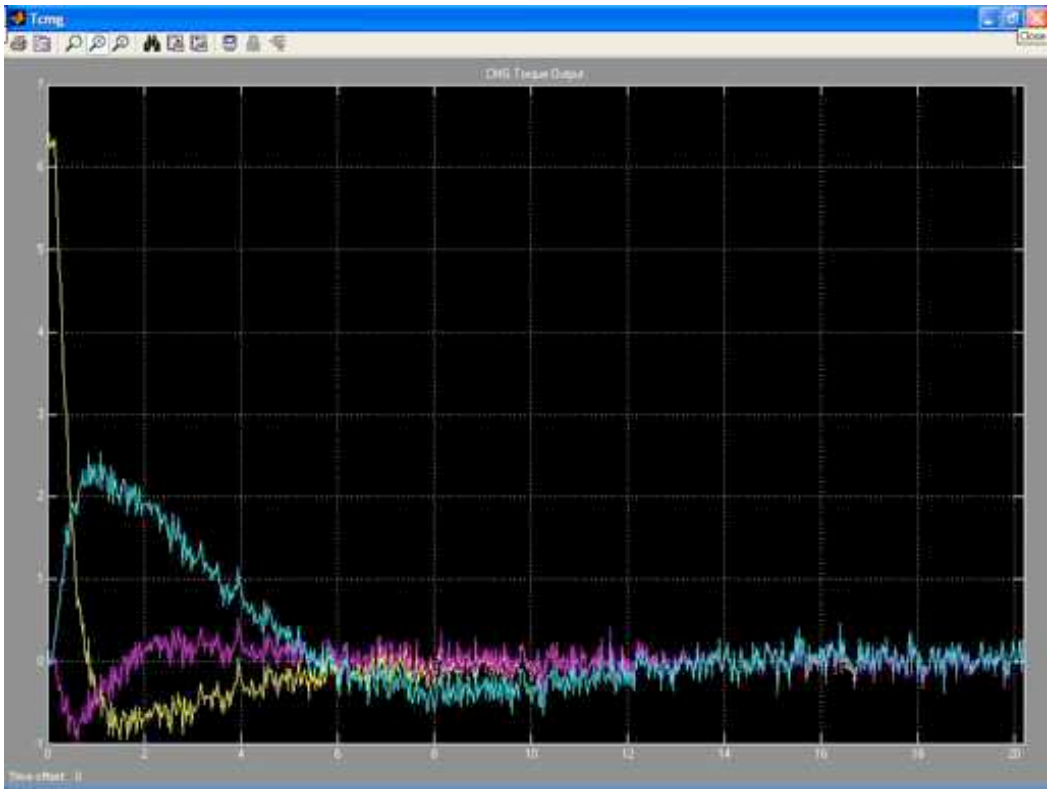

Figure 52. CMG torque, 2mm CG offset, worst case

The CMG torque in Figure 52 takes slightly longer to settle out than the ideal case in Figure 39. Noisy variations in torque can be observed as well.

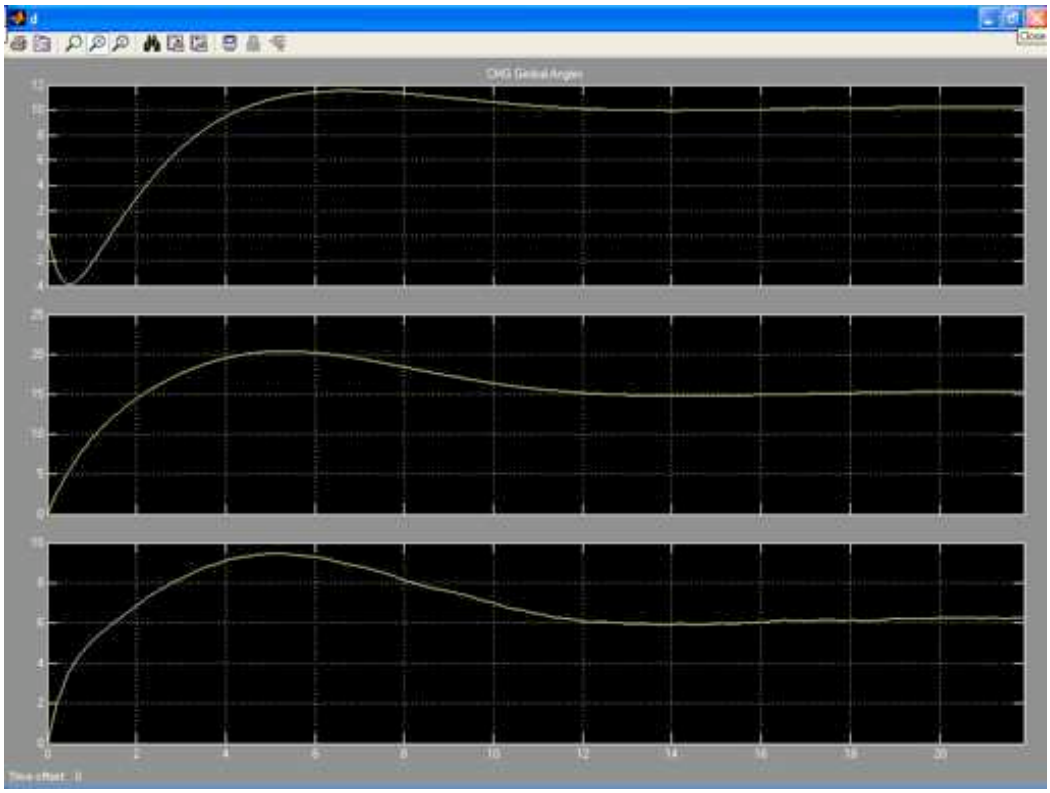

Figure 53. CMG gimbal angles, 2mm CG offset, worst

Figure 53 shows a much different CMG gimbal angle profile than the ideal condition. The gimbal angles in the worst case moved more than three times the magnitude of the ideal case. The peaks also took longer to occur.

The gimbal angles do not return to zero since there is a CG offset to counter. At the time the mass balancers compensate for the CG offset, the zero torque position for the gimbal angles has changed. Under the ideal case, the TASS was perfectly balanced and the change imparted to the gimbals was taken out to stop the TASS at the commanded attitude.

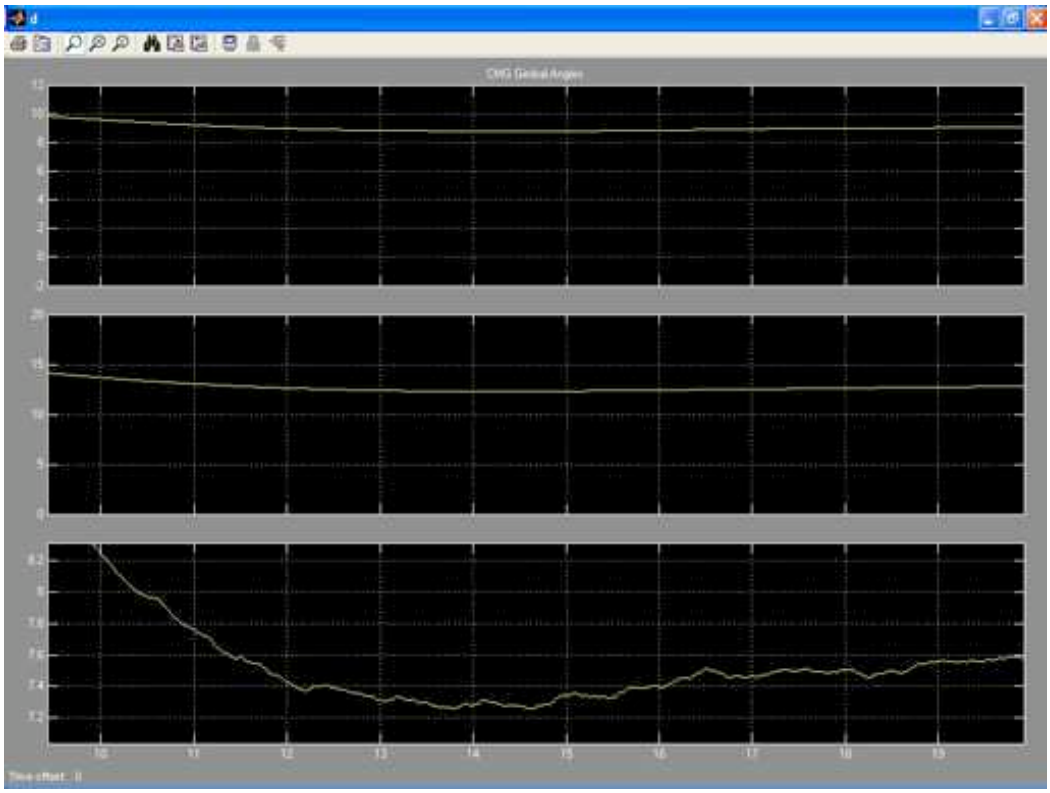

Figure 54. CMG gimbal angles, 2mm CG offset, zoomed

Figure 54 shows a zoomed in portion of Figure 53. Though noise in the system is causing the gimbal angle variation, this does not take into account friction. Friction was not modeled in the gimbal gearing or the bearings. Friction would likely reduce the gimbal angle variation.

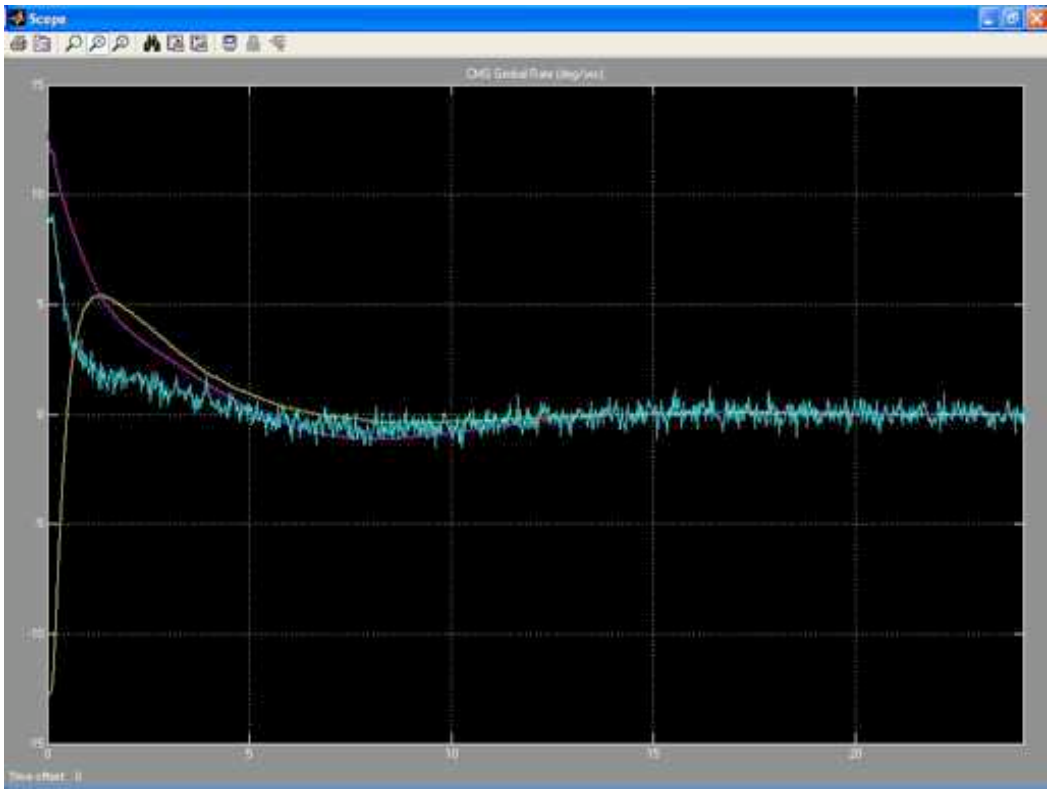

Figure 55. CMG gimbal rates, 2mm CG offset

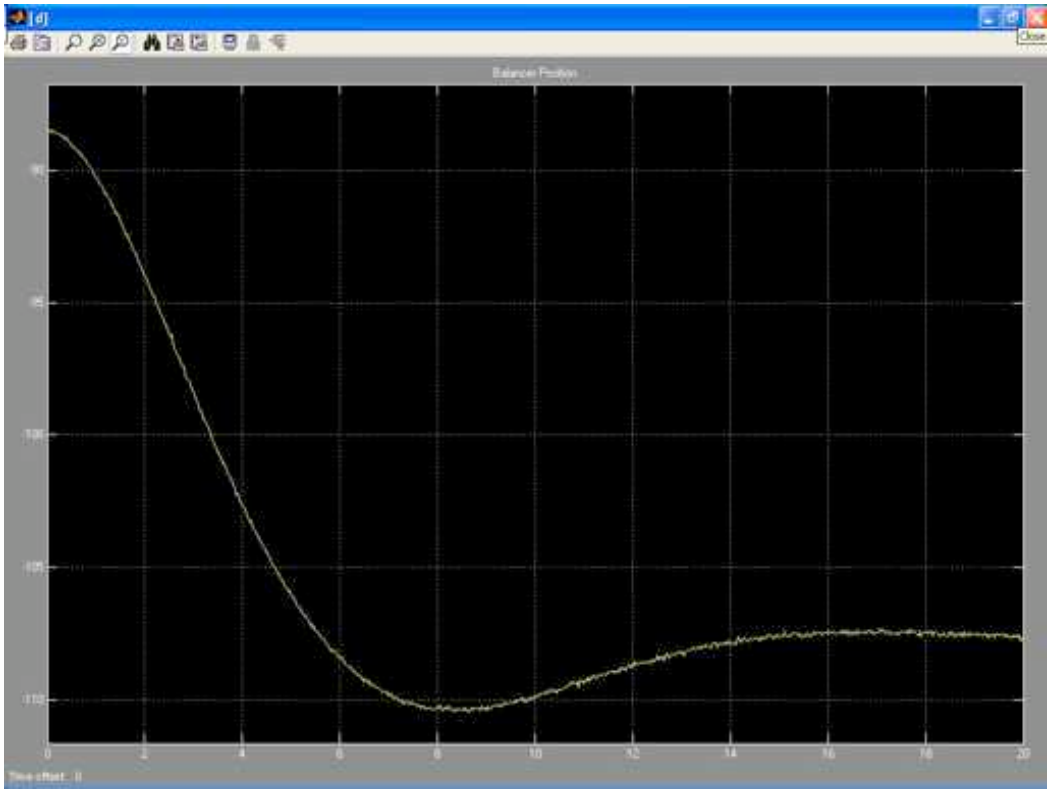

Figure 56. dx balance mass, 2mm CG offset, 5° +X

Figure 56 shows the mass balancer position change during the commanded maneuver. Since the CG offset was +2mm along the X axis, we expect to see the change in the X axis mass balancer to a more negative position. Here the move is about 34mm in the -X direction. This is well within the ±75mm travel limitation of the balancers.

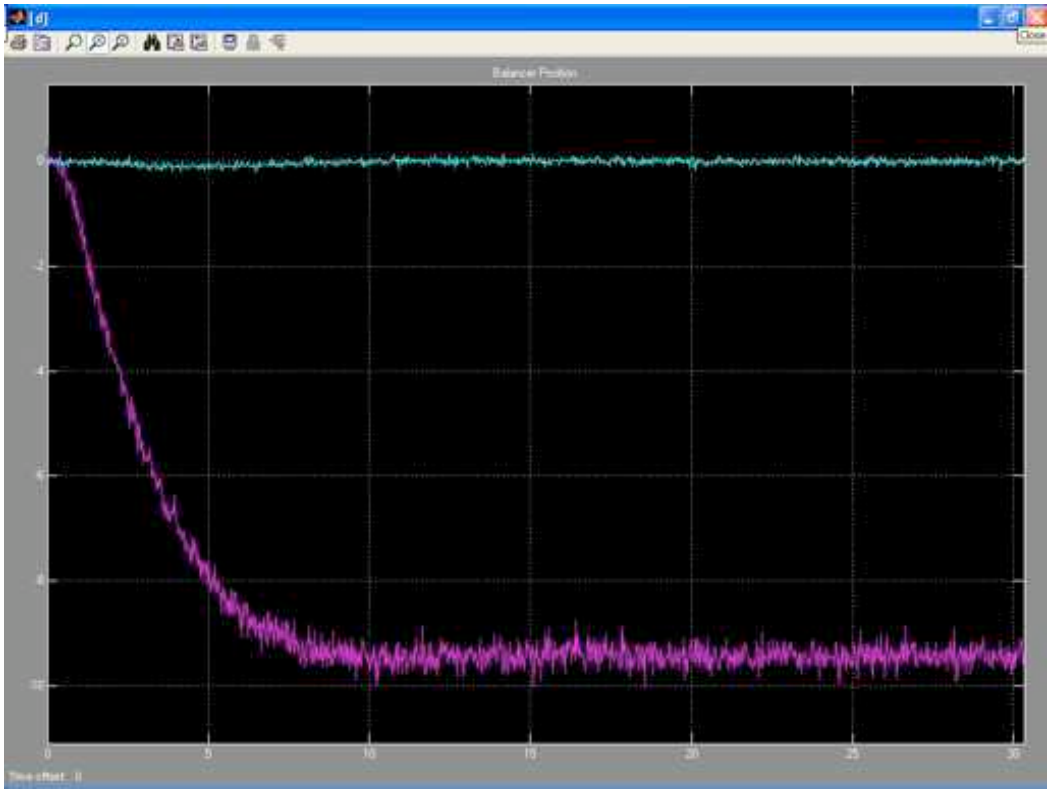

Figure 57. dy, dz balance masses, 2mm CG offset, 5° +X

Figure 57 shows a shift in the Y balance mass in the -Y direction by 9mm. This is also expected as the attitude increases in the +X direction. As the angle between the inertial horizontal and the +X axis increases, the Y balance mass is tilted back slightly and influences the overall CG correction. To aid in the correction, the Y balance mass moves downward slightly.

THIS PAGE INTENTIONALLY LEFT BLANK

VI. FUTURE WORK

A. EXPERIMENTATION AND SOFTWARE

Towards the end of research, one of the CMGs was returned to the manufacturer to upgrade the controller electronics and repair some sources of noise noted in II.C.2 and shown in Figure 12. Very little experimentation with the CMG Quaternion Controller, that was developed, was possible. Early in the development the CMGs were run and the controller seemed to perform in a stabilizing mode for a short period of time. Difficulty in determining adequate controller gains, problems with the CMG gearing set screws and a small field of view of the IR sensor (±10°) all combined to produce and unstable and divergent behavior with simulations greater than about 20 seconds or so. No data was gathered during this early development period.

System identification. Mass properties including moments of inertia were developed from the original spreadsheet by scaling for the change in mass from the delivered configuration to the configuration with the optical payload installed. Accurate determination of the mass properties will be needed. Friction modeling for CMG gimbal axes and bearings.

Sensor output filtering. Current sensor outputs are noisy even with the Extended Kalman Filter (EKF). Spikes of up to 1.5° were seen on some attitude sensors. This will not be acceptable for fine pointing modes of the simulator.

B. HARDWARE

1. Star Sensor

Incorporating the Star Sensor as researched by LT Connolly is also needed. The precision this sensor is

capable of will be required for fine pointing of the simulator.

2. Magnetometer

Integration of the three-axis magnetometer. Though difficult to calibrate in the presence of interference from environmental ferrous material, the Billingsley Magnetics TF100M-G2 could be accurate enough for determination of an inertial "North". Used differentially with a second magnetometer, it has a potential for high accuracy for position determination about the 'Y' axis or "pitch".

3. Optical Payload

The BFRM payload has a great deal of integration left. Jitter control, expanded field of view, beam front disturbance rejection, wireless connectivity and integration with the flight control unit are just a few areas.

4. Physical limits

To protect the simulator in the event of uncommanded torque inputs or flight software errors, a physical system around the base of the simulator is needed. This hardware will prevent the simulator lower deck from contacting the air bearing pedestal. A software implementation of possibly an auto-stabilizing LQR controller can be added as well.

5. CMGs

Singularity avoidance schemes will need to be pursued for full implementation of the CMGs. Position feedback filtering and optimization of the sampling bandwidth will need to be incorporated in the future.

VII. SUMMARY AND CONCLUSIONS

Much work has gone into the initial stages of developing the hardware, the software and dealing with each new anomaly that arose during testing. Quite a bit more work remains to be done.

Mass balancing was done with a KNOWN Cg offset. This was strictly to develop a working controller and simulation. Under real conditions the CG offset will not be known and would have to be determined from system parameters and repeated measurements in different attitudes. Some issues that present themselves for future work are finite positioning of the balance masses. Best stated accuracy for the installed balancers is 18 μm. Encoder scale factor is 191.63 counts per mm [Ref. 10]. This results in 1 count moving the mass ±5.2 μm along its respective axis. Working Equation 25 in reverse and solving for CG offset given a mass displacement, it is found a single mass can influence the CG by no more than .0955 μm. Being able to position the CG towards the CR within .0955 μm would result in a natural frequency of:

$$\omega_n = \sqrt{\frac{m \cdot \boldsymbol{g} \cdot \ell}{\mathrm{I}}}$$

$$= \sqrt{\frac{624Kg \cdot 9.81m \cdot 9.55 \times 10^{-8} m}{162.6Kg \cdot m^2 \cdot \sec^2}}$$

$$= 1.896 \times 10^{-3} \, rad/\sec = 3313.7 \, \sec/2\pi$$

If a specific ω_n is required to prevent the CMGs from saturating for some uninterrupted period, the above calculation can be reversed to calculate what CG offset is

required to produce that period. Once the period was obtained, the CG would be known within given bounds based on the stated period.

This thesis accomplished the objectives set at the beginning of development: to develop an initial CMG control program, develop and integrate the mass balancers with the TASS and flush out the initial anomalies associated with the development of a complicated mechanism such as the TASS.

APPENDIX A: MASS PROPERTIES SPREADSHEET

Component	Qty	Matl	OD/L-X (m)	ID/W-Z (m)	H/T-Y (m)	Volume (m^3)	Density (kg/m^3)	Weight ea (kg)
Optics Test Items - Upper Optical Deck	0		0	0	0	0.000E+00	0.000E+00	15.876
Upper Optical Deck Breadboard	1	6061-T6 Al	0.6096	0.4572	0.0127	1.622E-03	2.700E+03	9.253
Orion Telescope #1	1							2.200
Fast Steering Mirror #1	1							1.632
FSM Controller	1							1.087
Jitter PSD Controller	1							0.567
Video Camera #1	1							0.369
Mirror #1	1							0.257
Converging Lens	1							0.153
Beam Splitter	1							0.331
Jitter PSD	1							0.394
45 Degree Mirror #1	1							0.392
Optics Test Items - Optical Deck	0		0	0	0		0.000E+00	15.876
Optics Computer #1	1							4.800
Optics Computer #2	1							4.800
Orion Telescope #2	1							2.200
Fast Steering Mirror #2	1							1.632
Red Camera - Dalsa	1							0.953
Green Camera - Dalsa	1							0.953
Video Camera #2 - CCV	1							0.369
Mirror +Z	1							0.396
Mirror -Z	1							0.396
45 Degree Mirror #2	1							0.537
Beam Splitter - Star Sensor (X)	1							0.799
PSM - Star Sensor (X)	1							0.227
Laser Source - Star Sensor (X)	1							0.221
Optics PC	1							9.400
Beam Splitter - Star Sensor (-Z)	1							0.799
PSM - Star Sensor (-Z)	1							0.227
Laser Source - Star Sensor (-Z)	1							0.221
Balance mass	1							4.000
Balance mass	1							4.000
Equipment Deck Items								
UPS	1							9.300
Breadboard/Motor Flange	2	6061-T6 Al	0.29718	0.11938	0.0254	1.478E-03	2.700E+03	0.998
Hollow Shaft Motor	1		0.2921	0.11938	0.1016		0.000E+00	6.985
Motor Mounting Tube Assy	1	6061-T6 Al	0.254	0.2032	0.14605	2.664E-03	2.700E+03	1.996
Optical Deck	1	6061-T6 Al	1.2192	0.1524	0.0127	1.459E-02	2.700E+03	37.195

Component	Tot Weight (kg)	Assembly Weight (kg)	CGx (m)	Balx (kg-m)	(m from top equip plate)	(m fr CR to top equip plt)	Cgy (m from CR)
Optics Test Items - Upper Optical Deck	0.000		0.0000	0.0000	0.2413	0.2127	0.4540
Upper Optical Deck Breadboard	9.253		0.0000	0.0000	0.2291	0.2127	0.4418
Orion Telescope #1	2.200		0.1270	0.2794	0.4000	0.2127	0.6127
Fast Steering Mirror #1	1.632		0.2286	0.3731	0.4000	0.2127	0.6127
FSM Controller	1.087		0.2100	0.2283	0.3620	0.2127	0.5747
Jitter PSD Controller	0.567		0.2100	0.1191	0.2953	0.2127	0.5080
Video Camera #1	0.369		0.2540	0.0937	0.4000	0.2127	0.6127
Mirror #1	0.257		-0.2032	-0.0522	0.3715	0.2127	0.5842
Converging Lens	0.153		-0.1016	-0.0155	0.3715	0.2127	0.5842
Beam Splitter	0.331		-0.0762	-0.0252	0.3715	0.2127	0.5842
Jitter PSD	0.394		-0.1270	-0.0500	0.3715	0.2127	0.5842
45 Degree Mirror #1	0.392		0.0000	0.0000	0.3715	0.2127	0.5842
	0.000			0.0000		0.2127	0.2127
	0.000			0.0000		0.2127	0.2127
Optics Test Items - Optical Deck	0.000		0.0000	0.0000	0.0127	0.2127	0.2254
Optics Computer #1	4.800		0.2032	0.9754	0.0889	0.2127	0.3016
Optics Computer #2	4.800		-0.3048	-1.4630	0.0889	0.2127	0.3016
Orion Telescope #2	2.200		0.4191	0.9220	0.1587	0.2127	0.3714
Fast Steering Mirror #2	1.632		0.4572	0.7462	0.1524	0.2127	0.3651
Red Camera - Dalsa	0.953		0.4318	0.4115	0.2731	0.2127	0.4858
Green Camera - Dalsa	0.953		0.5588	0.5325	0.2191	0.2127	0.4318
Video Camera #2 - CCV	0.369		0.5207	0.1921	0.1778	0.2127	0.3905
Mirror +Z	0.396		0.2540	0.1006	0.1143	0.2127	0.3270
Mirror -Z	0.396		0.2159	0.0855	0.1143	0.2127	0.3270
45 Degree Mirror #2	0.537		0.0000	0.0000	0.0890	0.2127	0.3017
Beam Splitter - Star Sensor (X)	0.799		0.5330	0.4259	0.1143	0.2127	0.3270
PSM - Star Sensor (X)	0.227		0.5330	0.1210	0.0524	0.2127	0.2651
Laser Source - Star Sensor (X)	0.221		0.4064	0.0898	0.1143	0.2127	0.3270
Optics PC	9.400		-0.3048	-2.8651	0.1143	0.2127	0.3270
Beam Splitter - Star Sensor (-Z)	0.799		0.0000	0.0000	0.0762	0.2127	0.2889
PSM - Star Sensor (-Z)	0.227		0.0000	0.0000	0.0254	0.2127	0.2381
Laser Source - Star Sensor (-Z)	0.221		0.0000	0.0000	0.0889	0.2127	0.3016
Balance mass	4.000		0.0635	0.2540	0.0699	0.2127	0.2826
Balance mass	4.000		-0.3175	-1.2700	0.0699	0.2127	0.2826
Equipment Deck Items							
UPS	9.300			0.0000	0.1016	0.2127	0.3143
Breadboard/Motor Flange	1.996		0.0000	0.0000	0.1702	0.2127	0.3829
Hollow Shaft Motor	6.985		0.0064	0.0444	0.2007	0.2127	0.4134
Motor Mounting Tube Assy	1.996		0.0000	0.0000	0.1041	0.2127	0.3169
Optical Deck	37.195		0.0000	0.0000	0.0406	0.2127	0.2534

Component	Baly (kg-m)	CGz (m)	Balz (kg-m)	Comp Ixx (kg-m^2)	Comp Iyy (kg-m^2)	Comp Izz (kg-m^2)	Ixx (kg-m^2)
Optics Test Items - Upper Optical Deck	0.0000	0.0000	0.0000	0	0	0	0
Upper Optical Deck Breadboard	4.0879	0.0000	0.0000	0.286677139	0.4477387	0.161310304	2.092613879
Orion Telescope #1	1.3480	0.1778	0.3912	0	0	0	0.895485004
Fast Steering Mirror #1	1.0000	0.0000	0.0000	0	0	0	0.612694903
FSM Controller	0.6247	-0.1778	-0.1933	0	0	0	0.393402603
Jitter PSD Controller	0.2880	-0.1778	-0.1008	0	0	0	0.16425829
Video Camera #1	0.2261	0.1778	0.0656	0	0	0	0.150197258
Mirror #1	0.1501	0.2286	0.0588	0	0	0	0.101147739
Converging Lens	0.0894	0.0762	0.0117	0	0	0	0.053109276
Beam Splitter	0.1934	0.1778	0.0589	0	0	0	0.123438456
Jitter PSD	0.2302	-0.2413	-0.0951	0	0	0	0.157418247
45 Degree Mirror #1	0.2290	0.0000	0.0000	0	0	0	0.133794699
	0.0000		0.0000	0	0	0	
	0.0000		0.0000	0	0	0	
Optics Test Items - Optical Deck	0.0000	0.0000	0.0000	0	0	0	0
Optics Computer #1	1.4478	-0.3683	-1.7678	0	0	0	1.087773669
Optics Computer #2	1.4478	-0.2413	-1.1582	0	0	0	0.716161509
Orion Telescope #2	0.8171	0.4699	1.0338	0	0	0	0.789269418
Fast Steering Mirror #2	0.5959	-0.1016	-0.1658	0	0	0	0.234412605
Red Camera - Dalsa	0.4630	0.3556	0.3389	0	0	0	0.345436228
Green Camera - Dalsa	0.4115	0.1778	0.1694	0	0	0	0.207831529
Video Camera #2 - CCV	0.1441	0.3048	0.1125	0	0	0	0.090555888
Mirror +Z	0.1295	0.0000	0.0000	0	0	0	0.042349064
Mirror -Z	0.1295	0.3175	0.1257	0	0	0	0.082268339
45 Degree Mirror #2	0.1620	0.0000	0.0000	0	0	0	0.048885773
Beam Splitter - Star Sensor (X)	0.2613	0.0000	0.0000	0	0	0	0.085446722
PSM - Star Sensor (X)	0.0602	0.0000	0.0000	0	0	0	0.015955515
Laser Source - Star Sensor (X)	0.0723	0.0000	0.0000	0	0	0	0.0236342
Optics PC	3.0740	0.3048	2.8651	0	0	0	1.878544132
Beam Splitter - Star Sensor (-Z)	0.2308	-0.5534	-0.4422	0	0	0	0.311391335
PSM - Star Sensor (-Z)	0.0541	-0.5534	-0.1256	0	0	0	0.082390262
Laser Source - Star Sensor (-Z)	0.0667	-0.3810	-0.0842	0	0	0	0.052185973
Balance mass	1.1305	0.3810	1.5240	0	0	0	0.900140258
Balance mass	1.1305	-0.6096	-2.4384	0	0	0	1.805944898
Equipment Deck Items							
UPS							0.91881268
Breadboard/Motor Flange	0.7642	0.0000	0.0000	0.017018517	0.01279406	0.017018517	0.309628527
Hollow Shaft Motor	2.8876	0.1016	0.7097	0.102614683	0.08694456	0.102614683	1.368394212
Motor Mounting Tube Assy	0.6324	0.0000	0.0000	0.037488678	0.0263961	0.037488678	0.237868175
Optical Deck	9.4236	0.0000	0.0000	3.548845536	7.01896255	3.548845536	5.936413387

Component	Iyy (kg-m^2)	Izz (kg-m^2)	Ixy (kg-m^2)	Iyz (kg-m^2)	Izx (kg-m^2)
Optics Test Items - Upper Optical Deck	0	0	0	0	0
Upper Optical Deck Breadboard	0.286677139	2.092613879	0.90296837	-0.9029684	0
Orion Telescope #1	0.105032048	0.861420556	0.39522648	-0.3781943	-0.0170322
Fast Steering Mirror #1	0.085284991	0.697979894	0.26370496	-0.3063475	0.0426425
FSM Controller	0.082299857	0.406976146	0.15555137	-0.1623381	0.00678677
Jitter PSD Controller	0.04292918	0.17133851	0.06066455	-0.0642047	0.00354011
Video Camera #1	0.035471542	0.162338524	0.05736286	-0.0634335	0.00607063
Mirror #1	0.024041887	0.098329035	0.03855293	-0.0371436	-0.0014094
Converging Lens	0.002467737	0.053800242	0.02532077	-0.0256663	0.00034548
Beam Splitter	0.012385782	0.114896537	0.05552634	-0.0512554	-0.004271
Jitter PSD	0.029295748	0.140832151	0.06406125	-0.0557682	-0.008293
45 Degree Mirror #1	0	0.133794699	0.06689735	-0.0668973	0
			0	0	0
			0	0	0
Optics Test Items - Optical Deck	0	0	0	0	0
Optics Computer #1	0.849288624	0.634871349	0.11924252	0.10720864	-0.2264512
Optics Computer #2	0.725417904	0.882612789	-0.0046282	-0.0785974	0.08322564
Orion Telescope #2	0.872191804	0.689914778	-0.0414612	0.09113851	-0.0496773
Fast Steering Mirror #2	0.357986381	0.55870615	-0.0617869	-0.1003599	0.16214677
Red Camera - Dalsa	0.298196178	0.402616114	0.02362003	-0.05221	0.02858994
Green Camera - Dalsa	0.327708377	0.475285833	-0.0599384	-0.0737887	0.13372715
Video Camera #2 - CCV	0.134327635	0.156321079	-0.0218859	-0.0109967	0.0328826
Mirror +Z	0.025548336	0.0678974	0.00840036	-0.0211745	0.01277417
Mirror -Z	0.058377948	0.060807737	0.0119452	-0.0012149	-0.0107303
45 Degree Mirror #2	0	0.048885773	0.02444289	-0.0244429	0
Beam Splitter - Star Sensor (X)	0.226987111	0.312433833	-0.0707702	-0.0427234	0.11349356
PSM - Star Sensor (X)	0.064488203	0.080443718	-0.0242663	-0.0079778	0.0322441
Laser Source - Star Sensor (X)	0.036500572	0.060134772	-0.0064332	-0.0118171	0.01825029
Optics PC	1.746577152	1.878544132	0.06598349	-0.0659835	0
Beam Splitter - Star Sensor (-Z)	0.244694996	0.066696338	0.03334817	0.08899933	-0.1223475
PSM - Star Sensor (-Z)	0.069519104	0.012871158	0.00643558	0.02832397	-0.0347596
Laser Source - Star Sensor (-Z)	0.032080581	0.020105392	0.0100527	0.00598759	-0.0160403
Balance mass	0.596773	0.335625258	0.15168363	0.13057387	-0.2822575
Balance mass	1.88967364	0.722721258	-0.0418644	0.58347619	-0.5416118
Equipment Deck Items					
UPS	0	0.91881268			
Breadboard/Motor Flange	0.017018517	0.309628527	0.146305	-0.146305	0
Hollow Shaft Motor	0.175002764	1.296569462	0.59669572	-0.5607833	-0.0359124
Motor Mounting Tube Assy	0.037488678	0.237868175	0.10018975	-0.1001897	0
Optical Deck	3.548845536	5.936413387	1.19378393	-1.1937839	0

Optical Deck Isolators	16		0.0508	0.0127	0.0254		0.000E+00	0.057
Equipment Plate	1	6061-T6 Al	1.524	0.12065	0.0127	2.302E-02	2.700E+03	62.369
Standoffs	16	6061-T6 Al	0.0381	0	0.508	5.792E-04	2.700E+03	0.000
Lower Equipment Ring	1	6061-T6 Al	1.524	0.8001	0.0127	1.678E-02	2.700E+03	44.906
Ball Segment	1	15-5 SS	0.2794	0	0.1016	5.710E-03	7.810E+03	0.184
Ball Segment Adapter Tube	1	6061-T6 Al	0.3175	0.2921	0.19685	2.394E-03	2.700E+03	0.692
Manual X-Z Balance Block #1	1	6061-T6 Al	0.17145	0.17145	0.1016	2.987E-03	2.700E+03	8.064
Manual X-Z Balance Weight #1	1	Brass	0.1143	0.1143	0.08636	1.128E-03	8.670E+03	9.782
Manual Y Balance Weight #1	1	Brass	0.09144	0.01905	0.05334	3.351E-04	8.670E+03	2.905
Manual X-Z Balance Block #2	1	6061-T6 Al	0.17145	0.17145	0.1016	2.987E-03	2.700E+03	8.064
Manual X-Z Balance Weight #2	1	Brass	0.1143	0.1143	0.08636	1.128E-03	8.670E+03	9.782
Manual Y Balance Weight #2	1	Brass	0.09144	0.01905	0.05334	3.351E-04	8.670E+03	2.905
Manual X-Z Balance Block #3	1	6061-T6 Al	0.17145	0.17145	0.1016	2.987E-03	2.700E+03	8.064
Manual X-Z Balance Weight #3	1	Brass	0.1143	0.1143	0.08636	1.128E-03	8.670E+03	9.782
Manual Y Balance Weight #3	1	Brass	0.09144	0.01905	0.05334	3.351E-04	8.670E+03	2.905
Manual X-Z Balance Block #4	1	6061-T6 Al	0.17145	0.17145	0.1016	2.987E-03	2.700E+03	8.064
Manual X-Z Balance Weight #4	1	Brass	0.1143	0.1143	0.08636	1.128E-03	8.670E+03	9.782
Manual Y Balance Weight #4	1	Brass	0.09144	0.01905	0.05334	3.351E-04	8.670E+03	2.905
Manual X Balance Block #1	1	6061-T6 Al	0.15875	0.09525	0.09144	1.383E-03	2.700E+03	3.733
Manual X Balance Weight #1	1	Brass	0.0889	0.01905	0.0762	4.513E-04	8.670E+03	3.912
Manual X Balance Block #2	1	6061-T6 Al	0.15875	0.09525	0.09144	1.383E-03	2.700E+03	3.733
Manual X Balance Weight #2	1	Brass	0.0889	0.01905	0.0762	4.513E-04	8.670E+03	3.912
Manual Z Balance Block #1	1	6061-T6 Al	0.09525	0.15875	0.09144	1.383E-03	2.700E+03	3.733
Manual Z Balance Weight #1	1	Brass	0.0889	0.01905	0.0762	4.513E-04	8.670E+03	3.912
Manual Z Balance Block #2	1	6061-T6 Al	0.09525	0.15875	0.09144	1.383E-03	2.700E+03	3.733
Manual Z Balance Weight #2	1	Brass	0.0889	0.01905	0.0762	4.513E-04	8.670E+03	3.912
Power Switching & Control Electronics	1		0.2286	0.0762	0.1143	1.991E-03	9.800E-02	1.378
Sun Sensor Head	1		0.1143	0	0.1143			0.227
Switch Box	1		0.127	0.1778	0.0762	1.721E-03	9.800E-02	1.321
Industrial PC	1		0.19685	0.188468	0.181102	6.719E-03	9.800E-02	2.716
Auto Leveling Electronics #1	1		0.127	0.08255	0.028575	2.996E-04	9.800E-02	0.293
Auto Leveling Electronics #2	1		0.127	0.08255	0.028575			0.293
Auto Leveling Electronics #3	1		0.08255	0.127	0.028575			0.293
Wireless Ethernet	1		0.1920875	0.117475	0.04445			0.471
Inclinometers	1		0.0381	0.0381	0.0381	3.375E+00	9.800E-02	0.080
3-Axis Magnitometer	1		0.0635	0.09017	0.0381			0.255
IMU Interface	1		0.08255	0.127	0.028575			0.338
IMU	1		0.1016	0	0.10668	8.649E-04	9.800E-02	0.699
Top Deck Controller	1		0.08255	0.127	0.028575	-2.090E-04	9.800E-02	0.293
CMG Gimbal Controller #1	1		0.08255	0.028575	0.127	5.983E-04	9.800E-02	0.293
CMG Gimbal Controller #2	1		0.028575	0.08255	0.127	-5.983E-04	9.800E-02	0.295
CMG Gimbal Controller #3	1		0.08255	0.028575	0.127	5.983E-04	9.800E-02	0.293
Emoteq CMG Rotor Controllers #1	1		0.1397	0.1016	0.03048	2.201E-04		0.633
Emoteq CMG Rotor Controllers #2	1		0.1016	0.1397	0.03048			0.633
Emoteq CMG Rotor Controllers #3	1		0.1397	0.1016	0.03048			0.633

Optical Deck Isolators	0.907		0.0000	0.0000	0.0102	0.2127	0.2229
Equipment Plate	62.369		0.0000	0.0000	-0.0064	0.2127	0.2064
Standoffs	0.000		0.0000	0.0000	-0.2692	0.2127	-0.0565
Lower Equipment Ring	44.906		0.0000	0.0000	-0.5105	0.2127	-0.2978
Ball Segment	0.184		0.0000	0.0000	-0.2413	0.2127	-0.0286
Ball Segment Adapter Tube	0.692		0.0000	0.0000	-0.1111	0.2127	0.1016
Manual X-Z Balance Block #1	8.064		-0.5080	-4.0963	-0.0381	0.2127	0.1746
Manual X-Z Balance Weight #1	9.782		-0.6350	-6.2115	-0.0254	0.2127	0.1873
Manual Y Balance Weight #1	2.905		-0.5080	-1.4758	-0.1524	0.2127	0.0603
Manual X-Z Balance Block #2	8.064		-0.5080	-4.0963	-0.0381	0.2127	0.1746
Manual X-Z Balance Weight #2	9.782		-0.6350	-6.2115	-0.0254	0.2127	0.1873
Manual Y Balance Weight #2	2.905		-0.5080	-1.4758	-0.1524	0.2127	0.0603
Manual X-Z Balance Block #3	8.064		0.5080	4.0963	-0.0381	0.2127	0.1746
Manual X-Z Balance Weight #3	9.782		0.6350	6.2115	-0.0254	0.2127	0.1873
Manual Y Balance Weight #3	2.905		0.5080	1.4758	-0.1524	0.2127	0.0603
Manual X-Z Balance Block #4	8.064		0.5080	4.0963	-0.0381	0.2127	0.1746
Manual X-Z Balance Weight #4	9.782		0.6350	6.2115	-0.0254	0.2127	0.1873
Manual Y Balance Weight #4	2.905		0.5080	1.4758	-0.1524	0.2127	0.0603
Manual X Balance Block #1	3.733		-0.6807	-2.5412	-0.0254	0.2127	0.1873
Manual X Balance Weight #1	3.912		-0.8560	-3.3490	-0.0254	0.2127	0.1873
Manual X Balance Block #2	3.733		0.6807	2.5412	-0.0254	0.2127	0.1873
Manual X Balance Weight #2	3.912		0.8560	3.3490	-0.0254	0.2127	0.1873
Manual Z Balance Block #1	3.733		0.0000	0.0000	-0.5652	0.2127	-0.3524
Manual Z Balance Weight #1	3.912		0.0000	0.0000	-0.6223	0.2127	-0.4096
Manual Z Balance Block #2	3.733		0.0000	0.0000	-0.5652	0.2127	-0.3524
Manual Z Balance Weight #2	3.912		0.0000	0.0000	-0.6223	0.2127	-0.4096
Power Switching & Control Electronics	1.378		-0.4623	-0.6369	-0.1143	0.2127	0.0984
Sun Sensor Head	0.227		-0.7595	-0.1722	-0.0495	0.2127	0.1632
Switch Box	1.321		0.1600	0.2114	-0.0889	0.2127	0.1238
Industrial PC	2.716		-0.2235	-0.6070	-0.4128	0.2127	-0.2000
Auto Leveling Electronics #1	0.293		-0.2921	-0.0856	-0.4763	0.2127	-0.2635
Auto Leveling Electronics #2	0.293		-0.5080	-0.1488	-0.4763	0.2127	-0.2635
Auto Leveling Electronics #3	0.293		0.2692	0.0789	-0.4763	0.2127	-0.2635
Wireless Ethernet	0.471		-0.2184	-0.1029	-0.0381	0.2127	0.1746
Inclinometers	0.080		-0.5944	-0.0473	-0.0445	0.2127	0.1683
3-Axis Magnitometer	0.255		-0.5944	-0.1516	-0.0381	0.2127	0.1746
IMU Interface	0.338		0.1270	0.0430	-0.0381	0.2127	0.1746
IMU	0.699		0.3658	0.2555	-0.0635	0.2127	0.1492
Top Deck Controller	0.293		0.3378	0.0989	-0.0381	0.2127	0.1746
CMG Gimbal Controller #1	0.293		-0.9830	-0.2879	-0.3302	0.2127	-0.1175
CMG Gimbal Controller #2	0.295		0.0000	0.0000	-0.3302	0.2127	-0.1175
CMG Gimbal Controller #3	0.293		0.9830	0.2879	-0.3302	0.2127	-0.1175
Emoteq CMG Rotor Controllers #1	0.633		-0.5588	-0.3538	-0.4699	0.2127	-0.2572
Emoteq CMG Rotor Controllers #2	0.633		0.2057	0.1303	-0.4699	0.2127	-0.2572
Emoteq CMG Rotor Controllers #3	0.633		0.5639	0.3571	-0.4699	0.2127	-0.2572

Optical Deck Isolators	0.2022	0.0000	0.0000	0.002075673	1.9433E-05	0.002075673	0.047140526
Equipment Plate	12.8711	0.0000	0.0000	9.176288825	18.2205634	9.176288825	11.83249386
Standoffs	0.0000	0.0000	0.0000	0	0	0	0
Lower Equipment Ring	-13.3738	0.0000	0.0000	8.362748844	16.6304474	8.362748844	12.34573395
Ball Segment	-0.0053	0.0000	0.0000	0.002460144	0.0017988	0.002460144	0.002610716
Ball Segment Adapter Tube	0.0703	0.0000	0.0000	0.019401605	0.01610001	0.019401605	0.026544061
Manual X-Z Balance Block #1	1.4081	-0.5080	-4.0963	1.44015E-06	0.00987634	0.00667229	2.326821383
Manual X-Z Balance Weight #1	1.8323	-0.6350	-6.2115	0.004182289	0.00532483	0.004182289	4.291733485
Manual Y Balance Weight #1	0.1752	-0.5080	-1.4758	0.014497289	0.00316809	0.014497289	0.774773525
Manual X-Z Balance Block #2	1.4081	0.5080	4.0963	0.00667229	0.00987634	0.00667229	2.333492233
Manual X-Z Balance Weight #2	1.8323	0.6350	6.2115	0.004182289	0.00532483	0.004182289	4.291733485
Manual Y Balance Weight #2	0.1752	0.5080	1.4758	0.014497289	0.00316809	0.014497289	0.774773525
Manual X-Z Balance Block #3	1.4081	0.5080	4.0963	0.00667229	0.00987634	0.00667229	2.333492233
Manual X-Z Balance Weight #3	1.8323	0.6350	6.2115	0.004182289	0.00532483	0.004182289	4.291733485
Manual Y Balance Weight #3	0.1752	0.5080	1.4758	0.014497289	0.00316809	0.014497289	0.774773525
Manual X-Z Balance Block #4	1.4081	-0.5080	-4.0963	0.00667229	0.00987634	0.00667229	2.333492233
Manual X-Z Balance Weight #4	1.8323	-0.6350	-6.2115	0.004182289	0.00532483	0.004182289	4.291733485
Manual Y Balance Weight #4	0.1752	-0.5080	-1.4758	0.014497289	0.00316809	0.014497289	0.774773525
Manual X Balance Block #1	0.6993	0.0000	0.0000	0.001355909	0.00266565	0.002610334	0.13234858
Manual X Balance Weight #1	0.7329	0.0000	0.0000	0.003825711	0.00067377	0.003865152	0.141110148
Manual X Balance Block #2	0.6993	0.0000	0.0000	0.001355909	0.00266565	0.002610334	0.13234858
Manual X Balance Weight #2	0.7329	0.0000	0.0000	0.003825711	0.00067377	0.003865152	0.141110148
Manual Z Balance Block #1	-1.3157	-0.6807	-2.5412	0.002610334	0.00266565	0.001355909	2.1961758
Manual Z Balance Weight #1	-1.6025	-0.8560	-3.3490	0.003865152	0.00067377	0.003825711	3.526894368
Manual Z Balance Block #2	-1.3157	0.6807	2.5412	0.002610334	0.00266565	0.001355909	2.1961758
Manual Z Balance Weight #2	-1.6025	0.8560	3.3490	0.003865152	0.00067377	0.003825711	3.526894368
Power Switching & Control Electronics	0.1356	-0.2235	-0.3079	0.002166571	0.00166659	0.007499669	0.084344363
Sun Sensor Head	0.0370	0.0000	0.0000	0.08419198	0.08419198	0.073333673	0.090231784
Switch Box	0.1636	-0.5664	-0.7482	0.004119102	0.00131385	0.002414646	0.448175663
Industrial PC	-0.5432	0.3708	1.0070	0.015459912	0.0042017	0.016190779	0.497557154
Auto Leveling Electronics #1	-0.0772	-0.5359	-0.1570	0.000186256	0.00014	0.000413603	0.104655334
Auto Leveling Electronics #2	-0.0772	0.2743	0.0803	0.000186256	0.00014	0.000413603	0.042567765
Auto Leveling Electronics #3	-0.0772	-0.5080	-0.1488	0.000413603	0.00014	0.000186256	0.096339663
Wireless Ethernet	0.0823	0.5410	0.2549	0.000619378	0.0004976	0.001526183	0.152884196
Inclinometers	0.0134	-0.2464	-0.0196	1.92643E-05	4.8161E-06	1.92643E-05	0.007107379
3-Axis Magnitometer	0.0445	-0.3810	-0.0972	0.000203623	6.4615E-05	0.000116532	0.044995174
IMU Interface	0.0591	-0.3073	-0.1040	0.000477646	0.00016168	0.000215097	0.042741449
IMU	0.1042	-0.4064	-0.2839	0.006660617	0.00090133	0.006660617	0.137584827
Top Deck Controller	0.0511	-0.1016	-0.0298	0.000413603	0.00014	0.000186256	0.012367953
CMG Gimbal Controller #1	-0.0344	0.0000	0.0000	0.000413603	4.6564E-05	0.00056	0.004455983
CMG Gimbal Controller #2	-0.0346	0.9830	0.2898	0.000563702	4.6872E-05	0.000416337	0.289511686
CMG Gimbal Controller #3	-0.0344	0.0000	0.0000	0.000413603	4.6564E-05	0.00056	0.004455983
Emoteq CMG Rotor Controllers #1	-0.1629	-0.1930	-0.1222	0.000593723	0.00039363	0.001078846	0.066071948
Emoteq CMG Rotor Controllers #2	-0.1629	0.5537	0.3506	0.001078846	0.00039363	0.000593723	0.237108082
Emoteq CMG Rotor Controllers #3	-0.1629	0.2007	0.1271	0.000593723	0.00039363	0.001078846	0.06797159

Optical Deck Isolators	0.002075673	0.047140526	0.02253243	-0.0225324	0
Equipment Plate	9.176288825	11.83249386	1.32810252	-1.3281025	0
Standoffs	0	0	0	0	0
Lower Equipment Ring	8.362748844	12.34573395	1.99149255	-1.9914926	0
Ball Segment	0.002460144	0.002610716	7.5286E-05	-7.529E-05	0
Ball Segment Adapter Tube	0.019401605	0.026544061	0.00357123	-0.0035712	0
Manual X-Z Balance Block #1	4.16188448	2.326821383	-0.9175315	0.91753155	0
Manual X-Z Balance Weight #1	7.892813222	4.291733485	-1.8005399	1.80053987	0
Manual Y Balance Weight #1	1.513909215	0.774773525	-0.3695678	0.36956784	0
Manual X-Z Balance Block #2	4.16855533	2.333492233	-0.9175315	0.91753155	0
Manual X-Z Balance Weight #2	7.892813222	4.291733485	-1.8005399	1.80053987	0
Manual Y Balance Weight #2	1.513909215	0.774773525	-0.3695678	0.36956784	0
Manual X-Z Balance Block #3	4.16855533	2.333492233	-0.9175315	0.91753155	0
Manual X-Z Balance Weight #3	7.892813222	4.291733485	-1.8005399	1.80053987	0
Manual Y Balance Weight #3	1.513909215	0.774773525	-0.3695678	0.36956784	0
Manual X-Z Balance Block #4	4.16855533	2.333492233	-0.9175315	0.91753155	0
Manual X-Z Balance Weight #4	7.892813222	4.291733485	-1.8005399	1.80053987	0
Manual Y Balance Weight #4	1.513909215	0.774773525	-0.3695678	0.36956784	0
Manual X Balance Block #1	1.731234887	1.862227558	-0.7994432	-0.0654963	0.86493949
Manual X Balance Weight #1	2.870512482	3.007796919	-1.3647012	-0.0686422	1.43334339
Manual X Balance Block #2	1.731234887	1.862227558	-0.7994432	-0.0654963	0.86493949
Manual X Balance Weight #2	2.870512482	3.007796919	-1.3647012	-0.0686422	1.43334339
Manual Z Balance Block #1	1.732489313	0.466296821	0.23184324	0.63309625	-0.8649395
Manual Z Balance Weight #1	2.870551923	0.660207597	0.32817122	1.10517216	-1.4333434
Manual Z Balance Block #2	1.732489313	0.466296821	0.23184324	0.63309625	-0.8649395
Manual Z Balance Weight #2	2.870551923	0.660207597	0.32817122	1.10517216	-1.4333434
Power Switching & Control Electronics	0.365421639	0.309934401	-0.1405386	0.02774362	0.11279502
Sun Sensor Head	0.215003377	0.221043181	-0.0623858	-0.0030199	0.0654057
Switch Box	0.461748497	0.058196127	-0.0067864	0.20177618	-0.1949898
Industrial PC	0.524574336	0.259783549	-0.0135086	0.13239539	-0.1188868
Auto Leveling Electronics #1	0.109304823	0.045517477	-0.0023247	0.03189367	-0.0295689
Auto Leveling Electronics #2	0.097812094	0.096112317	-0.0276222	0.00084989	0.02677228
Auto Leveling Electronics #3	0.097230679	0.04198635	-0.0004455	0.02762216	-0.0271767
Wireless Ethernet	0.160998784	0.037465127	-0.0040573	0.06176683	-0.0577095
Inclinometers	0.03298168	0.030402737	-0.0129372	0.00128947	0.01164768
3-Axis Magnitometer	0.127301949	0.098061391	-0.0411534	0.01462028	0.02653311
IMU Interface	0.037883178	0.016247046	0.00242914	0.01081807	-0.0132472
IMU	0.215480796	0.115664477	-0.038948	0.04990816	-0.0109602
Top Deck Controller	0.036862673	0.042770208	-0.0122474	-0.0029538	0.01520113
CMG Gimbal Controller #1	0.283421579	0.287463959	-0.1394828	-0.0020212	0.14150399
CMG Gimbal Controller #2	0.285442582	0.004632805	0.00203455	0.14040489	-0.1424394
CMG Gimbal Controller #3	0.283421579	0.287463959	-0.1394828	-0.0020212	0.14150399
Emoteq CMG Rotor Controllers #1	0.221916218	0.240201637	-0.0779221	-0.0091427	0.08706484
Emoteq CMG Rotor Controllers #2	0.222029584	0.069763993	0.00753925	0.0761328	-0.083672
Emoteq CMG Rotor Controllers #3	0.22742722	0.243812998	-0.0797278	-0.0081929	0.0879207

Battery #1	1		0.175006	0.1651	0.17018			9.377
Battery #2	1		0.175006	0.1651	0.17018			9.377
DAQ Breakout Block #1	1		0.14224	0.14224	0.0762			0.227
DAQ Breakout Block #2	1		0.14224	0.14224	0.0762			0.227
Electronics Harness-Upper Deck	1		1.27	0.3048	0.0254			2.268
Electronics Harness-Lower Deck	1		1.27	0.8636	0.0254			2.268
HTVSCMG #1	1		0.1524	0.5207	0.26162			43.454
HTVSCMG #1 Pivot Assy	1		0.1143	0.127	0.0381			9.414
HTVSCMG #2	1		0.5207	0.1524	0.26162	2.076E-02		43.454
HTVSCMG #2 Pivot Assy	1		0.127	0.1143	0.0381			9.414
HTVSCMG #3	1		0.1524	0.5207	0.26162	2.076E-02		43.454
HTVSCMG #3 Pivot Assy	1		0.1143	0.127	0.0381			9.414
HTVSCMG #4 Ballast Weight	2	Lead	0.3302	0	0.0381	3.263E-03	1.134E+04	36.998
X- Axis CG Auto-Balance Actuator	1		0.1143	0.4826	0.0508	2.802E-03		4.763
X- Axis CG Auto-Balance Weight	1	Brass	0.1143	0	0.1143	1.173E-03	8.670E+03	10.886
Y- Axis CG Balance Actuator	1		0.1143	0.1016	0.4826	5.604E-03		6.804
Y- Axis CG Balance Weight	1	Brass	0.1143	0	0.1143	1.173E-03	8.670E+03	10.886
Z- Axis CG Balance Actuator	1		0.4826	0.1143	0.0508			4.763
Z- Axis CG Balance Weight	1	Brass	0.1143	0	0.1143	1.173E-03	8.670E+03	10.886
Foot Assy #1	1		0.0508	0	0.18796			1.134
Foot Assy #2	1		0.0508	0	0.18796			1.134
Foot Assy #3	1		0.0508	0	0.18796			1.134
Foot Assy #4	1		0.0508	0	0.18796			1.134
Ballast Weights #1	0		0	0	0			24.494
Ballast Weights #2	0		0	0	0			34.473
Ballast Weights #3	0		0	0	0			24.494

Battery #1	9.377		-0.5410	-5.0730	-0.0762	0.2127	0.1365
Battery #2	9.377		0.5436	5.0968	-0.0762	0.2127	0.1365
DAQ Breakout Block #1	0.227		0.3581	0.0812	-0.4890	0.2127	-0.2762
DAQ Breakout Block #2	0.227		0.3581	0.0812	-0.4890	0.2127	-0.2762
Electronics Harness-Upper Deck	2.268		0.0000	0.0000	-0.0064	0.2127	0.2064
Electronics Harness-Lower Deck	2.268		0.0000	0.0000	-0.5105	0.2127	-0.2978
HTVSCMG #1	43.454		-0.6731	-29.2490	-0.3302	0.2127	-0.1175
HTVSCMG #1 Pivot Assy	9.414		-0.8128	-7.6520	-0.5461	0.2127	-0.3334
HTVSCMG #2	43.454		0.0000	0.0000	-0.3302	0.2127	-0.1175
HTVSCMG #2 Pivot Assy	9.414		0.0000	0.0000	-0.5461	0.2127	-0.3334
HTVSCMG #3	43.454		0.6731	29.2490	-0.3302	0.2127	-0.1175
HTVSCMG #3 Pivot Assy	9.414		0.8128	7.6520	-0.5461	0.2127	-0.3334
HTVSCMG #4 Ballast Weight	73.997		0.0000	0.0000	-0.4724	0.2127	-0.2597
X- Axis CG Auto-Balance Actuator	4.763		-0.4623	-2.2017	-0.4763	0.2127	-0.2635
X- Axis CG Auto-Balance Weight	10.168		-0.3581	-3.6417	-0.3937	0.2127	-0.1810
Y- Axis CG Balance Actuator	6.804		-0.4763	-3.2404	-0.3556	0.2127	-0.1429
Y- Axis CG Balance Weight	10.168		-0.6223	-6.3277	-0.2921	0.2127	-0.0794
Z- Axis CG Balance Actuator	4.763		0.4521	2.1533	-0.4763	0.2127	-0.2635
Z- Axis CG Balance Weight	10.168		0.4521	4.5973	-0.3937	0.2127	-0.1810
Foot Assy #1	1.134		-0.4394	-0.4983	-0.6223	0.2127	-0.4096
Foot Assy #2	1.134		-0.4851	-0.5501	-0.6223	0.2127	-0.4096
Foot Assy #3	1.134		0.4724	0.5357	-0.6223	0.2127	-0.4096
Foot Assy #4	1.134		0.4521	0.5127	-0.6223	0.2127	-0.4096
Ballast Weights #1	0.000		-0.1651	0.0000	0.0488	0.2127	0.2615
Ballast Weights #2	0.000		0.4223	0.0000	0.0742	0.2127	0.2869
Ballast Weights #3	0.000		0.0000	0.0000	0.2540	0.2127	0.4667
		652.83	**-0.014326**	**-9.352529**			**-0.011898**

Battery #1	1.2801	0.2515	2.3579	0.043929336	0.01130776	0.04656192	0.811599822
Battery #2	1.2801	-0.2642	-2.4770	0.043929336	0.01130776	0.04656192	0.873002083
DAQ Breakout Block #1	-0.0626	0.5537	0.1256	0.000492122	0.00019119	0.000492122	0.087334395
DAQ Breakout Block #2	-0.0626	0.4115	0.0933	0.000492122	0.00019119	0.000492122	0.056197534
Electronics Harness-Upper Deck	0.4680	0.0000	0.0000	0.246594049	0.48358706	0.246594049	0.343183323
Electronics Harness-Lower Deck	-0.6754	0.0000	0.0000	0.339141346	0.66868165	0.339141346	0.54030221
HTVSCMG #1	-5.1050	0.0000	0.0000	1.22965659	0.26647738	0.331956349	1.829391258
HTVSCMG #1 Pivot Assy	-3.1385	0.0000	0.0000	0.013792443	0.00572576	0.011388256	1.060119802
HTVSCMG #2	-5.1050	0.6731	29.2490	0.331956349	0.26647738	1.22965659	20.61918596
HTVSCMG #2 Pivot Assy	-3.1385	0.8128	7.6520	0.011388256	0.00572576	0.013792443	7.277221553
HTVSCMG #3	-5.1050	0.0000	0.0000	1.22965659	0.26647738	0.331956349	1.829391258
HTVSCMG #3 Pivot Assy	-3.1385	0.0000	0.0000	0.013792443	0.00572576	0.011388256	1.060119802
HTVSCMG #4 Ballast Weight	-19.2184	-0.5893	-43.6047	0.739189697	0.50425034	0.739189697	31.42599884
X- Axis CG Auto-Balance Actuator	-1.2551	0.4674	2.2259	0.093461795	0.02440569	0.000192996	1.464522398
X- Axis CG Auto-Balance Weight	-1.8403	0.4674	4.7522	0.105155621	0.01777786	0.105155621	2.659216364
Y- Axis CG Balance Actuator	-0.9721	-0.4115	-2.7997	0.137906446	0.00331506	0.139461094	1.428811035
Y- Axis CG Balance Weight	-0.8072	-0.4115	-4.1840	0.105155621	0.10515562	0.01777786	1.890878906
Z- Axis CG Balance Actuator	-1.2551	-0.4674	-2.2259	0.006209448	0.02440569	0.093461795	1.377270051
Z- Axis CG Balance Weight	-1.8403	-0.3607	-3.6675	0.105155621	0.01777786	0.105155621	1.760997868
Foot Assy #1	-0.4645	-0.5359	-0.6077	0.017944822	0.0003658	0.017944822	0.533891957
Foot Assy #2	-0.4645	0.4674	0.5300	0.017944822	0.0003658	0.017944822	0.455866904
Foot Assy #3	-0.4645	0.4902	0.5559	0.017944822	0.0003658	0.017944822	0.480690065
Foot Assy #4	-0.4645	-0.5080	-0.5761	0.017944822	0.0003658	0.017944822	0.500816358
Ballast Weights #1	0.0000	-0.2667	0.0000	0	0	0	0
Ballast Weights #2	0.0000	0.1651	0.0000	0	0	0	0
Ballast Weights #3	0.0000	0.0000	0.0000				0
	-7.767070	**-0.017793151**	**-11.61591749**				**171.0872994**

Battery #1	3.381429601	2.963280254	-1.2849149	0.20907467	1.07584022
Battery #2	3.468663159	2.98911155	-1.2978305	0.2397758	1.05805473
DAQ Breakout Block #1	0.099119008	0.046887202	-0.0058923	0.0261159	-0.0202236
DAQ Breakout Block #2	0.067982147	0.046887202	-0.0058923	0.01054747	-0.0046552
Electronics Harness-Upper Deck	0.246594049	0.343183323	0.04829464	-0.0482946	0
Electronics Harness-Lower Deck	0.339141346	0.54030221	0.10058043	-0.1005804	0
HTVSCMG #1	20.91715153	21.5168862	-9.5438801	-0.2998673	9.84374747
HTVSCMG #1 Pivot Assy	6.233298381	7.27962574	-2.5865893	-0.5231637	3.10975297
HTVSCMG #2	20.01945129	0.931691017	0.29986733	9.54388014	-9.8437475
HTVSCMG #2 Pivot Assy	6.230894193	1.057715615	0.52316368	2.58658929	-3.109753
HTVSCMG #3	20.91715153	21.5168862	-9.5438801	-0.2998673	9.84374747
HTVSCMG #3 Pivot Assy	6.233298381	7.27962574	-2.5865893	-0.5231637	3.10975297
HTVSCMG #4 Ballast Weight	26.43459357	5.730594971	2.49570264	10.3519993	-12.847702
X- Axis CG Auto-Balance Actuator	2.15156735	1.442030113	-0.3435225	0.35476862	-0.0112461
X- Axis CG Auto-Balance Weight	3.630394251	1.742432587	-0.4855889	0.94398083	-0.4583919
Y- Axis CG Balance Actuator	2.833128806	1.820022724	-0.7021589	0.50655304	0.19560584
Y- Axis CG Balance Weight	5.764548802	4.106969982	-1.9368349	0.82878941	1.10804554
Z- Axis CG Balance Actuator	2.020067884	1.310530647	-0.3213989	0.35476862	-0.0333697
Z- Axis CG Balance Weight	3.506472637	2.516729469	-0.8727374	0.49487158	0.3778658
Foot Assy #1	0.562620413	0.427137004	-0.0143642	0.0677417	-0.0533775
Foot Assy #2	0.532529739	0.475071383	-0.0383314	0.02872918	0.00960224
Foot Assy #3	0.543562254	0.461280738	-0.0314361	0.04114076	-0.0097047
Foot Assy #4	0.54238438	0.43997657	-0.020784	0.0512039	-0.0304199
Ballast Weights #1	0	0	0	0	0
Ballast Weights #2	0	0	0	0	0
Ballast Weights #3	0	0	0	0	0
	243.9898794	**176.4333965**	**-36.91069636**	**34.23764782**	**2.673048534**

APPENDIX B: MATLAB/SIMULINK FILES

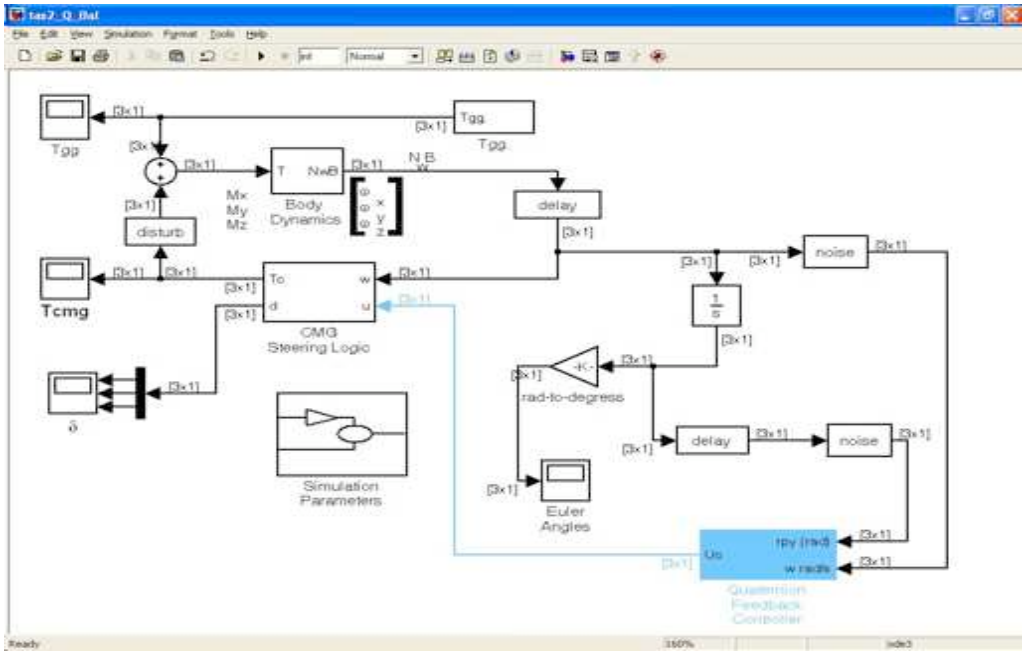

Figure 58. Simulation program

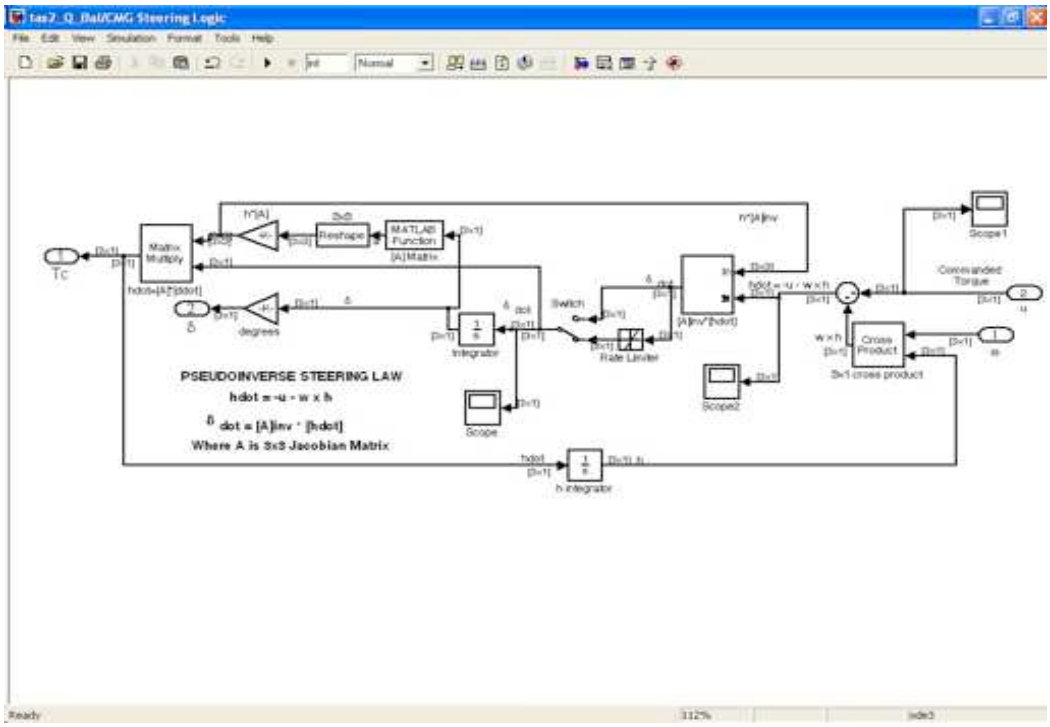

Figure 59. CMG steering

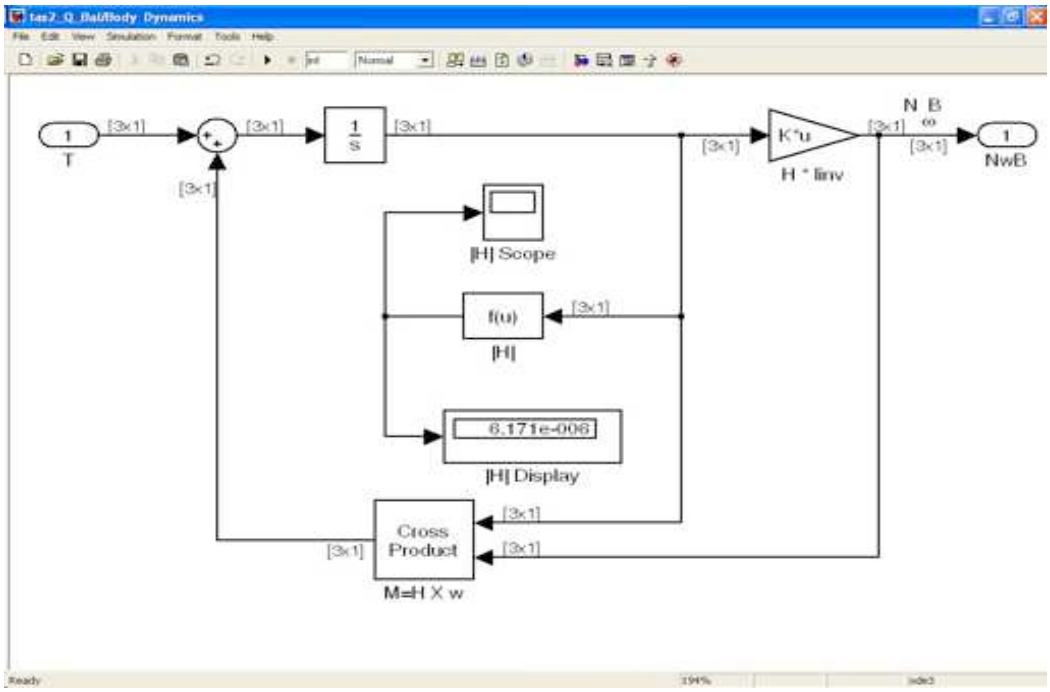

Figure 60. Body dynamics

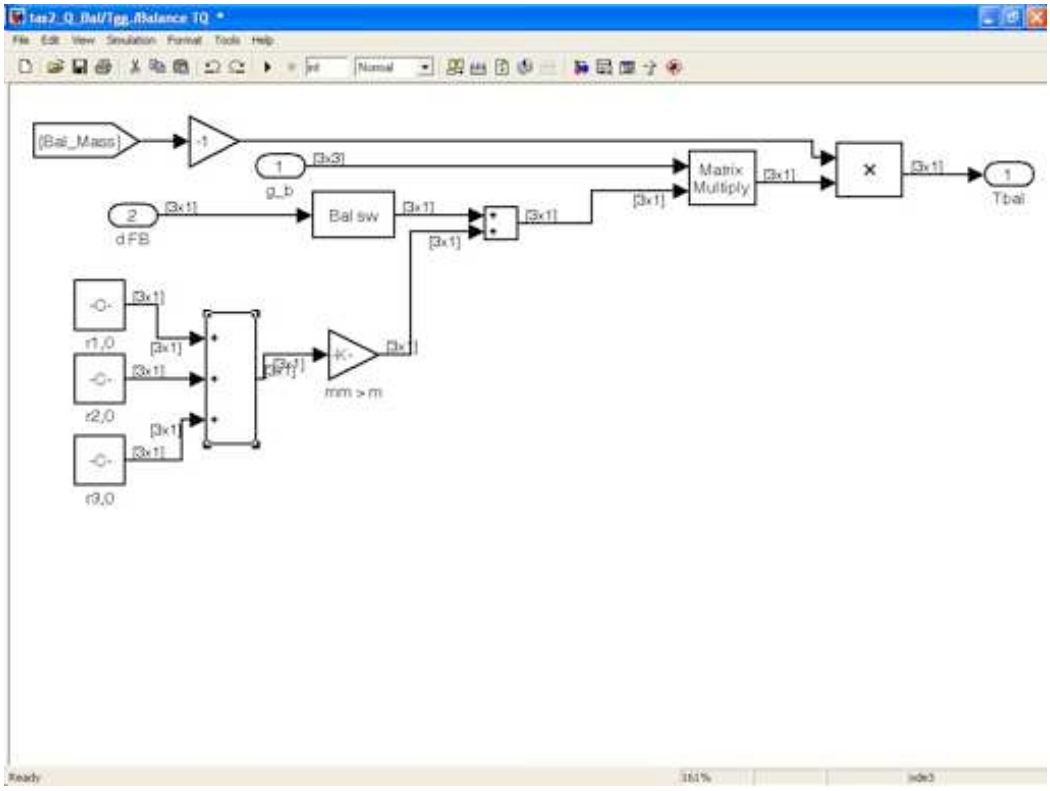

Figure 61. Balance torque calculation

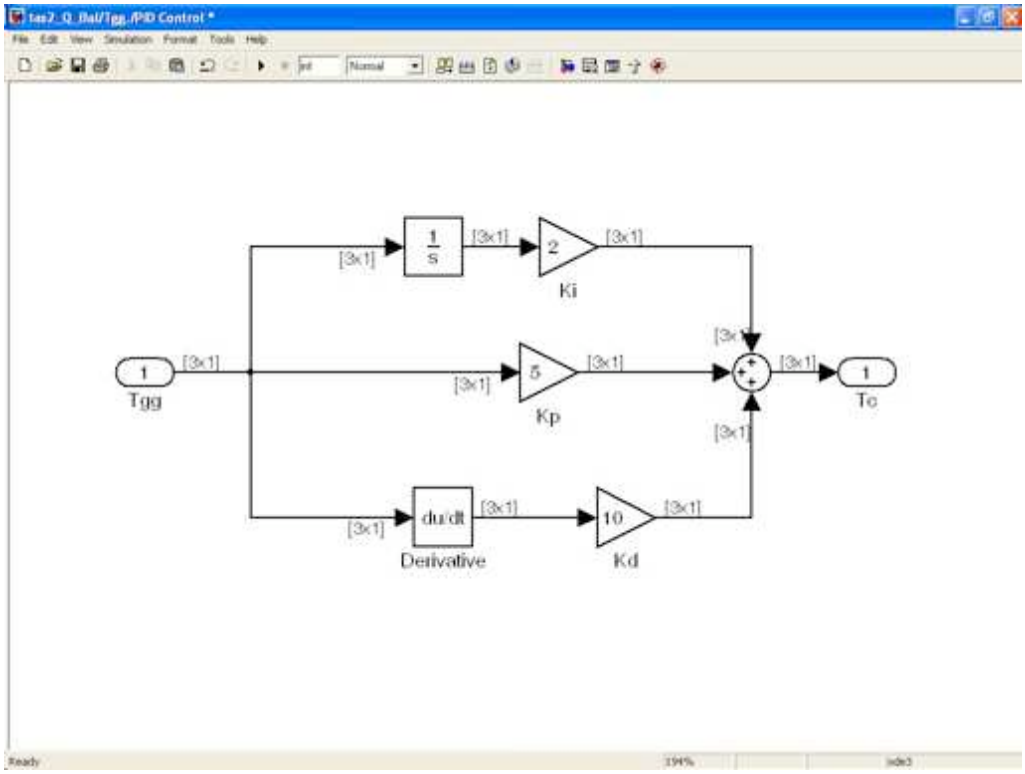

Figure 62. Balance PID controller

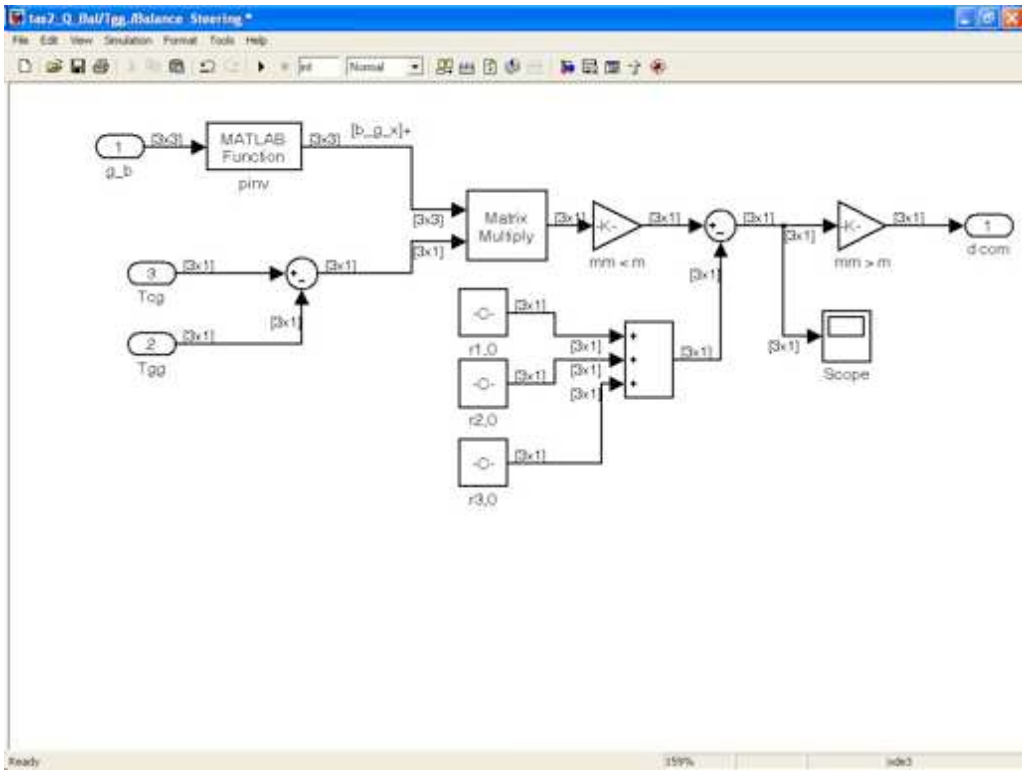

Figure 63. Balance steering

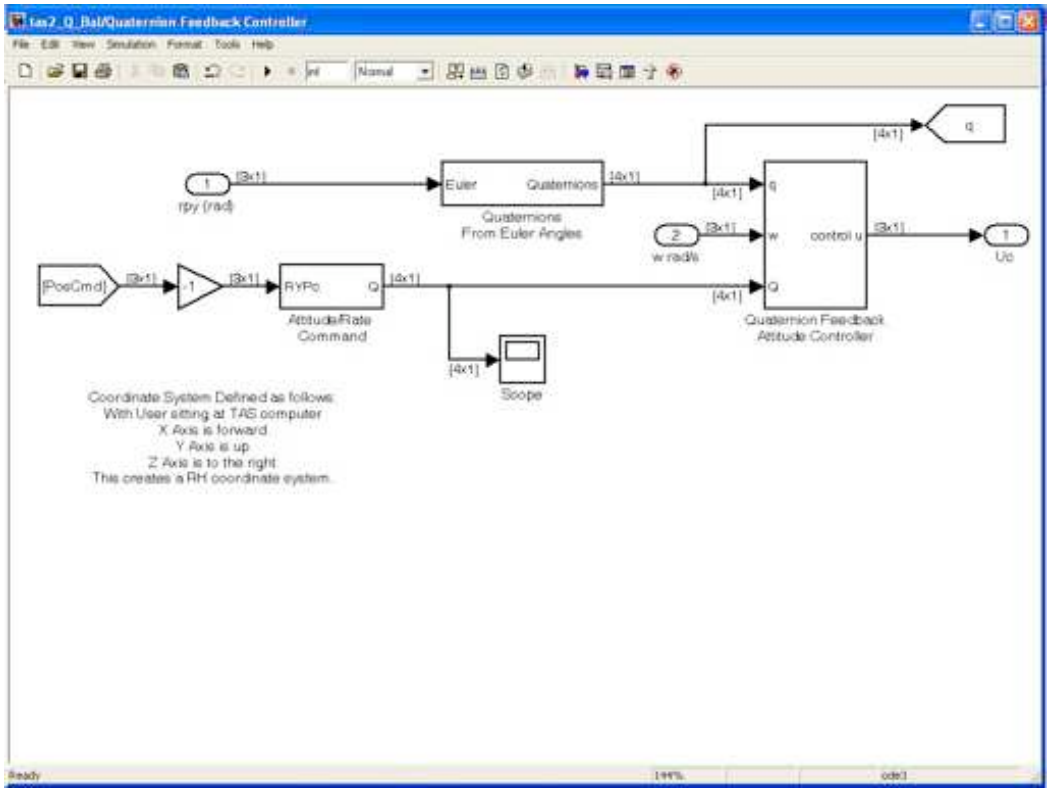

Figure 64. CMG quaternion attitude and feedback

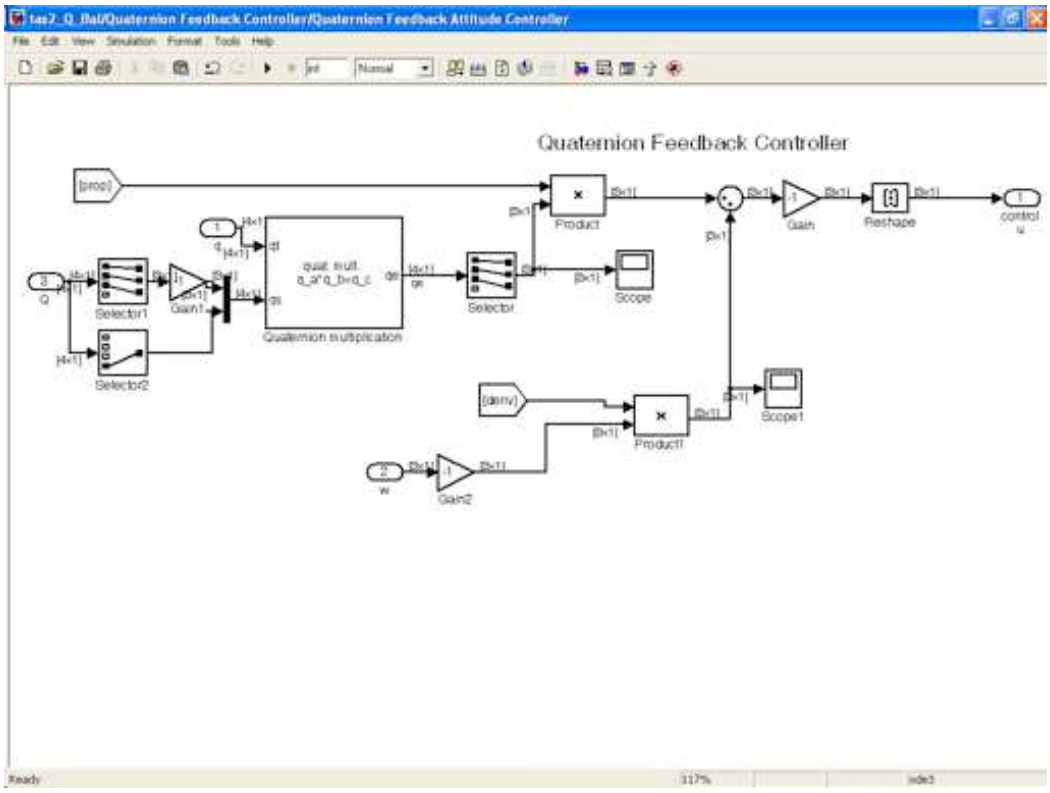

Figure 65. CMG quaternion feedback controller

```
%Bifocal Relay Mirror Spacecraft Dynamics Simulation
%TA Bands

clear all
close all
clc

%Constants%
Re=6371.1363e3;                    %earth radius
mu=398600.4415e9;                  %universal gravitation constant

%Spacecraft orbit
h=1;                               %orbit altitude
R=Re+h;                            %orbit radius from center of earth
we=0.00007292115855$;              %earth's angular velocity rad/solar
sec;Vallado)
wO=sqrt(mu/(Re+h)^3);              %orbit angular velocity
incln=36.6*pi/180;                 %Space Station Inclination
epsilon=12*pi/180;                 % earth magnetic dipole tilt
alpha0=0;                          % true anomoly
u0=0; n0=0;                        %Start S/C beneath subsolar point
beta=60;
gamma=1.5;

%Assumed spacecraft rectangular size
a=0.545491852;
b=0.314939867;
c=0.706226952;

Area=[1.719 2.1 1.718];            %projected area-m^2 in body x,y,z directions
density=4.974e-7;
Xpre=-9.9639/24/3600/180*pi*0;     %nodal precession constant assumed zero here
wn=Xpre*(Re/(Re+h))^3.5*cos(incln); %nodal precession (zero eccentricity)
V=wO*(Re+h);
rho=asin(Re/(O+Re));               %earth angular radius
Cd=2.2;                            %Drag coefficient
psun=4.5E-6;                       % solar pressure constant-N/m^2

%constants for aero and solar torque calculation
Kaero=-0.5*Cd*V^2; Ksolar=.501*psun;
dL=[0.000 -0.002 0.000];           %predicted distance between cp and cg
Rme=2.5190e-005;

%Spacecraft Magnetic Properties (assumed)
mresid=[0 0 0.01];                 %Spacecraft residual magnetic moment
M=mresid;                          %Magnetic unit dipole vector
B=7.943e15;
```

```
%Spacecraft Inertia conditions
mass = 624                          % mass in Kg
Ixx = .154136;  Iyy = .218868;   Izz = .172859;
Ixy = .032366;  Iyz = .022932;   Ixz = .009434;
Imo=[Ixx -Ixy  Ixz;
    -Ixy  Iyy  Iyz;
     Ixz  Iyz  Izz]*mass;          %Moment of inertia matrix (Kg-m^2) scaled
from original
IinV=inv(Imo);                     %Moment of inertia inverse goes in dynamics
block

%Spacecraft initial Euler state angles and rates
phio=0;thetao=0;psio=0;              %Initial Euler Angles
phidoto=0;thetadoto=0;psidoto=0;     %Initial Euler Rates

%Calculation of initial quaternion (qo) and angular momentum (Ho)
s1=sin(phio/2);
s2=sin(thetao/2);
s3=sin(psio/2);
c1=cos(phio/2);
c2=cos(thetao/2);
c3=cos(psio/2);
q1o=s1*c2*c3-c1*s2*s3;
q2o=c1*s2*c3+s1*c2*s3;               %Wie pg. 321
q3o=c1*c2*s3-s1*s2*c3;
q4o=c1*c2*c3+s1*s2*s3;
S1=sin(phio);
S2=sin(thetao);
S3=sin(psio);
C1=cos(phio);
C2=cos(thetao);
C3=cos(psio);
Wxo=phidoto-psidoto*S2-wo*S1*C2;
Wyo=thetadoto*C1+psidoto*C2*S1-wo*(C1*C1+S1*S2*S1);
Wzo=psidoto*C2*C1-thetadoto*S1-wo*(S3*S2*C1-C3*S1);
    qo=[q1o q2o q3o q4o];
    Ho=Imo*[Wxo Wyo Wzo]';
    norm(Ho)*1000;

%Calculate eclipse time for comparison with project EPS calculations
Te=100.87*2*V/2/pi;

%CMG Properties (in degrees)
Beta=54.73*pi/180;                   %Skew angle in degrees converted to
radians
GeltaBoughtX=60*pi/180;              %CMG X intial gimbal position
GeltaBoughtY=pi;                     %CMG Y intial gimbal position
GeltaBoughtZ=-60*pi/180;             %CMG Z intial gimbal position
```

Figure 66. Matlab 'M' file for CMG parameters

APPENDIX C: EQUIPMENT SPECIFICATION SHEETS

A. MAGNETOMETER

TFM100G2 / TFM100G2-S (Flight)

Ultra-miniature Triaxial Fluxgate Magnetometer

Ultra-miniature triaxial fluxgate magnetometer for spacecraft attitude control, general magnetic measurements in the laboratory or field applications. Underwater enclosure available.

TFM100G2 Specifications Download (.doc)

TFM100G2-S Specifications Download (.doc)

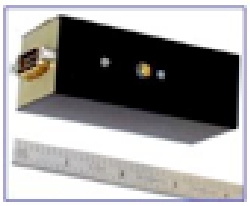

Specifications	
Radiation Tolerance	>10 kRADs (0 to 5 V option) >50 kRADs (weight 100 grams) >100 kRADs (weight 117 grams)
Axial Alignment (Orthogonality)	better than ±1° ; calibration data provided to ±0.1°
Input Voltage	+15 to +34 VDC 0 to +5 VDC
Input Current	30 mA @ 15 to 34 VDC
Noise	20 picoTesla RMS/ SQRT Hz @1 Hz* 10 picoTesla RMS/ SQRT Hz @1 Hz (Low Noise)* 8 picoTesla RMS/ SQRT Hz @1 Hz (Special)* *Not available on 0 to 5 Volt models
Field Measurement Range	± 100 µTesla = ± 10V (100 uV/nT)or 0 to + 5 Volts = ± 60 µTesla ±5 Volts = ± 60 µTesla
Accuracy	±0.75% of full scale (0.5% typical)
Linearity	±0.015% of full scale ± 0.15% of full scale (5 V option)
Scale Factor Temperature Shift	0.015% full scale per °C (typical)
Output Ripple	3 mV peak to peak at 2nd harmonic
Analog Output @ Zero Field	±0.025 V
Zero Shift with Temperature	±1.2 nanoTesla per °C
Susceptibility to Perming	± 8 nanoTesla shift with ± 5 Gauss applied
Output Impedance	332 Ohms ±5%
Frequency Response	3 dB at >500Hz Bandwidth: to >4 kHz (wideband) >150 Hz (5 Volt option)
EMI	CE01, CE03, RE02, CS01, CS02, CS06, RS01, RS02, RS03
Random Vibration	27G RMS (20 Hz to 2 KHz)
Shock	>230G
Temperature Range	-55° to +85°C operating
Weight	117 grams (shielded to 100 kRADs)
Size	3.51 cm x 3.23 cm x 8.26 cm
Connector (chassis mounted)	9 pin male 'D' type, gold-plated, mil-spec, non-magnetic (mating connector supplied)

B. MASS BALANCER

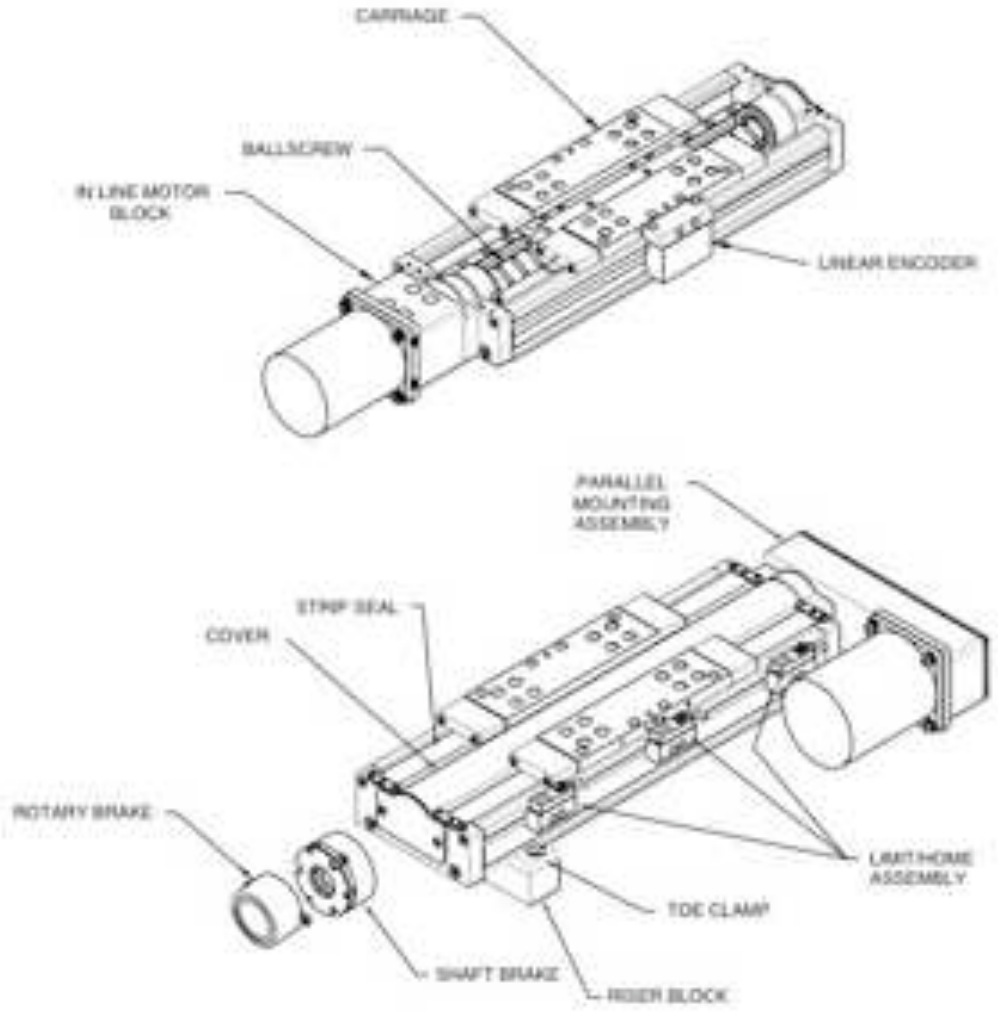

404XR Series

Common Characteristics	Precision	Standard
Performance		
Bidirectional Repeatability (µm)	±1.3	±5.0
Duty Cycle	100%	100%
Max Acceleration – m/sec² (in/sec²)	20 (773)	20 (773)
Rated Capacity[1]		
Normal load – kgf (lbs)	170 (375)	170 (375)
Axial load – kgf (lbs)	90 (198)	90 (198)
Motor Sizing		
Drive Screw Efficiency	90%	80%
Max Break-Away Torque – Nm (in-oz)	0,13 (18)	0,18 (26)
Max Running Torque – Nm (in-oz)	0,11 (16)	0,17 (24)
Linear Bearing – Coefficient of Friction	0.01	0.01
Ballscrew Diameter (mm)	16	16
Carriage Weight – kg (lbs)	0,70 (1.55)	0,70 (1.55)

404XR Series

Travel Dependent Characteristics

Travel (mm)	Positional[2] Accuracy (µm) Prec.	Std.	Straightness & Flatness Accuracy (µm) Prec./Std.	Input Inertia 10^{-5} kg-m² 5 mm	10 mm	20 mm	Max Screw Speed (Revs Per Second) Prec./Std.	Total Table Weight (kg) Prec./Std.
50	10	12	8	1,68	1,81	2,34	60	2,8
100	10	12	8	1,93	2,07	2,60	60	3,0
150	12	18	12	2,19	2,32	2,85	60	3,3
200	16	24	16	2,44	2,57	3,11	60	3,6
250	16	30	16	2,69	2,83	3,36	60	3,9
300	18	30	18	2,95	3,08	3,61	60	4,2
350	18	33	23	3,20	3,33	3,87	60	4,5
400	21	33	27	3,46	3,59	4,12	60	4,8
450	25	41	30	3,71	3,84	4,37	54	5,1
500	28	48	30	3,96	4,10	4,63	50	5,4
550	30	48	30	4,22	4,35	4,88	50	5,7
600	32	48	30	4,47	4,60	5,14	50	6,0

[2] Positional accuracy applies to in-line motor configurations only. Contact factory for parallel motor specifications.

C. IMU

LN-200

Description

The Northrop Grumman LN-200 family of inertial equipment uses fiber optic gyros (FOGs) and silicon accelerometers (SiACs) for measurement of vehicle angular rate and linear acceleration. It satisfies tactical missile and guided projectile guidance requirements and aircraft flight control systems. Its offers low cost and high reliability through the use of solid-state instruments. This results in both small size and light weight.

Summary of LN-200 IMU Characteristics

Physical		
	Weight	1.94 pounds (700 grams)
	Size	3.5 inches (8.9cm) diameter by 3.35 inches (8.5 cm high)
	Power	10 watts steady-state (nominal)
	Cooling	Conduction to mounting plate
	Mounting	4 mounting bolts - M4
Activation Time		0.8 sec (1 sec to full accuracy)
Performance - Gyro		
	Bias Repeatability	1deg./hr to 10deg./hr 1[sigma]
	Random Walk	0.04 to 0.1deg.[sqr root]hr power spectral density (PSD) level
	Scale Factor Stability	100 ppm 1[sigma]
	Bias Variation	0.35deg./hr 1[sigma] with 100-second correlation time
	Nonorthogonality	20 arcsec 1[sigma]
	Bandwidth	> 500 Hz
Performance - Accelerometer		
	Bias Repeatability	200 [micron]g to 1 milli-g, 1[sigma]
	Scale Factor Stability	300 ppm 1sigma
	Vibration Sensitivity	50 [micron]g/g2 1[sigma]
	Bias Variation	50 micro-g 1sigma with 60-second correlation time
	Nonorthogonality	20 arcsec 1[sigma]
	White Noise	50 micro[sqr root]Hz PSD level
	Bandwidth	100 Hz
Operating Range		

	Angular rate	±1000deg./sec
	Angular Acceleration	±100,000deg./sec/sec
	Acceleration	±40g
	Velocity Quantization	0.00169 fps
	Angular Attitude	Unlimited
Reliability (predicted)		32,995 hours MTBF (30deg.C missile launch environment)
Input/Output		RS-485 Serial Data Bus (SDLC)
Data Latency		< 1 msec
Environmental		
	Temperature	-54deg.C to +85deg.C operating (85deg.C intermittent)
	Vibration	11.9g rms - performance 17.9g rms - endurance
	Shock	90G, 6ms terminal sawtooth

Fiber Optic Gyro Advantages for (1deg./hr) Accuracy Applications

Characteristic	Comparative Advantages Over Competing Gyro Technologies (Tactical, RLG, DTG)
Performance	• Low random walk (no lock-in effects) • High bandwidth (no mechanical dither) • Low noise (no moving parts) • High rate capability
Environmental	• Full military temperature range • Extremely rugged • Excellent performance over full military vibration range (no isolators required)
Lifetime Reliability	• High MTBF (all solid-state) • No lifetime/dormancy limitations (no bearings, no gas leakage, low-voltage operation, no high energy mirror degredation, no cathode life limit)
Cost	• Lowest cost IMU
Production Baseline	• 300 IMUs/month capability (expandable)

THIS PAGE INTENTIONALLY LEFT BLANK

LIST OF REFERENCES

1 Peck, M. A., Miller, L., Cavender, A. R., Gonzalez, M., Hintz, T., "An Airbearing-Based Testbed for Momentum-Control Systems and Spacecraft Line of Sight," AAS paper 03-127, *AAS/AIAA Space Flight Mechanics Conference*, Ponce, Puerto Rico, Feb 9 – 12, 2003.

2 Peck M. A., Kim S. C., "New Results From the Spacecraft Momentum Control and Line of Sight Testbed," AAS paper 04-025, *27th Annual AAS Guidance and Control Conference*, Breckenridge, Colorado, Feb 4 – 8, 2004.

3 Romano M., Agrawal, B. N., "Acquisition, Tracking and Pointing Control of the Bifocal Relay Mirror Spacecraft," *Acta Astronautica*, Vol. 53, pp. 509-519, 2003.

4 Chernesky, V. S., "Development and Control of a Three-Axis Satellite Simulator for the Bifocal Relay Mirror Initiative," *M.S. Thesis, Naval Postgraduate School*, December, 2001.

5 Kurokawa, H. "A Geometric Study of Single Gimbal Control Moment Gyros," *Report of Mechanical Engineering Laboratory*, (175): 135-138, January 1998.

6 Jung, D., Tsiotras, P., A 3-DoF Experimental Test-Bed for Integrated Attitude Dynamics and Control Research, AIAA paper 03-5331, *AIAA Guidance, Navigation and Control Conference*, Austin, Texas, 2003.

7 Wie, B., *Space Vehicle Dynamics and Control*, American Institute of Aeronautics and Astronautics, Reston, Virginia, 1998.

8 Email between Mason A. Peck, Professor, Mechanical and Aerospace Engineering Department, Cornell University, 3 December 2004.

9 Mass Properties Spreadsheet prepared by Eric Rasmussen, Guidance Dynamics Corporation.

10 Automated Controlled Environments Inc., Three Axis Simulator II (TAS2), Electronics Operating Manual, Rev. A, California, 2003.

11 Sidi, M. J., *Spacecraft Dynamics and Control*, Cambridge University Press, Cambridge, United Kingdom, 1997.

12 Connolly, B. D., "Development of a High-Precision Sensor for the Attitude Determination of the Bifocal Spacecraft Simulator." *M.S. Thesis, Naval Postgraduate School*, June, 2004.

INITIAL DISTRIBUTION LIST

1. Defense Technical Information Center
   Ft. Belvoir, Virginia

2. Dudley Knox Library
   Naval Postgraduate School
   Monterey, California

3. Department Chairman, Code ME
   Department of Mechanical and Astronautical Engineering
   Naval Postgraduate School
   Monterey, California

4. Distinguished Professor Brij N. Agrawal, Code ME/Ag
   Department of Mechanical and Astronautical Engineering
   Naval Postgraduate School
   Monterey, California

5. Dr. Jong-Woo Kim, Code ME/Ki
   Department of Mechanical and Astronautical Engineering
   Naval Postgraduate School
   Monterey, California

6. Professor Mason A. Peck
   Department of Mechanical and Aerospace Engineering
   Cornell University
   Ithaca, New York

7. SRDC Research Library, Code ME
   Department of Mechanical and Astronautical Engineering
   Naval Postgraduate School
   Monterey, California